The Vortex in the $(2+1)$-dimensional $O(2)$ Model

and

Effective Low-Energy Theory for Spin Chains in a Strong Magnetic Field

Inauguraldissertation
der Philosophisch-naturwissenschaftlichen Fakultät
der Universität Bern

vorgelegt von

Manes Hornung

von Untereggen SG

Leiter der Arbeit:
Prof. Dr. Uwe-Jens Wiese

Albert Einstein Center for Fundamental Physics
Institut für Theoretische Physik, Universität Bern

source: https://doi.org/10.48549/3199 | downloaded: 17.4.2024

The Vortex in the $(2+1)$-dimensional $O(2)$ Model

and

Effective Low-Energy Theory for Spin Chains in a Strong Magnetic Field

Inauguraldissertation
der Philosophisch-naturwissenschaftlichen Fakultät
der Universität Bern

vorgelegt von

Manes Hornung

von Untereggen SG

Leiter der Arbeit:
Prof. Dr. U.-J. Wiese

Albert Einstein Center for Fundamental Physics
Institut für Theoretische Physik, Universität Bern

Von der Philosophisch-naturwissenschaftlichen Fakultät angenommen.

Bern, 2.7.2021

Der Dekan,

Prof. Dr. Zoltán Balogh

This work is licensed under a Creative Commons “Attribution 4.0 International” license.

Abstract

Part I The (2+1)-dimensional $O(2)$ model in the continuum limit at the Wilson-Fisher fixed point approached from the broken phase contains massless Goldstone bosons and vortices. The latter are infraparticles and therefore have a mass that is expected to diverge logarithmically with the volume due to the infinite cloud of massless Goldstone bosons that surrounds them. Making use of the exact duality that relates the $O(2)$ model on the lattice to a gauge theory with integer-valued link variables, we perform Monte Carlo simulations to calculate the mass of the vortex as a function of the finite and C-periodic volume non-perturbatively. We confirm the logarithmic divergence of the vortex mass numerically, and calculate the strength of the divergence that is related to the vortex charge, to be $b = 3.55(9)$. This constitutes a universal amplitude ratio associated with the Wilson-Fisher fixed point.

Part II In a large external magnetic field, spin chains saturate. We study defects in the saturated state for the XXZ Heisenberg spin chain as well as for a $SU(3)$ spin chain that is related to a regularization of the $\mathbb{C}P(2)$ model suitable for quantum simulation. The Hamiltonian is diagonalized in the one- and two-defects sectors and the results are matched to an effective theory of non-relativistic point particles with a contact interaction. We find that the defects in the saturated state of the $SU(3)$ spin chain are equivalent to the ones in an antiferromagnetic, anisotropic XXZ Heisenberg spin chain, and that they interact repulsively.

Acknowledgements

First and foremost, I thank Uwe-Jens Wiese for the excellent supervision during the work on my Ph.D.. While his literal office door is usually closed, the figurative version could not be more open. Despite his busy schedule, he always had time and an open ear to discuss the many challenges that arose during the work on this thesis. I am also thankful for his understanding and support during the second part of my Ph.D., when the birth of my son shifted much of my time and focus. I also thank Shailesh Chandrasekharan for agreeing to be the external examiner in my Ph.D. defense.

Furthermore, I thank my collaborators, Urs Gerber, Stephan Caspar, Alessandro Mariani and João Pinto Barros, who contributed significantly to this work, and who made working in this research group such a pleasant experience.

Many thanks also go to my fellow doctoral students, for the fun and inspiring conversations over lunch, coffee and beer. I would also like to thank Günhan Akarçay, for supporting my decision to start over in theoretical physics, even if it meant that I left his group. Special thanks go to Jonas Hagen for the countless discussions over afternoon-tea, providing inspiration, encouragement, comfort, or distraction, whichever was needed.

Last but not least, I am deeply thankful to my friends and family, who have been supportive through all these years in so many ways. Annsophie and Seraphin, without your unfailing support and encouragement this would not have been possible.

Contents

1. Introduction

Magnetic phenomena have fascinated humanity for thousands of years. Mentions of the magnetic properties of lodestone, a naturally occurring permanent magnet, can be found in Greek texts from as early as 800 B.C.. The ability of lodestone to attract and move iron even led Thales to attribute a soul to it. While the technological application of magnetism in the form of the compass had a great impact on navigation, its origins remained mysterious [1]. For example, it was widely believed well into the seventeenth century that garlic diminishes the force exhibited by a magnet [2]. Even today, one of the very few experimental hints of physics beyond the Standard Model of particle physics is in the intrinsic magnetic properties of the muon [3].

The understanding of the relationship between electricity and magnetism started in the nineteenth century and culminated in 1861 in the work of James C. Maxwell, whose famous equations give a coherent picture of electromagnetism. In 1928, Werner Heisenberg [4] proposed what is now known as the quantum Heisenberg model, a simple yet extremely successful model that describes magnetism in solids as a collective phenomenon based on the exchange interaction of electron spins.

Figure 1.1 shows the magnetization of five different materials as a function of temperature close to their critical point compared to predictions of the quantum Heisenberg model. Magnetization and temperature are scaled by appropriate powers of an external magnetic field. Two things are remarkable in Figure 1.1: Even though the five materials differ substantially in their microscopic properties ($CrBr_3$ has an anisotropic lattice structure, Pd_3Fe is an alloy and YIG is a ferrimagnet), they show the same dependence of the scaled magnetization on the temperature. Moreover, despite its idealized simplicity, the quantum Heisenberg model makes accurate predictions. In fact, one could use an even simpler model, the classical Heisenberg model where the quantum spins are replaced by classical unit vectors. The additional Euclidean time dimension that implements the temperature in the quantum Heisenberg model in the calculation of thermal expectation values, only affects its critical structure at zero temperature.

This is an instance of what is known as universality. Close to a continuous phase transition, many properties of a considered system (such as the rescaled magnetization of a magnet) become independent of the microscopic details of the system and only depend on its symmetry properties and the number of its dimensions. Thus, continuous phase transitions can be classified in different universality classes.

This phenomenon can be understood in terms of renormalization group (RG) theory [6–8]. Each universality class can be associated with an RG fixed point. Universality is also part of the reason why physics is so successful at explaining certain aspects of our world. For instance, to accurately describe the phase transition in a ferromagnetic material, one does not have to include the details of the atomic structure of the material

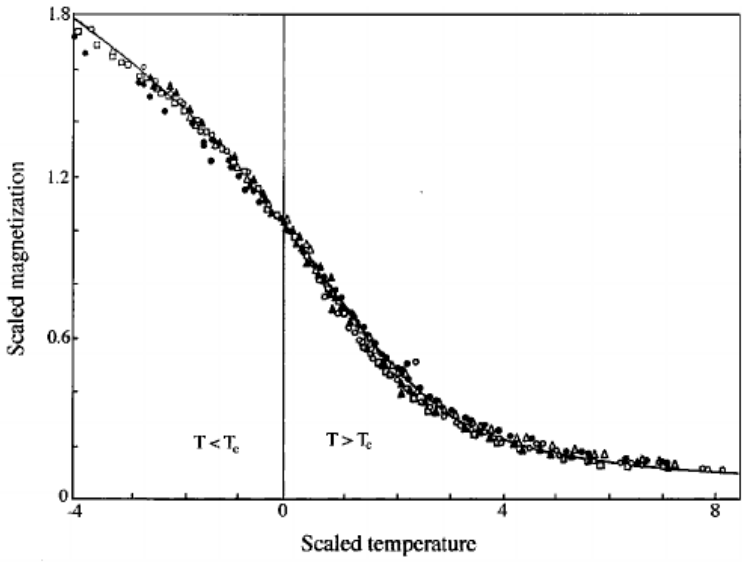

Figure 1.1.: The magnetization of several magnetic materials as a function of temperature. Magnetization and temperature are scaled by an appropriate power of the externally applied magnetic field. The solid line is the prediction of the quantum Heisenberg model in three spatial dimensions. The materials are: △ $CrBr_3$, ○ EuO, ▲ Ni, • Pd_3Fe, □ YIG. Reprinted figure with permission from [5] Copyright (1999) by the American Physical Society.

and can simply use an idealized system with the same symmetry properties, such as the (quantum) Heisenberg model. Another example is the liquid-vapor transition at the critical point of a fluid that can be described by the Ising model, a model system even simpler than the Heisenberg model.

This applies not only to phase transitions in condensed matter physics but also to certain aspects of quantum field theory. The continuum limit of a quantum field theory can be attributed to a universality class. To calculate e.g., the mass of a particle, one can then again use a (relatively) simple model system in the same universality class, for which it is possible to perform computer simulations.

Part I of the present thesis is concerned with the $O(2)$ model, a simple model within the three-dimensional XY universality class, where the defining symmetry properties of the interactions are invariance under rotations and reflections in the plane. This universality class contains the critical point in magnets with an easy-plane anisotropy, several phase transitions in liquid crystals and is relevant for type-II superconductors (see e.g. [9] and references therein). Moreover, the phase transition between liquid and superfluid ^{4}He along the λ-line also lies within the three-dimensional XY universality class. We study the $O(2)$ model, as a quantum field theory in $(2+1)$ dimensions, and calculate the mass of the vortex, a topological excitation, in a finite volume. This mass

is a universal quantity that can be attributed to the Wilson-Fisher fixed point.

Vortices play an important role in the physics of superfluids. In 1949, Lars Onsager first predicted the existence of quantized vortices in superfluids [10]. This idea was further developed by Feynman [11] and also applied to superconductors by Abrikosov [12]. The existence of quantized vortices in liquid helium was confirmed first indirectly in 1956 by Hall and Vinen [13] and directly in 1961 by Vinen [14]. Because they are coupled to massless Goldstone bosons, static vortices have an energy, or equivalently a rest mass, that diverges with the volume. Concerning the kinetic mass, the situation is less clear. Different ways of assigning such a mass to the vortex exist. Mapping vortices and phonons in a superfluid to charged particles and photons in electrodynamics, Popov concluded that the kinetic mass of a vortex corresponds to the static energy divided by the square of the speed of sound [15]. A similar conclusion was reached by Duan based on fluid dynamics arguments [16]. From the velocity dependence of the energy change induced by a moving vortex he extracted the kinetic mass and found it to diverge logarithmically with the volume. He further argued, that what he calls the dynamic mass can be obtained from the velocity dependence of the total momentum of the same system and that it coincides with the kinetic mass. On the other hand, a finite core-mass can be attributed to the vortex as kinetic mass. According to Baym and Chandler [17] the core-mass corresponds to the mass of the superfluid within the core. An equivalent concept, the Kopnin-mass exists for superconductors and fermionic superfluids [18–20]. In 2007, Thouless and Anglin [21] studied the reaction of a vortex to an external force by a pinning potential by means of the Gross-Pitaevskii equation [22, 23]. They found that the kinetic vortex mass contains an infinite contribution (confirming Duan and Popov) and that it depends on the form of the pinning potential, from which they concluded that the kinetic vortex mass is ambiguous. Their conclusion was later questioned by Simula [24], who studied the circular motion of a vortex without external forces, and obtained a kinetic vortex mass in line with the core-mass suggested by Baym and Chandler [17] as well as Kopnin [19], again, based on the Gross-Pitaevskii equation.

In the framework of the $O(2)$ model as a quantum field theory in $(2+1)$ dimensions, vortices are topological excitations. In the symmetric phase, the vortices condense and in the broken phase they correspond to topologically charged particles. Also in this context, the mass of the vortex is somewhat controversial: The $(2+1)$-dimensional $O(2)$ model is exactly dual to a lattice gauge theory with integer-valued link variables [25–27]. The latter corresponds to a certain limit of non-compact scalar quantum electrodynamics. This duality was exploited to study properties of vortices in the dual gauge theory, that is related to superconductivity in [28–31]. The vortices and Goldstone bosons in the $O(2)$ model are dual to the charged scalar particles and photons, respectively. Charged particles are so-called infraparticles [32–34] and as such surrounded by a cloud of soft dual photons that extends to infinity. In two spatial dimensions where the Coulomb potential is logarithmic, this photon cloud gives the dual charged particle, and thus the vortex, a mass that diverges logarithmically with the volume. This expectation is contrasted by a relatively recent study [35], where the vortex mass in the $(2+1)$-dimensional $O(2)$ model was found to be finite.

Topological excitations, such as the vortex are often quantized semi-classically [36, 37], but there exists also a rigorous non-perturbative approach in the framework of lattice field theory due to Fröhlich and Marchetti, based on disorder operators [38]. They gave a quite generic construction of the soliton sectors in a broad class of quantum field theories [39] and applied it to a variety of models (e.g., vortices in the abelian Higgs model in $(2+1)$ dimensions [40], monopoles in the $(3+1)$ dimensional $U(1)$ gauge theory [41] and kinks in $(1+1)$-dimensional ϕ^4-theory [42]).

Along these lines, we construct the vortex two-point function for the (2+1)-dimensional $O(2)$ model in a finite volume. Topological reasons forbid the existence of field configurations containing a single vortex in a periodic geometry. To overcome this obstruction, we make use of C-periodic boundary conditions [43, 44]. From the vortex two-point function, we extract the vortex mass. The numerical calculations are carried out in the dual formulation of the theory, i.e., the integer gauge theory. We calculate the mass of the vortex as a function of the fixed physical volume in the continuum limit at the Wilson-Fisher fixed point approached from the broken phase. We confirm that the vortex mass diverges logarithmically with the volume. The strength of the logarithmic divergence that is related to the Coulomb charge of the vortex, represents a new universal quantity associated with the Wilson-Fisher fixed point.

The first part of the present thesis is organized as follows. In Chapter 2, we consider the vortex as a field configuration in the classical $O(2)$ model. The non-perturbative formulation of the vortex two-point function is then reviewed in Chapter 3. In Chapter 4 we discuss the details of the duality that maps the vortex to a dual charged particle before describing the Monte Carlo calculation of the vortex mass in the continuum limit in Chapter 5. Finally, we present our conclusions and a summary in Chapter 6.

Part II of the thesis is again related to the Heisenberg model. Spin models such as the Heisenberg model and generalizations thereof, so-called quantum link models [45–49], also provide an alternative non-perturbative regularization for strongly coupled quantum field theories such as quantum chromodynamics (QCD). While the standard lattice formulation of quantum field theory due to Wilson [50] proves to be highly successful for e.g., hadron spectroscopy [51, 52], sign and complex action problems prohibit its use for the exploration of the non-zero density and real-time physics of QCD [53]. A long-standing proposal for an alternative approach is the use of quantum simulators [54–59], where a quantum system in a laboratory, e.g., ultracold atoms in an optical lattice, is specifically designed to encode the quantum field theory of interest.

The quantum spin or quantum link regularization is extremely well suited for such a quantum simulation experiment. However, many challenges remain to be solved before such experiments can be performed for full QCD [60]. For example, the regularization of QCD in terms of quantum links [48], contains an additional spatial dimension that has to be encoded in the internal degrees of freedom in a quantum simulation experiment.

The $\mathbb{C}P(2)$ model in (1+1) dimensions [61, 62] shares many features with QCD, such as a non-perturbatively generated mass gap, asymptotic freedom and non-trivial topology. At the same time it is much simpler than QCD, and therefore a natural candidate to

explore the challenges that lie on the path towards quantum simulation of QCD. It can be regularized in terms of a $(2+1)$-dimensional ladder of $SU(3)$-symmetric quantum spins [63, 64]. Moreover, it is possible to perform quantum simulation experiments of this regularization with currently available technology [65].

In [66], we have explored the finite density phase diagram of the $\mathbb{C}P(2)$ model at zero temperature to provide a benchmark for possible quantum simulation experiments. We have used the same regularization in terms of $SU(3)$ quantum spins to perform Monte Carlo simulations on a classical computer. The symmetry group $SU(3)$ has rank two, and thus two commuting generators, T^3 and T^8. To each of those a chemical potential, μ_3 and μ_8, can be associated. Figure 1.2 shows a sketch of the zero temperature phase diagram of the $\mathbb{C}P(2)$ model in the μ_3-μ_8 plane. If the chemical potential is large enough to overcome the mass gap, particles are created. They interact repulsively and form a gas that undergoes the Kosterlitz-Thouless phenomenon and condenses. Along the lines that pass through the corners of the vacuum hexagon, a two-component ferromagnetic condensate is formed. This can be understood as follows: While a generic chemical potential breaks the global $SU(3)$ symmetry down to $U(1)_3 \times U(1)_8$, along the line $\mu_3 = 0$, $\mu_8 \neq 0$ for example, the global symmetry is broken down to $SU(2)_{123} \times U(1)_8$.

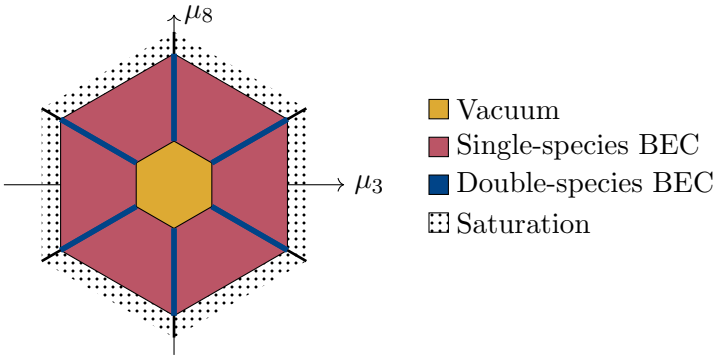

Figure 1.2.: A sketch of the zero temperature phase diagram of the $(1+1)$-dimensional $\mathbb{C}P(2)$ model, according to [66]. If the chemical potential is large enough to overcome the mass gap, particles are created. They interact repulsively and form a gas that undergoes the Kosterlitz-Thouless phenomenon. Only the region close to the vacuum was explored in [66], the extension of the condensate phase all the way to a saturated phase was conjectured.

For very large values of the chemical potentials, the spin ladders saturate, i.e. the spins align with the direction of the chemical potential. In [66] only the region close to the vacuum was explored, the extension of the condensate phase all the way to a saturated phase was conjectured. If interactions between defects in the saturated state are attractive, this would be a strong indication that another phase transition should exist in between.

In this work, we study a chain of $SU(3)$ spins with a large chemical potential μ_3, close to saturation. This system can be treated analytically in closed form. We find

that the defects in the saturated state are completely equivalent to the defects in an antiferromagnetic XXZ quantum spin chain and that they interact repulsively. While this result still needs to be generalized to a $(2+1)$-dimensional ladder to make a definite statement on the phase structure of the $\mathbb{C}P(2)$ model, it is still a strong hint.

Furthermore, this work can be viewed as a simple and pedagogical example for the use of effective theory methods. We show that the low-energy physics of the defects in the saturated state of the considered spin chains can be effectively described in terms of the quantum mechanics of non-relativistic particles with contact interactions in a continuous space.

The second part of the present thesis is organized as follows. In Chapter 7, we diagonalize the Hamiltonian of the XXZ-chain in the one- and two-defect sectors. To do so, we explicitly solve the recursion relation corresponding to the stationary Schrödinger equation. We show in Chapter 8 that the defects in the saturated state of the $SU(3)$ spin chain are equivalent to the defects in a specific anisotropic XXZ spin chain, and therefore, the same methods can be applied there. We then provide a consistent effective description of the low-energy physics of these defects in terms of non-relativistic point particles in Chapter 9. Finally, we summarize the results and conclude in Chapter 10.

Part I.

The Vortex in the $(2+1)$-dimensional $O(2)$ Model

2. The Vortex in the $O(2)$ Symmetric Classical Field Theory

2.1. The $O(2)$ Model as a Classical Field Theory

In this chapter, we consider the $O(2)$ model in two spatial and one temporal dimension as a classical field theory. A simple yet nontrivial classical field theory that is invariant under a global $O(2)$ symmetry is the scalar field theory of a complex scalar field with a quartic interaction — ϕ^4 theory. The Lagrangian density is

$$\mathcal{L} = \frac{1}{2}\partial^\mu \phi^* \partial_\mu \phi - V(\phi)\,, \tag{2.1}$$

with the potential

$$V(\phi) = \frac{\lambda}{4!}\left(|\phi|^2 - v^2\right)^2\,, \tag{2.2}$$

and ϕ, a complex valued scalar field such that,

$$\phi(x) = \phi_1(x) + i\phi_2(x)\,. \tag{2.3}$$

The Lagrangian density is invariant under global $O(2)$ or $U(1)$ field rotations of the form

$$\phi(x)' = \phi(x)\exp(i\varphi)\,, \tag{2.4}$$

and of course under Poincaré transformations and charge conjugation, that is

$${}^C\phi(x) = \phi(x)^*\,. \tag{2.5}$$

In three space-time dimensions (and in units where $c = 1$), the Lagrangian density has the following dimension,

$$[\mathcal{L}] = \frac{\text{energy}}{\text{length}^2}\,. \tag{2.6}$$

From that we can infer the units of the field and the parameters,

$$[\phi] = \text{energy}^{1/2}\,, \qquad [v] = \text{energy}^{1/2}\,, \qquad [\lambda] = \text{energy}^{-1}\text{length}^{-2}\,. \tag{2.7}$$

The dimensionful parameters, v and λ, thus define the characteristic length and energy scales, $\lambda^{-1/2}v^{-1}$ and v^2.

The Hamiltonian density is obtained from the canonically conjugate momenta to ϕ_1

and ϕ_2,

$$\pi_i = \frac{\delta \mathcal{L}}{\delta \partial_t \phi_i} = \partial_t \phi_i \,, \tag{2.8}$$

as

$$\begin{aligned} \mathcal{H} &= \pi_1 \partial_t \phi_1 + \pi_2 \partial_t \phi_2 - \mathcal{L} \\ &= \frac{1}{2} \partial_t \phi^* \partial_t \phi + \frac{1}{2} \partial_i \phi^* \partial_i \phi + V(\phi) \\ &= \frac{1}{2} \pi_i^* \pi_i + \frac{1}{2} \partial_i \phi^* \partial_i \phi + V(\phi) \,. \end{aligned} \tag{2.9}$$

The Euler-Lagrange equations of motion,

$$\frac{\delta \mathcal{L}}{\delta \phi_i} = \partial_\mu \left(\frac{\delta \mathcal{L}}{\delta \partial_\mu \phi} \right) , \tag{2.10}$$

are

$$\partial_\mu \partial^\mu \phi_i = \frac{\partial V(\phi)}{\partial \phi_i} = \frac{\lambda}{6} \left(|\phi|^2 - v^2 \right) \phi_i \,. \tag{2.11}$$

For static solutions, the time derivative vanishes and the equations of motion become

$$\Delta \phi = \frac{\lambda}{6} \left(|\phi|^2 - v^2 \right) \phi \,. \tag{2.12}$$

The lowest energy solution to the equations of motion is the trivial vacuum solution $\phi(x,t) = v$.

2.2. Vortices as Classical Field Configurations

Besides the trivial solution there are other static field configurations that solve the equations of motion. Here we are interested in solutions of the form

$$\phi(r, \varphi) = f(r) \exp(il\varphi) \,. \tag{2.13}$$

Since the argument of ϕ wraps around the unit circle l times while it is traced along a closed loop around the origin, we will refer to these solutions as vortex-like or simply vortex field configurations. If the ansatz of eq. (2.13) is plugged into the equations of motion, an ordinary differential equation for the radial function $f(r)$ is obtained. Making use of the Laplacian in polar coordinates,

$$\Delta = \partial_r^2 + \frac{1}{r} + \frac{1}{r^2} \partial_\varphi^2 \,, \tag{2.14}$$

we obtain

$$\left(\partial_r^2 + \frac{1}{r} \partial_r - \frac{l^2}{r^2} \right) f(r) = -\frac{\lambda}{6} \left(f(r)^2 - v^2 \right) f(r) \,. \tag{2.15}$$

We are not aware of a closed form solution to this nonlinear differential equation and we will be satisfied with a numerical solution and a discussion of the asymptotic behavior. We start with a discussion of the asymptotic form of $f(r)$ around $r = 0$. In order for $\phi(r, \varphi)$ to be continuous, $f(r)$ must vanish at $r = 0$. Using an ansatz of the form,

$$f(r) = \sum_{n=1}^{\infty} a_n r^n \,, \tag{2.16}$$

the differential eq. (2.15) turns into a recursion relation for the a_i, namely,

$$\begin{aligned} a_1(1 - l^2) &= 0 \,, \\ \frac{6}{\lambda}\left((n+2)^2 - l^2\right) a_{n+2} + v^2 a_n &= \sum_{i=1}^{n} \sum_{j=1}^{i} a_j a_{i-j} a_{n-i} \,. \end{aligned} \tag{2.17}$$

For the first few values of n, the recursion evaluates to

$$\begin{aligned} a_1(1 - l^2) &= 0 \,, \\ a_2\left(4 - l^2\right) &= 0 \,, \\ a_3\left(9 - l^2\right) &= -v^2 a_1 \,, \\ a_4\left(16 - l^2\right) &= \frac{a_1^3 \lambda}{6} - a_2 v^2 \,, \\ a_5\left(25 - l^2\right) &= \frac{1}{6}\left(a_2 a_1^2 + 2 a_2^2 a_1\right)\lambda - a_3 v^2 \,. \end{aligned} \tag{2.18}$$

Thus the power series expansion of $f(r)$, eq. (2.16), starts at $n = l$, and the first two terms are

$$\begin{aligned} l = 1 : &\qquad f(r) = ar - \frac{av^2}{8} r^3 + O(r^4) \,, \\ l = 2 : &\qquad f(r) = ar^2 - \frac{av^2}{12} r^4 + O(r^6) \,, \\ l = 3 : &\qquad f(r) = ar^3 - \frac{av^2}{16} r^5 + O(r^7) \,, \end{aligned} \tag{2.19}$$

with $a = a_l$ unconstrained. For large values of r, we expect $f(r)$ to approach v, and make the ansatz

$$f(r) = v - \frac{c}{r^\alpha} \,. \tag{2.20}$$

We plug it into the equation of motion, eq.(2.15), and obtain

$$-\frac{c\alpha(\alpha+1)}{r^{\alpha+2}}+\frac{c\alpha}{r^{\alpha+2}}-\frac{l^2v}{r^2}+\frac{cl^2}{r^{\alpha+2}}=\frac{\lambda v}{6}\left(-\frac{2cv}{r^\alpha}+\frac{c^2}{r^{2\alpha}}\right)+\frac{\lambda}{6}\frac{2c^2v}{r^{2\alpha}}$$
$$\frac{cl^2-c\alpha^2}{r^{\alpha+2}}-\frac{l^2v}{r^2}=\frac{\lambda vc^2}{2r^{2\alpha}}-\frac{\lambda v^2c}{3r^\alpha} \tag{2.21}$$

This implies that $\alpha = 2$. From the terms proportional to r^{-2}, we can then read off

$$c=\frac{3l^2}{v\lambda}\,. \tag{2.22}$$

In order for this to be consistent for the terms of the order of r^{-4}, a term c_2r^{-4} has to be added to the ansatz. Then $-v^2\lambda/6f(r)$ gives rise to another term proportional to r^{-4}, and with a suitable choice of c_2, the differential equation can be solved to the order r^{-4}.

Eq. (2.15) can also be solved numerically as a boundary value problem with the boundary conditions $f(0) = 0$ and $f(R) = v - 3l^2/v\lambda R^2$. To do so we solve the equation with the help of `solve_bvp` from the SciPy library [67] in units, where $\lambda = 1$ and $v = 1$ and therefore also the field is dimensionless. The result is shown in Figure 2.1 for $l = 1, 2, 3$. To impose the asymptotic boundary condition, we have chosen a value of $R = 80/v\sqrt{\lambda}$ which is well in the asymptotic regime. Two-dimensional visualizations of the vortex field configurations are shown in Figure 2.2.

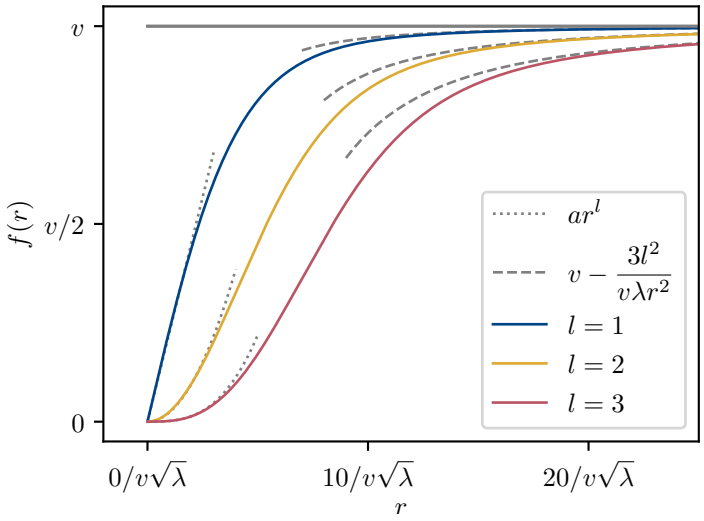

Figure 2.1.: The radial profile $f(r)$ for field configurations of the form $\phi(r,\varphi) = f(r)\exp(il\varphi)$ with vortex number $l = 1, 2, 3$. The dashed grey lines show the asymptotic approach to v for $r \to \infty$, and the dotted lines the behavior around $r = 0$ with the prefactor a fitted to the numerical solution.

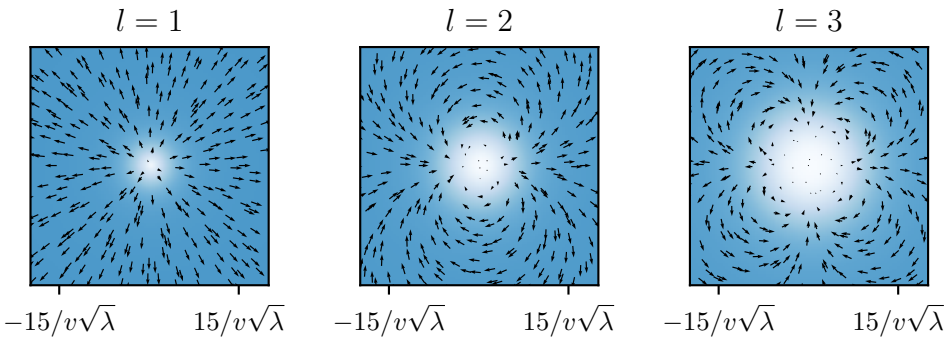

Figure 2.2.: The vortex field configuration $\phi(r, \varphi) = f(r) \exp(il\varphi)$. The background color indicates the absolute value $|\phi(r, \varphi)|$ from 0 (white) to v (light blue). The arrows' vertical and horizontal component correspond to the real and imaginary part of ϕ, respectively. The polar angle is zero along the positive y axis and increases clockwise. The arrows are drawn on random positions in order for the otherwise appearing grid pattern not to distract the eye.

2.3. The Vortex in a Finite Volume

In the following, we discuss the vortex inside a finite box. That is, static field configurations, $\phi(x)$, which obey the equations of motion and for which the field is confined to a box of size $L \times L$, as

$$x_i \in [-L/2, L/2] \ . \tag{2.23}$$

In order to do so, boundary conditions have to be imposed. Periodic boundary conditions are often used since they preserve translation invariance and thus the momentum structure of the theory. However, a vortex solution similar to the solutions considered previously cannot exist in that geometry for topological reasons: For a continuous periodic field configuration, the integral of the complex phase around the boundary of the finite box is always zero since the contributions from opposite boundaries cancel each other. For a field configuration that contains a single vortex, it should be 2π. A natural candidate to cure this problem and still preserve translation invariance are C-periodic boundary conditions [43, 44].

As we will see, purely C-periodic boundary conditions do not support continuous vortex solutions with a form akin to the infinite volume configurations that we have discussed in Section 2.2. Instead we will make a more general ansatz for the boundary conditions that includes twists at the spatial boundaries. After discussing how these boundary conditions affect the symmetries of the model, we will constrain them by demanding that a vortex configuration similar to the infinite volume vortex solution is continuous at the boundaries.

Twisted C-periodic boundary conditions have the following form,

$$\begin{aligned}\phi(x+e_1L) &= \phi(x)^* \exp(ib_1)\\ \phi(x+e_2L) &= \phi(x)^* \exp(ib_2)\,.\end{aligned} \tag{2.24}$$

The twists, b_1 and b_2, are constrained by a cocycle condition,

$$\begin{aligned}\phi(x+e_1L+e_2L) &= \phi(x+e_1)^* \exp(ib_2) = \phi(x)\exp(i(b_1-b_2))\\ &= \phi(x+e_2)^* \exp(ib_1) = \phi(x)\exp(i(b_2-b_1))\,,\end{aligned} \tag{2.25}$$

in order to be consistent. It follows that

$$b_1 - b_2 = b_2 - b_1 \mod 2\pi \tag{2.26}$$

and therefore

$$b_1 - b_2 \mod 2\pi \in \{0,\pi\}\ . \tag{2.27}$$

These boundary conditions clearly break rotation invariance to 90 degrees rotation invariance. Also the internal $O(2)$ symmetry,

$$\begin{aligned}\phi(x)' &= \phi(x)\exp(i\gamma)\,,\\ \phi(x)' &= \phi(x)^*\,,\end{aligned} \tag{2.28}$$

is affected. While the potential term of the Lagrangian density is still invariant under the full $O(2)$ symmetry, the term $\partial_\mu\phi\partial^\mu\phi^*$ is not. Consider e.g.,

$$\begin{aligned}\partial_1\phi(e_1L)\partial_1\phi(e_1L)^* &= \lim_{\epsilon\to 0}\frac{1}{\epsilon^2}|\phi(e_1(L+\epsilon)) - \phi(e_1L)|^2\\ &= \lim_{\epsilon\to 0}\frac{1}{\epsilon^2}|\phi(e_1\epsilon)^*\exp(ib_1) - \phi(e_1L)|^2\,.\end{aligned} \tag{2.29}$$

Under a global transformation $\phi(x)' = \phi(x)\exp(i\gamma)$, this expression transforms into

$$\partial_1\phi(e_1L)'\partial_1\phi(e_1L)'^* = \lim_{\epsilon\to 0}\frac{1}{\epsilon^2}|\phi(e_1\epsilon)^*\exp(ib_1)\exp(-i\gamma) - \phi(e_1L)\exp(i\gamma)|^2\,. \tag{2.30}$$

It is only invariant for $\gamma \in \{0,\pi\}$. The same is true for an equivalent term at the other boundary. The transformation ${}^C\phi = \phi^*$, charge conjugation, is also no longer a symmetry. To see this, we consider the transformation $\phi'(x) = \phi^*(x)\exp(i\gamma)$,

$$\partial_1\phi'(e_1L)\partial_1\phi'^*(e_1L) = \lim_{\epsilon\to 0}\frac{1}{\epsilon^2}|\phi(e_1\epsilon)\exp(ib_1)\exp(-i\gamma) - \phi(e_1L)^*\exp(i\gamma)|^2\,, \tag{2.31}$$

which only is an invariance if $\gamma = b_1 + m\pi$ for an integer m. At the other boundary we find $\gamma = b_2 + m\pi$. This is consistent if the cocycle condition $b_1 - b_2 = m\pi$ is taken into account. Thus, the twisted C-periodic boundary conditions explicitly break the global

$O(2)$ symmetry down to $\mathbb{Z}_2 \times \mathbb{Z}_2$ given by

$$\begin{aligned} R\phi(x) &= -\phi(x) \\ \widetilde{C}\phi(x) &= \phi(x)^* \exp(ib_1)\,. \end{aligned} \tag{2.32}$$

Note that the twisted C-periodic boundary conditions can be expressed in terms of theses symmetry operations as

$$\begin{aligned} \phi(x + e_1 L) &= \widetilde{C}\phi(x) \\ \phi(x + e_2 L) &= R^m C\phi(x) \\ \phi(x + e_2 L + e_1 L) &= R^m \phi(x)\,, \end{aligned} \tag{2.33}$$

with $m = (b_1 - b_2)\pi$.

We will now discuss for which values of b_1 and b_2 continuous vortex solutions are naturally supported by the boundary conditions. In polar coordinates, a general field configuration can be written as

$$\phi_l(r, \varphi) = f(r, \varphi) \exp(il\theta(r, \varphi) + i\beta)\,. \tag{2.34}$$

In the infinite volume, the vortex field configurations have the following symmetries,

$$\begin{aligned} \phi(r, \varphi) &= \phi(r, \varphi - \delta) \exp(+il\delta) \\ \phi(r, \varphi) &= \phi(r, -\varphi)^*\,. \end{aligned} \tag{2.35}$$

They combine spatial rotation and reflection with the internal $O(2)$ symmetry. In a finite box, the spatial rotation symmetry can only be assumed to hold for $\delta = n\pi/2$ with $n \in \mathbb{Z}$. Imposing these symmetries on the general form of eq. (2.34) yields the following constraints,

$$\begin{aligned} f(r, \varphi) &= f\left(r, \varphi + n\frac{\pi}{2}\right)\,, & f(r, \varphi) &= f\left(r, -\varphi\right)\,, \\ \theta(r, \varphi) &= \theta\left(r, \varphi + n\frac{\pi}{2}\right) - \frac{n\pi}{2}\,, & \theta(r, \varphi) &= -\theta\left(r, -\varphi\right)\,. \end{aligned} \tag{2.36}$$

If furthermore

$$\int_0^{2\pi} \theta(r, \varphi) d\varphi = 2\pi\,, \tag{2.37}$$

the field configuration $\phi_l(r, \varphi)$ is indeed an l-fold vortex. This condition is however not necessary for the following discussion. We now consider a point on the boundary normal to the e_1 direction, p_1, as illustrated in Figure 2.3. The field configuration $\phi_l(r, \phi)$ is

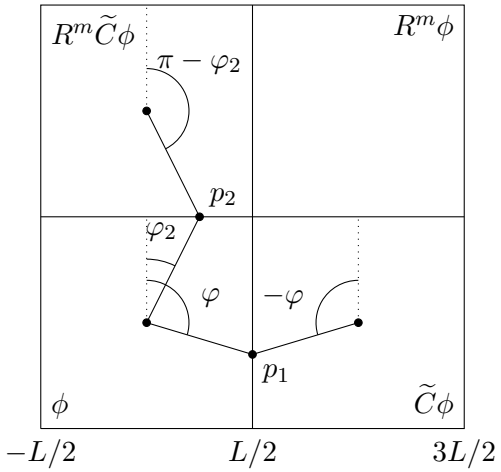

Figure 2.3.: A schematic drawing of the twisted C-periodic geometry. Demanding continuity for ϕ at the generic points p_1 and p_2 constrains the twists at the boundaries that support vortex field configurations.

continuous at p_1, if the field value agrees with its twisted C-periodic copy,

$$\begin{aligned} \phi_l(r,\varphi) &= \phi_l(r,-\varphi)^* \exp(ib_1)\,, \\ f(r,\varphi)\exp(il\theta(r,\varphi)+i\beta) &= f(r,-\varphi)\exp(-il\theta(r,-\varphi)-i\beta+ib_1) \\ &= f(r,\varphi)\exp(il\theta(r,\varphi)-i\beta+ib_1)\,. \end{aligned} \tag{2.38}$$

It follows that

$$\beta = b_1 - \beta \mod 2\pi\,. \tag{2.39}$$

A similar equation arises from considering a point p_2 on the other boundary (confer Figure 2.3). The field configuration is continuous if

$$\begin{aligned} \phi_l(r,\varphi) &= \phi_l(r,\pi-\varphi)^* \exp(ib_2)\,, \\ f(r,\varphi)\exp(il\theta(r,\varphi)+i\beta) &= f(r,\pi-\varphi)\exp(-il\theta(r,\pi-\varphi)-i\beta+ib_2) \\ &= f(r,\varphi)\exp(il\theta(r,\varphi)-il\pi-i\beta+ib_2)\,. \end{aligned} \tag{2.40}$$

This implies that

$$\beta = -l\pi - \beta + b_2 \mod 2\pi\,. \tag{2.41}$$

From eqs. (2.39) and (2.41) we deduce that

$$b_1 - b_2 = l\pi \mod 2\pi\,. \tag{2.42}$$

That is, for a vortex configuration with $l = 1$ to naturally fit into the C-periodic geometry, twists that differ by an odd multiple of π have to be imposed on the two boundaries. Specifically, pure C-periodic boundary conditions do not support such a field configu-

ration. They do support a two-fold vortex field configuration with $l = 2$, however. In summary, a twisted C-periodic box with twists b_1 and b_2, naturally supports vortex field configurations with the phase dependence on the polar angle, $\exp(il\theta(\varphi, r) + i\beta)$ with

$$l = \frac{\pm(b_1 - b_2)}{\pi} + 2n\,, \qquad \beta = \frac{b_1}{2} + k\pi\,, \tag{2.43}$$

for $n, k \in \mathbb{Z}$. This amounts to a total of four distinct field configurations for given $|l|$ and $\theta(r, \varphi)$, as well as $f(r, \varphi)$. They can be labeled as $\phi_{l\pm\pm}(r, \varphi)$ with the first $\pm$ referring to the sign of l and the second to whether k is even $(+)$ or odd $(-)$. These configurations are related by R and $\widetilde{C}$ as

$$\widetilde{C}\phi_{l\pm\pm} = \phi_{l\mp\pm}\,, \qquad R\phi_{l\pm\pm} = \phi_{l\pm\mp}\,. \tag{2.44}$$

2.4. Numerical Solutions in the Finite Volume

Here we discuss numerical solutions of the equations of motion (2.10), subject to the boundary conditions discussed in the previous section. After a qualitative discussion of these vortex-like solutions, we will also look at the scaling of their energy with the size of the C-periodic box.

To solve the equations of motion numerically, we discretize the system on an $N \times N$ lattice Λ and minimize the lattice energy,

$$\begin{aligned} E &= a^2 \sum_{x\in\Lambda} H(x) \\ &= v^2 \sum_{x\in\Lambda} \left(\sum_{i=1}^{2} \frac{1}{2} |\tilde{\phi}(x + e_i) - \tilde{\phi}(x)| + \lambda a^2 \left(|\tilde{\phi}(x)|^2 - 1 \right)^2 \right) . \end{aligned} \tag{2.45}$$

Here, a denotes the lattice spacing and the fields are rescaled to be dimensionless as

$$\tilde{\phi}(x)v = \phi(x)\,. \tag{2.46}$$

Furthermore, we impose the 90 degrees rotation invariance, described in eq. (2.35), explicitly by considering only the quadrant $0 \le x_1 < L/2$, $0 < x_2 < L/2$ of the lattice, and continue the field to the other quadrants according to

$$\widetilde{\phi}(r, \varphi + n\pi/2) = \widetilde{\phi}(r, \varphi) \exp(iln\pi/2)\,, \tag{2.47}$$

for $n \in \{1, 2, 3\}$. In addition, we choose $\widetilde{\phi}(0, 0) = 0$. The minimization is performed with a cooling algorithm: In a sweep through the lattice, at each site the field $\widetilde{\phi}(x)$ is set to the value that minimizes its contribution to the total energy,

$$\widetilde{H}(x) = H(x) + \sum_{i=1}^{2} H(x + e_i) + H(x - e_i)\,. \tag{2.48}$$

This field value corresponds to one of the three solutions to

$$\partial_{\phi_1(x)}\widetilde{H}(x) = 0\,, \qquad\qquad \partial_{\phi_2(x)}\widetilde{H}(x) = 0\,.$$

They can be obtained in closed form as

$$\begin{aligned}
\widetilde{\phi}_1 &= -\frac{i\left(\sqrt[3]{2}\alpha^{2/3} + 2\sqrt[3]{3}a^2\lambda\left(a^2\lambda - 24\right)c_r^2\left(c_i^2 + c_r^2\right)\right)}{6^{2/3}a^2\sqrt[3]{\alpha}\lambda c_r\left(c_i + ic_r\right)}\,,\\
\widetilde{\phi}_2 &= \frac{2^{2/3}\sqrt[3]{3}\left(\sqrt{3}+i\right)\alpha^{2/3} + 2i\sqrt[3]{2}\sqrt[6]{3}\left(\sqrt{3}+3i\right)a^2\lambda\left(a^2\lambda-24\right)c_r^2\left(c_i^2+c_r^2\right)}{12a^2\sqrt[3]{\alpha}\lambda c_r\left(c_i+ic_r\right)}\,,\\
\widetilde{\phi}_3 &= \frac{2\sqrt[3]{2}\sqrt[6]{3}\left(3+i\sqrt{3}\right)a^2\lambda\left(a^2\lambda-24\right)c_r^2\left(c_i^2+c_r^2\right) - 2^{2/3}\sqrt[3]{3}\left(\sqrt{3}-i\right)\alpha^{2/3}}{12a^2\sqrt[3]{\alpha}\lambda c_r\left(c_i+ic_r\right)}\,,
\end{aligned} \tag{2.49}$$

where

$$\begin{aligned}
c_r &= 2\,\mathrm{Re}\left(\sum_{i=1}^{2}\widetilde{\phi}(x+e_i) + \widetilde{\phi}(x-e_i)\right)\,,\\
c_i &= 2\,\mathrm{Im}\left(\sum_{i=1}^{2}\widetilde{\phi}(x+e_i) + \widetilde{\phi}(x-e_i)\right)\,,
\end{aligned} \tag{2.50}$$

and

$$\begin{aligned}
\alpha = \sqrt{3}\sqrt{-a^6c_r^6\lambda^3\left(c_i^2+c_r^2\right)^3\left(4a^6\lambda^3 - 288a^4\lambda^2 - 27a^2\lambda\left(9c_i^2+9c_r^2-256\right) - 55296\right)}\\
- 27a^4c_r^3\lambda^2\left(c_i^2+c_r^2\right)^2\,.
\end{aligned} \tag{2.51}$$

At each step, $\widetilde{\phi}_1$, $\widetilde{\phi}_2$ and $\widetilde{\phi}_3$ are evaluated, and $\widetilde{\phi}$ is then set to the one that minimizes $\widetilde{H}(x)$. The cooling is stopped if in ten consecutive sweeps, the total energy changes by less than $10^{-8}v^2$. In smaller systems, where the cooling can be continued to machine precision in a reasonable time, we have observed that this stopping criterion yields energy values that differ from the machine precision result by roughly 10^{-6}. As an initial guess, we take the infinite volume vortex field configuration,

$$\widetilde{\phi}_0(r,\varphi) = \exp\left(il\varphi\right)\,, \tag{2.52}$$

for $r > 0$. If instead a random initial configuration is used, the algorithm takes significantly more time to stop, but eventually converges to the same vortex like field configuration as with the educated initial guess.

Before discussing the scaling of the energy we will take a qualitative look at the numerical solutions in order to confirm the conclusions of Section 2.3. Figure 2.4 shows the numerical solution to the equations of motion for various twisted C-periodic geometries. In addition to the actual box in the lower left corner, the continuation into three adjacent boxes according to the boundary conditions is shown. A further continuation

then simply corresponds to a periodic repetition of the four displayed boxes. The boundaries are marked by white lines. In the top two rows, the difference between the twists is $b_1 - b_2 = \pi$ and, as expected, single vortex solutions are supported. The value b_1 determines the overall orientation of the vortex, and can indeed be identified with 2β. Furthermore, for each value of b_1, the four types of vortices, $\phi_{\pm\pm}$, appear in the four adjacent boxes. In the bottom row, $b_1 - b_2 = 0$ and only two-fold vortices are supported. Here no reflection R is applied at either of the boundaries and only two types of two-fold vortices appear in the four adjacent boxes. The case of $b_1 = b_2 = 0$ (bottom left) corresponds to C-periodic boundary conditions without a twist. It seems difficult to construct numerical solutions for larger values of l because the boundary conditions do still allow the solutions with $l = 1$ or $l = 2$ and the algorithm converges to those even with initial conditions $\exp(il\varphi)$ with $l > 2$. The phase pattern, $\theta(r, \varphi)$ in Section 2.3, is very similar to the one of the infinite volume solutions (confer Figure 2.2).

Let us now turn to the scaling of the energy of the single vortex field configuration, $l = 1$, with the box size L. We use system extents $L \in \{10a_0, 15a_0, 20a_0, 25a_0, 30a_0\}$ and lattice spacings $a \in \{a_0, a_0/2, a_0/4, a_0/5, a_0/6\}$. In addition, we set $\lambda a_0^2 = 10$. With this choice of parameters, the vortex core is significantly smaller than the box and at the same time still reasonably resolved in the discretized field. For the smallest box this corresponds to $L \approx 32/v\sqrt{\lambda}$ and for the largest box to $L \approx 95v\sqrt{\lambda}$. This is several times the vortex core size in the infinite volume, if we estimate it crudely as $10/v\sqrt{\lambda}$ from Figure 2.1.

At a given physical system size, the energy dependence on the lattice spacing is well described by $E(a) = \alpha a^2 + \beta a + E(0)$. The linear term is necessary to describe the dependence on the lattice spacing a satisfactorily. An example is shown in Figure 2.5. Since the quantities $E(a)$ do not come with a statistical error, it is not straightforward to assess the quality of the fits. We do so according to the following ad hoc scheme. If a relative error of 10^{-5} is assumed on $E(a)$, the chi square per degree of freedom is of order 1. This relative error is comparable to the expected accuracy of the energy values. On the other hand, if the linear term is left out of the fit, the artificial relative error has to be increased to 10^{-3} in order to get a chi square per degree of freedom that is of the order of one.

Figure 2.6 shows the dependence of $E(0)$ on L and a fit of the form $b\log(L/a_0) + c$. The best fit estimate of the prefactor of the log is $b = 3.139$. To give an order of magnitude estimate, of the systematic uncertainty of this number, we compare it to the result obtained from a fit to $E(1/6a_0)$. There we find $b(1/6a_0) = 3.155$. Taking $|(b - b(1/6a_0))/2|$ as a rough estimate for the systematic error, we find

$$b = 3.139(8) \tag{2.53}$$

as a final estimate for the prefactor of the log, which is well compatible with the infinite volume value of $b = \pi$. We recover not only the logarithmic scaling of the large volume energy but also find a prefactor consistent with the rotation invariant large volume result.

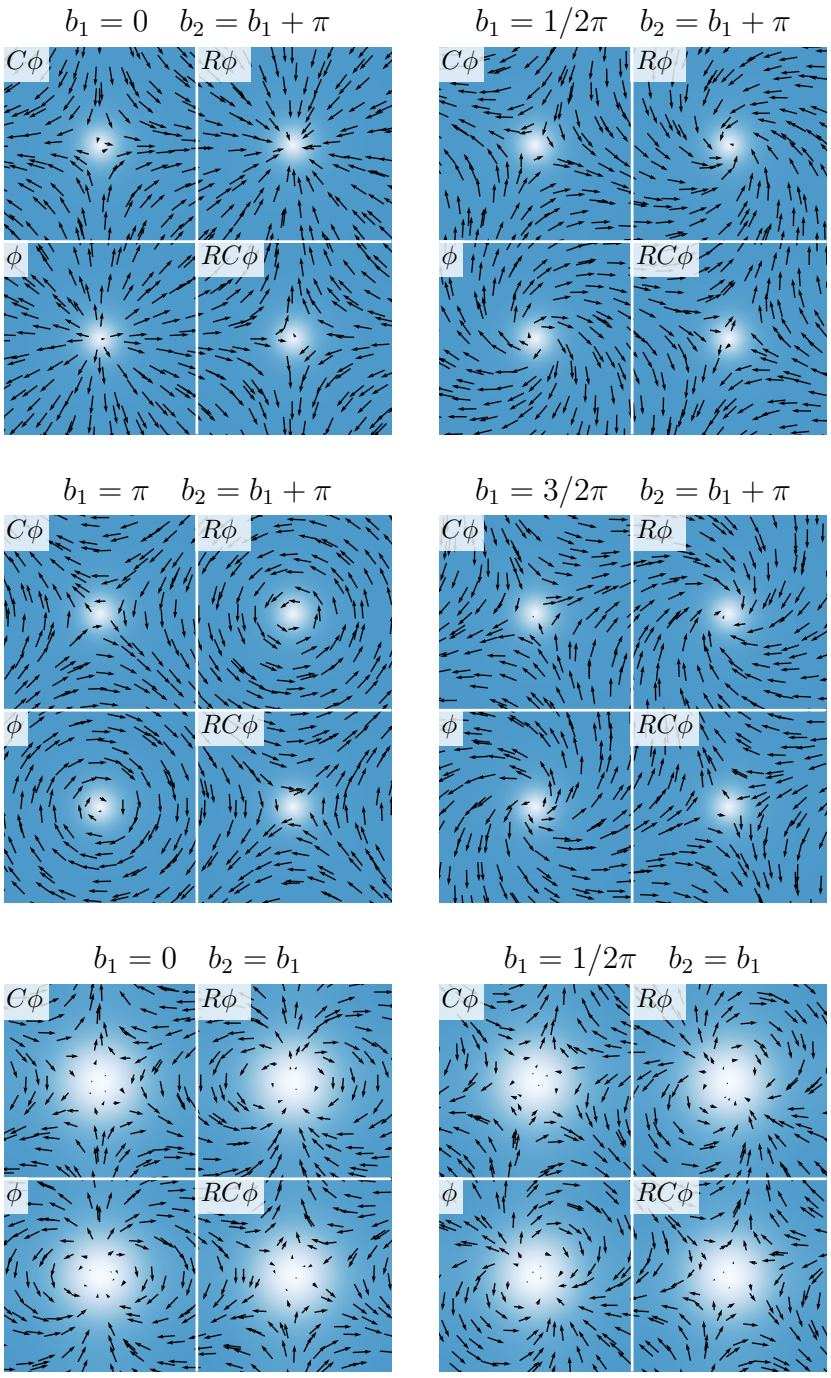

Figure 2.4.: Vortex field configurations in various twisted C-periodic geometries. The background indicates the absolute value of $\phi(x)$ and the vertical and horizontal component of the arrows correspond to the real and imaginary part of ϕ. The size of the box is $L \approx 31.6/v\sqrt{\lambda}$. For $b_2 - b_1 = \pi$, as in the top two rows, the resulting configuration is a single vortex ($l = 1$) and for $b_2 = b_1$ (bottom rows) it is a two-fold vortex, i.e., $l = 2$.

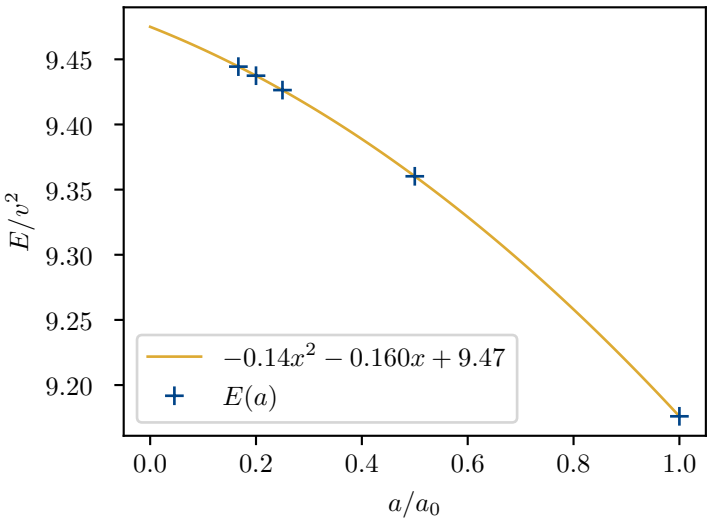

Figure 2.5.: The continuum limit of the vortex energy at $L = 10a_0$.

2.5. Vortices and Charged Particles

In this section, we look at a classical Coulomb point charge in a two-dimensional C-periodic geometry and show that it exhibits a logarithmic divergence of the energy with the box size. This allows us to relate the prefactor of the logarithmic divergence to the charge of the vortex.

In two spatial dimensions, the Coulomb potential generated by a point particle with charge e is logarithmic,

$$V(r) = -\frac{e}{4\pi} \log\left(\frac{r}{r_0}\right) , \tag{2.54}$$

where r_0 is an integration constant and we have used units where $\epsilon_0 = 1$. A particle of charge e in a box of size L with C-periodic boundary conditions can equivalently be described as an infinite checkerboard, where the black and white squares correspond to periodic and C-periodic copies of the original box. That is, a particle with charge e sitting in the center of each black square, and a particle with charge $-e$ in the centers of all white squares. The energy of a particle in a C-periodic box corresponds to the energy per particle in the (infinite) checkerboard system. This can be calculated as the energy of a point charge in the Coulomb potential exhibited by all its infinite periodic and C-periodic copies. A part of an infinite checkerboard is visualized in Figure 2.7. The squares of size $L \times L$ are labeled with $n_x \in \mathbb{Z}$ and $n_y \in \mathbb{Z}$, such that the coordinates of the point particles correspond to $L(n_x, n_y)$. The energy of the particle at $(0, 0)$ in the

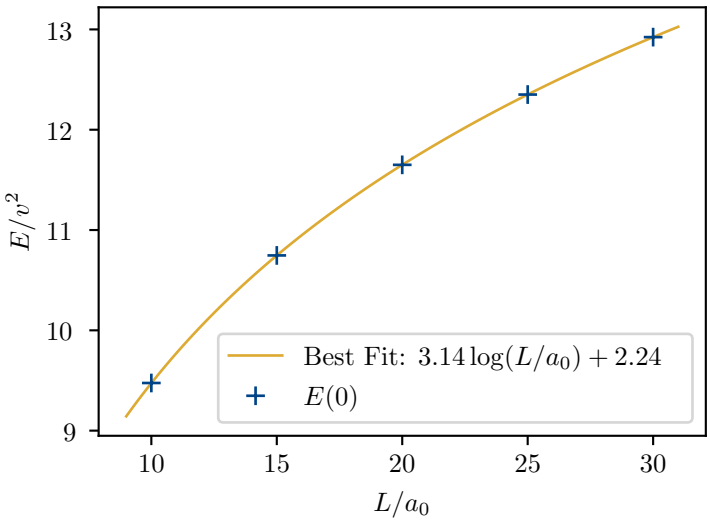

Figure 2.6.: The logarithmic scaling of the vortex energy with the system extent L.

Coulomb potential generated by its copies is

$$E = -\frac{e^2}{4\pi} \sum_{n_x, n_y \neq (0,0)} (-1)^{n_x+n_y} \log\left(\frac{L\sqrt{n_x^2+n_y^2}}{r_0}\right) . \tag{2.55}$$

In order for this sum to be well-defined, it has to be set up as a limit, where it is important to consider only systems with an even number of boxes such that the overall charge vanishes,

$$E = -\lim_{N\to\infty} \frac{e^2}{4\pi} \sum_{n_x=-N+1}^{N} \sum_{\substack{n_y=-N+1 \\ (n_x,n_y)\neq(0,0)}}^{N} (-1)^{n_x+n_y} \log\left(\frac{L\sqrt{n_x^2+n_y^2}}{r_0}\right) . \tag{2.56}$$

To infer the scaling with the box size L, we separate the logs as

$$E = -\lim_{N\to\infty} \frac{e^2}{4\pi} \sum_{n_x=-N+1}^{N} \sum_{\substack{n_y=-N+1 \\ (n_x,n_y)\neq(0,0)}}^{N} (-1)^{n_x+n_y} \left(\log\left(\frac{L}{r_0}\right) - \log\left(\sqrt{n_x^2+n_y^2}\right)\right) . \tag{2.57}$$

Since the point $n_x = n_y = 0$ is left out in the sum, there is one more contribution of $+\log(L/r_0)$ than there is of $-\log(L/r_0)$, independent of N, and the energy is simply

$$E = \frac{e^2}{4\pi} \log\left(\frac{L}{r_0 N_0}\right) , \tag{2.58}$$

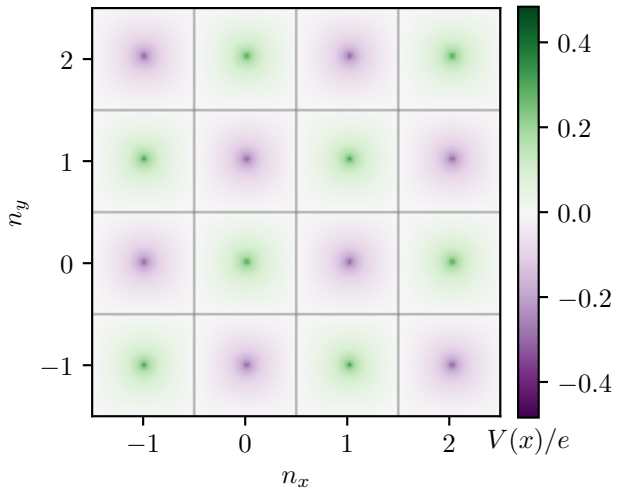

Figure 2.7.: The Coulomb potential in a part of the infinite checkerboard array equivalent to a charged particle in a C-periodic box. The potential has been calculated numerically according to eq.qeq:coulombenergy. The sums were truncated at $|n_i| = 20$.

with

$$\log(N_0) = -\lim_{N\to\infty} \frac{e^2}{4\pi} \sum_{n_x=-N+1}^{N} \sum_{\substack{n_y=-N+1 \\ (n_x,n_y)\neq(0,0)}}^{N} (-1)^{n_x+n_y} \log\left(\sqrt{n_x^2+n_y^2}\right) . \tag{2.59}$$

The exact value of N_0 is not so interesting, however, it is important that it converges. Although not a proof [68], in order to justify this, we will be satisfied with a numerical calculation of N_0 at $N = 10$, $N = 100$ and $N = 1000$. We find that

$$\begin{aligned} N = 10 : &\qquad N_0 = 0.5400271938\,, \\ N = 100 : &\qquad N_0 = 0.5393593431\,, \\ N = 1000 : &\qquad N_0 = 0.5393526686\,. \end{aligned} \tag{2.60}$$

The identification of the vortex as a charged Coulomb particle will become clear in Chapter 4. Granted this equivalence, we conclude that the Coulomb charge of the vortex in the classical $2+1$-d $O(2)$ model is

$$e = 2\pi v\,. \tag{2.61}$$

3. The Vortex in the $O(2)$ Symmetric Quantum Field Theory

3.1. The $O(2)$ Model as a Quantum Field Theory on the Lattice

In the context of lattice quantum field theory, the mass of a particle can be obtained from Euclideantime two-point functions,

$$\langle O_1(0)O_2(t)\rangle = \sum_n \langle 0|\hat{O}_1|n\rangle \, \langle n|\hat{O}_2|n\rangle \exp(-E_n t)\,. \tag{3.1}$$

If $\hat{O}_1$ and $\hat{O}_2$ are chosen such that they create and annihilate the particle of interest respectively, the t-dependence of the two-point function at large t is dominated by an exponential decay with the inverse mass of that particle as decay length at large t. In order to calculate this two-point function as a path integral, we regularize the $(2+1)$-dimensional $O(2)$ model on a Euclidean space-time lattice, and represent the $O(2)$ symmetric scalar field by an angle φ_{c_0} attached to each lattice site c_0. We make use of the formalism of differential forms on the lattice, which is briefly reviewed in appendix A. The Euclidean time path integral then reads

$$\langle O_1(0)O_2(t)\rangle = \frac{1}{Z}\prod_{c_0}\int_{-\pi}^{\pi} d\varphi_{c_0}\frac{1}{2\pi}\exp(-S[\varphi])O_1[\phi(\cdot,0)]O_2[\phi(\cdot,t)]\,. \tag{3.2}$$

The operator insertions, $O_1[\phi(\cdot,0)]$ and $O_2[\phi(\cdot,t)]$, are functionals of the field configurations in the Euclidean time slices at 0 and t. This is indicated by the dot in the spatial argument of ϕ. The normalization constant Z, the partition function, corresponds to the above path integral without operator insertions. In the context of statistical mechanics, this model is usually referred to as the XY-model, originally proposed to describe the λ transition in liquid helium [69, 70]. The standard action is

$$S[\varphi] = \sum_{c_1}\frac{-1}{g^2}\cos\left(d\varphi_{c_1}\right)\,. \tag{3.3}$$

Another choice for the action, that is very convenient to do calculations with, and that we will therefore mostly adopt in the next sections, is the Villain action [71],

$$\exp(-S[\varphi]) = \prod_{c_1} \sum_{n_{c_1}\in\mathbb{Z}} \exp\left(-\frac{1}{2g^2}\left\|d\varphi - 2\pi n\right\|^2\right) . \tag{3.4}$$

Both actions are, of course, invariant under global $O(2)$ symmetry transformations of the form $\varphi'_{c_0} = \varphi_{c_0} + \alpha$.

To calculate the vortex mass, it remains to find a suitable operator, Φ, that creates or annihilates a vortex. Following Banks [25], the $O(2)$ model in three space-time dimensions can be rewritten as a Coulomb gas of closed vortex world lines. This construction is reviewed in Section 3.2. The vortex correlation function can then be found by inserting an additional open vortex world line [39]. We will discuss this in Section 3.3. The whole construction is analogous to the one given in [72] for magnetic monopoles in scalar QED in four space-time dimensions and we will follow the derivation there quite closely.

3.2. The $O(2)$ Model as a Gas of Vortex World Lines

We start with the partition function of the $(2+1)$-dimensional $O(2)$ model with the Villain action,

$$Z = \prod_{c_0} \int_{-\pi}^{\pi} d\varphi_{c_0} \prod_{c_1} \sum_{n_{c_1}\in\mathbb{Z}} \exp\left(-\frac{1}{2g^2}\left\|d\varphi + 2\pi n\right\|^2\right) . \tag{3.5}$$

Here, n is a 1-form that associates an integer to each link, and can be hodge-decomposed into

$$n = d\Delta^{-1}\delta n + \delta\Delta^{-1} dn\,. \tag{3.6}$$

Introducing $m = dn$ and $l = \Delta^{-1}\delta n$, the sum over n can be replaced by sums over m and l.

$$Z = \prod_{c_0} \int_{-\pi}^{\pi} d\varphi_{c_0} \sum_{l_{c_0}\in\mathbb{Z}} \prod_{c_2} \sum_{\substack{m_{c_2}\in\mathbb{Z} \\ dm=0}} \exp\left(-\frac{1}{2g^2}\left\|d\varphi + 2\pi d\, l + 2\pi\delta\Delta^{-1} m\right\|^2\right) \tag{3.7}$$

In order not to enlarge the configuration space, the 2-form m, is subject to the constraint $dm = 0$. An equivalent constraint, $\delta l = 0$, would have to be imposed on l, but is trivially fulfilled since l is a 0-form. A non-compact field, $A = (\varphi + 2\pi dl)$, can now be introduced and the partition function reads

$$Z = \prod_{c_2} \sum_{\substack{m_{c_2}\in\mathbb{Z} \\ dm=0}} \prod_{c_0} \int_{-\pi}^{\pi} dA_{c_1} \exp\left(-\frac{1}{2g^2}\left\|dA + 2\pi\delta\Delta^{-1} m\right\|^2\right) . \tag{3.8}$$

The newly introduced field, A, decouples from m since

$$\begin{aligned}\left\|dA + 2\pi\delta\Delta^{-1}m\right\|^2 &= (dA + 2\pi\delta\Delta^{-1}m, dA + 2\pi\delta\Delta^{-1}m) \\ &= \|dA\|^2 + 4\pi(dA, \delta\Delta^{-1}m) + \left\|2\pi\delta\Delta^{-1}m\right\|^2 \\ &= \|dA\|^2 + 4\pi(A, \delta^2\Delta^{-1}m) + \left\|2\pi\delta\Delta^{-1}m\right\|^2 \\ &= \|dA\|^2 + \left\|2\pi\delta\Delta^{-1}m\right\|^2 . \end{aligned} \tag{3.9}$$

In the second last step we have used partial integration. Furthermore, again making use of partial integration, one finds that

$$\left\|\delta\Delta^{-1}m\right\|^2 = (\delta\Delta^{-1}m, \delta\Delta^{-1}m) = (d\delta\Delta^{-1}m, \Delta^{-1}m) . \tag{3.10}$$

Since $dm = 0$, it follows that $\Delta m = d\delta m$, and thus

$$(d\delta\Delta^{-1}m, \Delta^{-1}m) = (m, \Delta^{-1}m). \tag{3.11}$$

Putting it all together, we obtain

$$Z = \prod_{c_2} \sum_{m_{c_2}\in\mathbb{Z}\, dm=0} \prod_{c_0} \int_{-\pi}^{\pi} dA_{c_1} \exp\left(-\frac{1}{2g^2}\|dA\|^2\right) \exp\left(-2\kappa\pi^2(m, \Delta^{-1}m)\right) . \tag{3.12}$$

This partition function can be interpreted as the one of a Coulomb gas of vortex world lines. The 2-form m counts the vorticity of the individual plaquettes. Its dual form ${}^*m$, associated to dual links, describes the world lines of vortices on the dual lattice. The constraint, $dm = 0$, is equivalent to a continuity equation, $\delta{}^*m = 0$, and implies that the vortex world lines are closed loops and thus vorticity is conserved. In $(m, \Delta^{-1}m)$, the expression $\Delta^{-1}m$ is nothing but the Coulomb potential generated by m. The vortex world lines form a Coulomb gas.

To develop some intuition on why m corresponds to the vorticity of a plaquette, consider a plaquette with the four attached angles labeled by φ_i, $1 \le i \le 4$. To assess whether this plaquette contains a vortex, one considers the sum of the differences of these angles,

$$m = \frac{1}{2\pi}\left((\varphi_2 - \varphi_1)) + (\varphi_3 - \varphi_2) + (\varphi_4 - \varphi_3) + (\varphi_1 - \varphi_4)\right) . \tag{3.13}$$

If the φ_i were non-compact real numbers, this would trivially add up to zero. The difference of two angles, however, is only unique up to an integer multiple of 2π, depending on the interpolation that is implicitly assumed between the individual spins. In the Villain action, these interpolations are all explicitly accounted for by the term $2\pi n$, that is added to $d\varphi$ at each link. We can therefore think of a configuration of n as an interpolation prescription for each link. The sum of the difference of the angles around our example

plaquette according to this interpolation prescription is then

$$m = n_{21} + n_{32} + n_{43} + n_{14}\,, \tag{3.14}$$

where n_{ij} is the integer added to the link connecting the sites that φ_i and φ_j are attached to. If the orientation of the links is taken into account, this is equivalent to dn evaluated at that plaquette. Thus $m = dn$ does indeed account for the vorticity of a plaquette.

3.3. The Vortex Two-Point Function

Following Fröhlich and Marchetti [39], the vortex two-point function is given as

$$\begin{aligned}\langle \Phi(x_1)\Phi^*(x_2)\rangle &= \frac{\prod_{c_2}\sum_{m_{c_2}\in\mathbb{Z},dm=-dB}\exp\left(-\frac{2\pi^2}{g^2}(m+B,\Delta^{-1}(m+B))\right)}{\prod_{c_2}\sum_{m_{c_2}\in\mathbb{Z},dm=0}\exp\left(-\frac{2\pi^2}{g^2}(m,\Delta^{-1}(m))\right)} \\ &= \frac{Z(x_1,x_2)}{Z}\,.\end{aligned} \tag{3.15}$$

The partition function, $Z(x_1, x_2)$, describes a Coulomb gas of closed vortex world lines with an additional open world line that starts at the dual lattice point x_1 and ends at the dual lattice point x_2. This is illustrated schematically in Figure 3.1. To implement

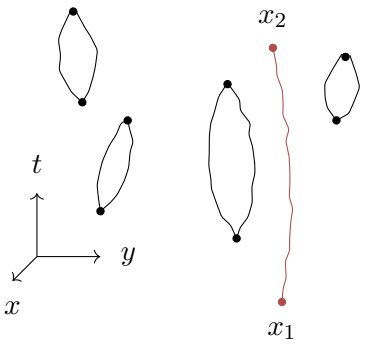

Figure 3.1.: A schematic drawing of a configuration contributing to $Z(x_1, x_2)$. The lines correspond to vortex world lines that form closed loops of vortex antivortex pairs, with the exception of a single open world line that starts at x_1 and ends at x_2, where an single vortex is created and anihilated.

this, an external 2-form field B is added with

$$dB = {}^*\delta_{x_1} - {}^*\delta_{x_2}, \tag{3.16}$$

where ${}^*\delta_x$ is a 2-form Kronecker delta function that is equal to 1 on the space-time cube dual to x and 0 otherwise. The field B is not uniquely defined by the constraint of

eq. (3.16). A suitable choice is to take

$$B = B_{x_1} - B_{x_2}\,, \tag{3.17}$$

with $dB_{x_i} = {}^*\delta_{x_i}$, and B_{x_i} nonzero only on plaquettes dual to links in the dual time slice that contains x_i. The field B_{x_i} is then given by

$$B_{x_i} = \delta_2 \Delta_2^{-1} {}^*\delta_{x_i}\,. \tag{3.18}$$

The subscript 2 indicates, that δ_2 and Δ_2 refer to the two-dimensional coderivative and Laplacian respectively. Confer Figure 3.2.

In the original formulation of the Villain model in terms of angles, φ_{c_0}, the vortex two-point function is

$$\langle \Phi(x_1)\Phi^*(x_2)\rangle = \frac{1}{Z}\prod_{c_0}\int_{-\pi}^{\pi} d\varphi_{c_0} \prod_{c_1}\sum_{n_{c_1}\in\mathbb{Z}} \exp\left(-\frac{1}{2g^2}\left\|d\varphi + 2\pi n + 2\pi\delta\Delta^{-1}(B-\omega)\right\|^2\right). \tag{3.19}$$

In addition to the field B, another 2-form field ω appears that describes the Dirac string, connecting the vortex creation point x_1 to its annihilation point x_2. It is integer-valued and fulfills

$$d\omega = {}^*\delta_{x_1} - {}^*\delta_{x_2}\,, \tag{3.20}$$

but is otherwise arbitrary. A simple realization is, $\omega = 1$ on plaquettes dual to links on a path that connects x_1 to x_2 on the dual lattice and zero otherwise. Figure 3.2 illustrates this geometry. The vortex two-point function does not depend on the exact form of ω and the Dirac string is invisible. To see this, we consider two realizations ω_1 and ω_2. Since $d\omega_1 = d\omega_2$ they differ by an exact form. We therefore consider the transformation

$$\omega' = \omega + d\xi \tag{3.21}$$

with ξ an integer valued 1-form. Under such a transformation,

$$\begin{aligned} 2\pi\delta\Delta^{-1}(B-\omega') &= 2\pi\delta\Delta^{-1}(B-\omega) - 2\pi\delta\Delta^{-1}d\xi \\ &= 2\pi\delta\Delta^{-1}(B-\omega) - 2\pi\xi + 2\pi d\Delta^{-1}\delta\xi\,, \end{aligned} \tag{3.22}$$

where we have used the Hodge decomposition of ξ,

$$\xi = d\Delta^{-1}\delta\xi + \delta\Delta^{-1}d\xi. \tag{3.23}$$

This leaves the vortex correlation function, eq. (3.19), invariant since the terms $2\pi\xi$ and $2\pi d\Delta^{-1}\delta\xi$ can be absorbed into n and φ by simple shifts.

It is easy to see that the vortex correlation function in terms of the angle field φ, eq. (3.19), is indeed equivalent to the formulation in terms of vortex world lines, eq. (3.15). In fact the only modification to the previous derivation of the equivalence of the respective partition functions is that m is replaced by $m+B-\omega$. The non-compact field, $A = \varphi + 2\pi l$,

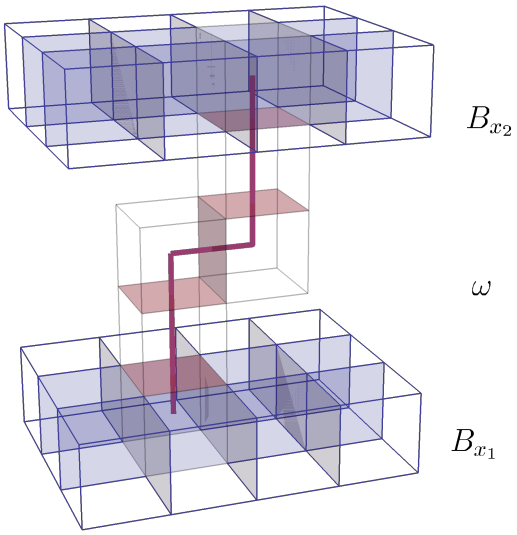

Figure 3.2.: An illustration of the geometry employed in the vortex correlation function. The thick red line corresponds to the path on the dual lattice that connects the vortex creation point x_1 to the annihilation point x_2. The fields, B_{x_i}, are nonzero only in the (blue) plaquettes within the time slices of the vortex creation and annihilation point.

still decouples from $m + B - \omega$, since

$$(dA, 2\pi\delta\Delta^{-1}(m + B - \omega)) = (A, 2\pi\delta^2\Delta^{-1}(m + B - \omega)) = 0 \tag{3.24}$$

and furthermore

$$\begin{aligned} \left\|2\pi\delta\Delta^{-1}(m + B - \omega)\right\|^2 &= 4\pi^2(\delta\Delta^{-1}(m + B - \omega), \delta\Delta^{-1}(m + B - \omega)) \\ &= 4\pi^2\left(d\delta\Delta^{-1}(m + B - \omega), \Delta^{-1}(m + B - \omega)\right) \\ &= 4\pi^2\left(m + B - \omega, \Delta^{-1}(m + B - \omega)\right) , \end{aligned} \tag{3.25}$$

since $d(m + B - \omega) = 0$. To obtain eq. (3.15) one finally replaces m by $m - \omega$.

We now have a fully non-perturbative formulation of the vortex correlation function. And in principle it is possible to evaluate it with Monte Carlo techniques in order to retrieve, for instance, the vortex mass. However, neither of the representations, eq. (3.19) and eq. (3.15), are practically suited to do numerical calculations. Their evaluation amounts to the measurement of ratios of Boltzmann weights, quantities that typically vary over many orders of magnitude. Fortunately there is a way out. The vortex in the $O(2)$ model in $(2 + 1)$ dimensions is exactly dual to an ordinary charged particle in an integer valued gauge theory, whose correlation function is calculable with Monte Carlo simulations. The concept of duality is interesting on its own, beyond being a mere trick that enables numerical calculations and is discussed in the next chapter.

4. The Vortex as a Dual Charged Particle

4.1. Kramers-Wannier Duality

While a dualism (such as in "mind matter dualism") refers to something consisting of two completely separate parts, the term duality means that there are two different perspectives on a single entity with possibly different emphasis. Dualities are ubiquitous in mathematics and physics [73]. Examples in physics range from the classic electromagnetic duality over wave-particle duality up to gauge-gravity duality.

Here, we will be concerned with a duality in the spirit of the self-duality of the two-dimensional Ising model described in 1941 by Kramers and Wannier [74]. They discovered a symmetry that relates the high-temperature to the low-temperature physics of the two-dimensional Ising model: The partition function at inverse temperature β can be rewritten again as an Ising model partition function (up to an overall factor) with inverse temperature, $\widetilde{\beta}$, that is a monotonically decreasing function of β, namely,

$$\widetilde{\beta} = -\frac{1}{2}\log\left(\tanh(\beta)\right) . \tag{4.1}$$

Assuming that the Ising model has only a single phase transition, this relation allows the exact determination of the critical temperature as follows. At the critical point, the free energy, $F(\beta)$, is non analytic. Since

$$F(\beta) = -\sinh(2\widetilde{\beta}) + F(\widetilde{\beta}) , \tag{4.2}$$

a non-analyticity can only occur if $\beta = \widetilde{\beta}$ and the critical temperature is obtained as the solution to

$$\beta_c = -\frac{1}{2}\log\left(\tanh(\beta_c)\right) . \tag{4.3}$$

The extra sinh term in eq. (4.2) accounts for the overall factor that relates original partition function to its dual.

By now it is understood that this symmetry is an instance of a more general duality transform that can be applied to a broad class of lattice systems [75, 76]. This duality transform is a kind of Fourier transform of the path integral. We consider models whose partition functions are of the following form

$$Z = \prod_{c_k} \int_G d\phi_{c_k} \prod_{c_{k+1}} W(d\phi_{c_{k+1}}) , \tag{4.4}$$

i.e., the degrees of freedom are associated to the cells c_k (e.g. points, c_0, for a spin model or links, c_1, for a gauge theory) and take on values in an Abelian group G. Furthermore the Boltzmann weight of a configuration can be expressed as a product over $(k+1)$-cells of local weights, that depend only on $d\phi_{c_{k+1}}$. In the first step of the duality transform, the integration over the field variables, ϕ_{c_k}, is replaced by an integration over a newly introduced $(k+1)$-form, $\chi_{c_{k+1}} = d\phi_{c_{k+1}}$. In order not to enlarge the configuration space, one has to ensure that the integration is only over configurations of χ that can indeed be obtained as an exterior derivative of some ϕ. This is ensured by inserting a constraint, $\delta(d\chi_{c_{k+2}})$, for each $(k+2)$-cell,

$$Z = \prod_{c_{k+1}} \int_G d\chi c_{k+1} \prod_{c_{k+1}} W(\chi_{c_{k+1}}) \prod_{c_{k+2}} \delta(d\chi_{c_{k+2}}) \,. \tag{4.5}$$

The delta function on an Abelian group can be expressed as a sum or integral over its characters, that form the dual group $\widetilde{G}$. The latter corresponds to the group of one-dimensional unitary representations of G. Doing so yields,

$$Z = \prod_{c_{k+1}} \int_G d\chi c_{k+1} \prod_{c_{k+2}} \int_{\widetilde{G}} dk_{c_{k+2}} \prod_{c_{k+1}} W(\chi_{c_{k+1}}) \exp(i(k, d\chi)) \,. \tag{4.6}$$

With a partial integration, $(k, d\chi)$ is then replaced by $(\delta k, \chi)$ and the integration over χ is carried out as

$$Z = \prod_{c_{k+2}} \int_{\widetilde{G}} dk_{c_{k+2}} \prod_{c_{k+1}} \widetilde{W}(\delta k_{c_{k+1}}) \,, \tag{4.7}$$

where $\widetilde{W}$ is the Fourier transform of W. For an abelian group it is given by

$$\widetilde{W}(\delta k_{c_{k+1}}) = \int_G d\chi_{c_{k+1}} W(\chi_{c_{k+1}}) \exp(i\delta k_{c_{k+1}} \chi_{c_{k+1}}) \,. \tag{4.8}$$

Eq. (4.7) can be interpreted as the partition function of a model with degrees of freedom attached to dual $k+1$ cells on the dual lattice,

$$Z = \prod_{{}^*c_{k+2}} \int_{\widetilde{G}} d^* k_{{}^*c_{k+1}} \widetilde{W}(d^* k_{{}^*c_{k+1}}) \,. \tag{4.9}$$

Therefore, in two dimensions, a spin model, i.e. a model with degrees of freedom attached to the sites c_0 is dual to a spin model with degrees of freedom attached to the dual lattice sites, ${}^*c_2$. In three dimensions on the other hand, ${}^*c_2$ refers to the links of the dual lattice and therefore a spin model is dual to a gauge theory.

Two comments are in order. First, the delta function constraints only ensure the integration over χ to be over the correct configuration space if the lattice has a trivial cohomology and therefore by virtue of the Poincaré lemma, all closed forms are exact. This is not the case, e.g., for a square lattice with periodic boundary conditions: In the case of a spin model ($k = 0$), there exist configurations of χ that obey the constraint

$d\chi = 0$ but cannot be obtained as $\chi = d\phi$ for some ϕ. One example is $\chi_{c_1} = const.$ The case of nontrivial cohomology has been discussed in [77]. Second, the above duality construction also fails if the symmetry group, be it local or global, is non-Abelian. Several attempts for generalizations to non-Abelian models exist, e.g. [78].

4.2. Duality of the Villain Model

Applying the duality transform described in Section 4.1 to the $(2+1)$-dimensional $O(2)$ model yields an integer valued gauge theory. In the following, we review this duality on the level of partition functions and for the vortex correlation function.

The $O(2)$ model partition function in the Villain formulation reads

$$Z = \prod_{c_0} \int_{-\pi}^{\pi} d\varphi_{c_0} \prod_{c_1} \sum_{n_{c_1} \in \mathbb{Z}} \exp\left(-\frac{1}{2g^2} \left\| d\varphi + 2\pi n \right\|^2 \right) . \tag{4.10}$$

We start the dualization by replacing the spin field associated to lattice sites, φ, by a field that is associated to the links, χ. In order not to enlarge the configuration space, we have to add an additional delta function constraint, that ensures that the 1-form χ can indeed be obtained from a 0-form φ as en exterior derivative. Expressed in this way, the partition function reads

$$Z = \prod_{c_1} \int_{-\pi}^{\pi} d\chi_{c_1} \prod_{c_1} \sum_{n_{c_1} \in \mathbb{Z}} \exp\left(-\frac{1}{2g^2} \left\| \chi + 2\pi n \right\|^2 \right) \prod_{c_2} \delta(d\chi_{c_2}) . \tag{4.11}$$

The delta function can be rewritten as a sum of exponentials as

$$Z = \prod_{c_1} \int_{-\pi}^{\pi} d\chi_{c_1} \prod_{c_1} \sum_{n_{c_1} \in \mathbb{Z}} \exp\left(-\frac{1}{2g^2} \left\| \chi + 2\pi n \right\|^2 \right) \prod_{c_2} \sum_{k_{c_2} \in \mathbb{Z}} \exp\left(i \left(k, d\chi \right) \right) . \tag{4.12}$$

We can now perform a partial integration, $(k, d\chi) = (\delta k, \chi)$, and add a trivial $2\pi n$ to χ in the second term, to obtain

$$Z = \prod_{c_1} \int_{-\pi}^{\pi} d\chi_{c_1} \prod_{c_1} \sum_{n_{c_1} \in \mathbb{Z}} \prod_{c_2} \sum_{k_{c_2} \in \mathbb{Z}} \exp\left(-\frac{1}{2g^2} \left\| \chi + 2\pi n \right\|^2 + i \left(\delta k, \chi + 2\pi n \right) \right) . \tag{4.13}$$

In the next step, the field χ is replaced by the non-compact field $A = \chi + 2\pi n$ that is integrated over the real numbers. We find that

$$Z = \prod_{c_1} \int_{-\infty}^{\infty} dA_{c_1} \prod_{c_2} \sum_{k_{c_2} \in \mathbb{Z}} \exp\left(-\frac{1}{2g^2} \left\| A \right\|^2 + i \left(\delta k, A \right) \right) . \tag{4.14}$$

The integral over A is Gaussian and can be explicitly performed. The result is,

$$Z = \prod_{c_2} \sum_{k_{c_2} \in \mathbb{Z}} \exp\left(-\frac{g^2}{2}\|\delta k\|^2\right) = \prod_{{}^*c_2} \sum_{k_{{}^*c_2} \in \mathbb{Z}} \exp\left(-\frac{g^2}{2}\|d^* k\|^2\right) . \tag{4.15}$$

This is the partition function of a $(2+1)$-dimensional pure gauge theory on the dual lattice with integer-valued link variables.

The duality transformation can also be performed for the vortex correlation function, eq. (3.19). The transformation is analogous to the one for the partition function. The additional term $2\pi\delta\Delta^{-1}(B-\omega)$ is included in the non-compact field, A, which in this case is

$$A = \chi + 2\pi n + 2\pi\delta\Delta^{-1}(B-\omega) . \tag{4.16}$$

The vortex correlation function before the integration of the non-compact field, the analog of eq. (4.14) is,

$$\begin{aligned}&\langle \Phi(x_1)\Phi^*(x_2)\rangle = \\ &\frac{1}{Z}\prod_{c_1}\int_{-\pi}^{\pi} d\chi_{c_1} \prod_{c_2}\sum_{k_{c_2}\in\mathbb{Z}} \exp\left(-\frac{g^2}{2}\|A\|^2 + i(dA,k) - i(2\pi d\delta\Delta^{-1}(B-\omega),k)\right) .\end{aligned} \tag{4.17}$$

Because $d(B-\omega)=0$, it holds that $d\delta\Delta^{-1}(B-\omega) = (B-\omega)$ and we find

$$\begin{aligned}\langle \Phi(x_1)\Phi^*(x_2)\rangle &= \frac{1}{Z}\prod_{c_2}\sum_{k_{c_2}\in\mathbb{Z}} \exp\left(-\frac{g^2}{2}\|\delta k\|^2\right)\exp\left(-2\pi i((B-\omega),k)\right) \\ &= \frac{1}{Z}\prod_{c_2}\sum_{k_{c_2}\in\mathbb{Z}} \exp\left(-\frac{g^2}{2}\|\delta k\|^2\right)\exp\left(-2\pi i(B,k)\right) \\ &= \frac{1}{Z}\prod_{{}^*c_2}\sum_{{}^*k_{{}^*c_2}\in\mathbb{Z}} \exp\left(-\frac{g^2}{2}\|d^* k\|^2\right)\exp\left(-2\pi i({}^*B,{}^*k)\right) .\end{aligned} \tag{4.18}$$

In the second step we have used that ω is integer-valued and thus $\exp(-2\pi i(\omega,k)) = 1$. This form of the vortex two-point function suggests to use the following definition for the vortex creation operator,

$$\Phi(x) = \exp(-2\pi i({}^*B_x, {}^*k)) . \tag{4.19}$$

With ${}^*B_x$ given by eq. (3.18), the classical electric field generated by a point charge.

The vortex creation operator is invariant under gauge transformations of the dual theory,

$${}^*k' = {}^*k + d^*\alpha , \tag{4.20}$$

again, because $\exp(-2\pi i({}^*B_x, {}^*d\alpha)) = 1$ for α integer-valued.

4.3. The Vortex as a Charged Particle

As realized by Fröhlich and Marchetti [41], the dual integer gauge theory corresponds to a limit of non-compact scalar QED with a $U(1)$ valued scalar field, ${}^*\phi_{{}^*c_3} = \exp(i{}^*\eta_{{}^*c_3})$. The partition function reads,

$$Z = \prod_{{}^*c_2} \int_{-\infty}^{\infty} d^*A_{{}^*c_2} \prod_{{}^*c_3} \int_{-\pi}^{\pi} d^*\eta_{{}^*c_3} \exp\left(-\frac{1}{2e^2} \left\| d^*A \right\|^2 + \kappa \sum_{{}^*c_2} \cos\left(d^*\eta_{{}^*c_2} + {}^*A_{{}^*c_2} \right) \right) . \tag{4.21}$$

In unitary gauge, where ${}^*\eta = 0$, it simplifies to

$$Z = \prod_{{}^*c_2} \int_{-\infty}^{\infty} d^*A_{{}^*c_2} d\eta \exp\left(-\frac{1}{2e^2} \left\| d^*A \right\|^2 + \kappa \sum_{{}^*c_2} \cos\left({}^*A_{{}^*c_2} \right) \right) . \tag{4.22}$$

In the limit $\kappa \to \infty$, the second term in the action fixes the gauge field ${}^*A_{{}^*c_2}$ to take on values of an integer multiple of 2π,

$${}^*A_{{}^*c_2} = {}^*k_{{}^*c_2} 2\pi \, . \tag{4.23}$$

In this limit the partition function reads,

$$\lim_{\kappa \to \infty} Z = \prod_{{}^*c_2} \sum_{{}^*k_{{}^*c_2} \in \mathbb{Z}} \exp\left(-\frac{2\pi^2}{e^2} \left\| d^*k \right\|^2 \right) , \tag{4.24}$$

which is equal to the partition function of the integer gauge theory given in eq. (4.15) if the couplings are related as

$$e = \frac{2\pi}{g} \, . \tag{4.25}$$

The photon is dual to the massless Goldstone boson and the vortex can be identified with the charged scalar particle in this dual QED. To create a physical charged scalar particle, one needs a gauge invariant operator and cannot simply use ${}^*\phi$. Under a gauge transformation, the fields transform as

$$\begin{aligned} {}^*A' &= {}^*A + d^*\alpha \\ {}^*\phi' &= {}^*\phi \exp(ie{}^*\alpha) \, . \end{aligned} \tag{4.26}$$

Furthermore, charged particles are infraparticles and always surrounded by a cloud of massless photons, that extends to infinity. To construct a gauge invariant operator that creates a charged particle, this photon cloud has to be taken into account. A possible choice, following Dirac [79], is,

$${}^*\phi_c(x) = {}^*\phi(x) \exp(i(E_x, A)) \, , \tag{4.27}$$

where E_x is the classical electric field of a point charge located at x and thus equals B_x. It

is now clear, that the vortex in the $(2+1)$-dimensional $O(2)$ model is dual to the charged particle in the $\kappa \to \infty$ limit of scalar QED. The infinite dual photon cloud surrounding a charged particle gives it a mass that diverges logarithmically with the system extent. In the next section we will therefore address the vortex in a finite volume.

4.4. The Vortex in a Box

Here we discuss the integer gauge theory, defined by eq. (4.15), in a finite volume. Before looking at the implications of the finite system extent on the vortex creation operator, we start with a brief discussion of the symmetries of the gauge theory subject to periodic and C-periodic boundary conditions. We consider the theory on a $(2+1)$-dimensional Euclidean space-time lattice that extends over $N_i = L_i/a$ lattice sites in the direction specified by the unit vector e_i.

We start by addressing periodic boundary conditions of the form

$$ {}^*k_{{}^*c_2'} = {}^*k_{{}^*c_2} \,, \tag{4.28} $$

where ${}^*c_2'$ is a periodic copy of the dual lattice site ${}^*c_2$, i.e., if ${}^*c_2$ is located at x, ${}^*c_2'$ is located at $x + Le_i$ for some i. First and foremost there is gauge invariance. Under a periodic (dual) gauge transformation ${}^*\alpha$, the gauge field transforms as

$$ {}^*k' = {}^*k + d{}^*\alpha \,, \tag{4.29} $$

and the action is invariant, since $dd{}^*\alpha = 0$. We have already seen, that also the vortex operator is invariant under gauge transformations in Section 4.2. In addition, there is charge conjugation C that operates as

$$ Ck = -k \,. \tag{4.30} $$

This is again a symmetry of the action. Furthermore, there is a $\mathbb{Z}^3$ global symmetry, that is given by

$$ {}^*k'_{{}^*c_2} = {}^*k_{{}^*c_2} + q_i \,, \quad \forall {}^*c_2 \in {}^*S_i \,, \tag{4.31} $$

where q_j is an integer and ${}^*S_j$ is a lattice slice perpendicular to e_j. The location of the slice does not matter since for different choices of slices (but the same values for the q_j), the ${}^*k'$ are related by gauge transformations. In Section 2.3 we have seen that classically, a single vortex cannot exist in the $(2+1)$-dimensional $O(2)$ model with periodic boundary conditions. The same is also true for the charged particle, because the charge creation operator refers to the field

$$ B_x = \delta_2 \Delta_2^{-1} {}^*\delta_x \,, \tag{4.32} $$

which is ambiguous with periodic boundary conditions since the Laplacian has zero-modes, the constant forms, and is thus not invertible.

This problem does not occur when C-periodic boundary conditions, of the form

$$ {}^*k_{{}^*c_2'} = {}^C{}^*k_{{}^*c_2} = -{}^*k_{{}^*c_2}\,, \tag{4.33} $$

are employed. Then the Laplacian does not have zero-modes and B_x in eq. (4.32) is well defined. We will use C-periodic boundary conditions in space and periodic boundary conditions in Euclidean time, nevertheless, we will refer to these mixed boundary conditions sometimes simply as C-periodic boundary conditions. These boundary conditions break the global symmetry defined in eq. (4.31): While for dual plaquettes in the bulk d^*k remains invariant, for dual plaquettes that extend over a boundary and contain a modified link as well as a C-periodic copy of a modified link, it does not. Under the transformation $k' = k' + q_i$, such a plaquette transforms as $d^*k' = d^*k + 2q_i$. If however $q = q_i = q_j$, for all directions i, j, and the S_i are chosen as the boundaries of the lattice, d^*k is invariant also on these plaquettes. This transformation has the form of a global constant gauge transformation,

$$ {}^*k' = {}^*k + d^*\varphi\,, \qquad\qquad \varphi(c_0) = \frac{q}{2} \tag{4.34} $$

The gauge group being $\mathbb{Z}$, for even q this is a proper gauge transformation, for odd q it is not. The remaining global symmetry up to gauge transformations is therefore reduced to $\mathbb{Z}_2$ and is given as

$$ {}^*k'_{{}^*c_2} = {}^*k_{{}^*c_2} + q\,, \qquad \forall {}^*c_2 \in S_i\,, \tag{4.35} $$

with $q \in \{0, 1\}$. Under this transformation, the vortex creation operator transforms as

$$ \begin{aligned} \Phi(x)' &= \Phi(x) \exp\left(-2\pi i \left({}^*B_x, d^*\varphi\right)\right) \\ &= \Phi(x) \exp\left(-2\pi i \left(\delta_x, \varphi\right)\right) \\ &= -\Phi(x)\,. \end{aligned} \tag{4.36} $$

In the following, we will refer to this transformation as vortex field reflection or simply R. Under charge conjugation, the vortex creation operator transforms as,

$$ {}^C\Phi(x) = \Phi^*(x)\,. \tag{4.37} $$

Its C-even and C-odd components are

$$ \begin{aligned} {}^C\operatorname{Re}\Phi(x) &= \operatorname{Re}\Phi(x) \\ {}^C\operatorname{Im}\Phi(x) &= -\operatorname{Im}\Phi(x)\,. \end{aligned} \tag{4.38} $$

Thus in a C-periodic volume, the real part of $\Phi(x)$ is periodic and the imaginary part is anti-periodic. This implies that they have different allowed spatial momenta, (p_1, p_2),

namely,

$$\begin{aligned} \mathrm{Re}\,\Phi: &\qquad p_i = \frac{2\pi n_i}{L} &&\qquad n_i \in \mathbb{Z}\,, \\ \mathrm{Im}\,\Phi: &\qquad p_i = \frac{2\pi\left(n_i + \frac{1}{2}\right)}{L} &&\qquad n_i \in \mathbb{Z}\,. \end{aligned} \tag{4.39}$$

We introduce the vortex creation operators at fixed spatial momentum as

$$\begin{aligned} \mathrm{Re}\,\Phi(p_1, p_2, t) &= \sum_{x_1, x_2} \exp(ip_1 x_1 + p_2 x_2)\,\mathrm{Re}\,\Phi(x_1, x_2, t)\,, \\ \mathrm{Im}\,\Phi(p_1, p_2, t) &= \sum_{x_1, x_2} \exp(ip_1 x_1 + p_2 x_2)\,\mathrm{Im}\,\Phi(x_1, x_2, t)\,. \end{aligned} \tag{4.40}$$

In order to obtain the mass of the vortex from numerical simulations we will consider the correlation functions of the operators

$$\begin{aligned} \Phi_+(t) &= \mathrm{Re}\,\Phi(0, 0, t)\,, \\ \Phi_-(t) &= \mathrm{Im}\,\Phi(\pi/L, \pi/L, t)\,. \end{aligned} \tag{4.41}$$

For large Euclidean time differences, their correlation functions decay exponentially

$$\begin{aligned} c_+(t) &= \langle \Phi_+(0)\Phi_+(t)\rangle \sim \exp(-mt) \\ c_-(t) &= \langle \Phi_-(0)\Phi_-(t)\rangle \sim \exp(-Et) \end{aligned} \tag{4.42}$$

where m is the energy of the lowest energy state $|V^+\rangle$ for which

$$\langle 0|\Phi_+|V^+\rangle \neq 0\,, \tag{4.43}$$

and E, the energy of the lowest energy state $|V^-\rangle$ for which

$$\langle 0|\Phi_-|V^-\rangle \neq 0\,. \tag{4.44}$$

The states $|V^+\rangle$ and $|V^-\rangle$ are even and odd, respectively, under charge conjugation, i.e. they are eigenstates of C with eigenvalues plus and minus one. Charged vortex and anti-vortex states should be formed as

$$\begin{aligned} |V\rangle &= \frac{1}{\sqrt{2}}\left(|V^+\rangle + |V^-\rangle\right) \\ |\overline{V}\rangle &= \frac{1}{\sqrt{2}}\left(|V^+\rangle - |V^-\rangle\right)\,. \end{aligned} \tag{4.45}$$

Then indeed the charge conjugated state of the vortex is the anti-vortex, ${}^C|V\rangle = |\overline{V}\rangle$. However, in the finite volume with C-periodic boundary conditions the states $|V\rangle$ and $|\overline{V}\rangle$ are not energy eigenstates since $|V^+\rangle$ and $|V^-\rangle$ have different momenta. This is a manifestation of the infraparticle nature of the vortex.

In a finite volume, a vortex or its dual charged particle is always surrounded by a cloud of massless bosons that extends to the boundary, and the global $U(1)$ symmetry is broken to the $\mathbb{Z}_2$ vortex reflection symmetry by the C-periodic boundary conditions. In the infinte volume, where the $U(1)$ symmetry is restored, the energies of $|V_+\rangle$ and $|V_-\rangle$ become degenerate as the momentum π/L of the C-odd state vanishes. There, charged states can be formed albeit with infinite energy.

4.5. Twisted C-Periodic Boundary Conditions

In the previous section, we have imposed C-periodic boundary conditions (and periodic boundary conditions in time) on the gauge fields. It is, however, more natural to impose the boundary conditions on gauge invariant quantities only. This is achieved with twisted boundary conditions, where the vector potential is periodic or C-periodic only up to a gauge transformation. Twisted boundary conditions were first introduced in [80]. In this section, we will be rather explicit, and therefore switch back to component notation for the gauge field, i.e., the value of ${}^*k(c_2)$ is denoted as $k_\mu(x)$, where $\mu \in \{1,2,3\}$ denotes the direction in which the link dual to c_2 points from the site x. With that notation, we express the twisted C-periodic boundary conditions as

$$\begin{aligned} k_\mu(x + L_i e_i) &= -k_\mu(x) + \partial_\mu \varphi_i(x)\,, \\ k_\mu(x + L_3 e_3) &= k_\mu(x) + \partial_\mu \varphi_3(x)\,, \end{aligned} \tag{4.46}$$

with $i \in \{1,2\}$.

The functions φ_μ are known as transition functions and are subject to cocycle conditions, i.e. consistency conditions for shifts in two directions. Specifically, $k_\mu(x + L_\mu e_\mu + L_\rho e_\rho)$ is expressed in terms of $k_\mu(x)$ and the transition function has to be single-valued, independent of the order in which the boundary conditions are applied. We start by considering the two spatial directions,

$$\begin{aligned} k_\mu(x + L_1 e_1 + L_2 e_2) &= -k_\mu(x + L_1 e_1) + \partial_\mu \varphi_2(x + L_1 e_1) \\ &= k_\mu(x) - \partial_\mu \varphi_1(x) + \partial_\mu \varphi_2(x + L_1 e_1)\,, \\ k_\mu(x + L_2 e_2 + L_1 e_1) &= -k_\mu(x + L_2 e_2) + \partial_\mu \varphi_1(x + L_2 e_2) \\ &= k_\mu(x) - \partial_\mu \varphi_2(x) + \partial_\mu \varphi_1(x + L_2 e_2)\,. \end{aligned} \tag{4.47}$$

This leads to the following consistency condition,

$$\partial_\mu \left(\varphi_2(x + L_1 e_1) - \varphi_1(x + L_2 e_2) - \varphi_1(x) + \varphi_2(x)\right) = 0\,. \tag{4.48}$$

It is fulfilled if the so-called twist tensor, or rather its spatial component, introduced as

$$n_{12} = \varphi_2(x + L_1 e_1) - \varphi_1(x + L_2 e_2) - \varphi_1(x) + \varphi_2(x) \tag{4.49}$$

is constant. Furthermore it is antisymmetric, $n_{12} = -n_{21}$. Next, we consider a spatial direction, i, and the temporal direction. The equations analogous to the spatial cocylce

conditions, eqs. (4.47), read,

$$\begin{aligned} k_\mu(x + L_i e_i + L_3 e_3) &= k_\mu(x + L_i e_i) + \partial_\mu \varphi_3(x + L_i e_i) \\ &= -k_\mu(x) + \partial_\mu \varphi_i(x) + \partial_\mu \varphi_3(x + L_i e_i) \\ k_\mu(x + L_3 e_3 + L_i e_i) &= -k_\mu(x + L_3 e_3) + \partial_\mu \varphi_i(x + L_3 e_3) \\ &= -k_\mu(x) - \partial_\mu \varphi_3(x) + \partial_\mu \varphi_i(x + L_3 e_3)\,. \end{aligned} \tag{4.50}$$

The resulting consistency condition is fulfilled if the space-time components of the twist tensor,

$$n_{3i} = \varphi_3(x + L_i e_i) - \varphi_i(x + L_3 e_3) + \varphi_i(x) + \varphi_3(x)\,, \tag{4.51}$$

are constant. Note that also the space-time part of the twist tensor is antisymmetric and n_{i3} therefore is

$$n_{i3} = \varphi_i(x + L_i e_i) - \varphi_3(x + L_3 e_3) - \varphi_i(x) - \varphi_3(x)\,. \tag{4.52}$$

A further constraint on the twist tensor arises from considering

$$\begin{aligned} &\varphi_i(x + L_j e_j + L_3 e_3) - \varphi_j(x + L_3 e_3) + \varphi_3(x) \\ &\qquad = \varphi_j(x + L_i e_i + L_3 e_3) - \varphi_i(x + L_3 e_3) + \varphi_3(x) + n_{ij} \\ &\qquad = \varphi_j(x + L_i e_i + L_3 e_3) - \varphi_3(x + L_i e_i) - \varphi_i(x) + n_{ij} + n_{3i} \\ &\qquad = \varphi_3(x + L_i e_i + L_j e_j) + \varphi_j(x + L_i e_i) - \varphi_i(x) + n_{ij} + n_{3i} + n_{j3}\,, \end{aligned} \tag{4.53}$$

on the one hand, and

$$\begin{aligned} &\varphi_i(x + L_j e_j + L_3 e_3) - \varphi_j(x + L_3 e_3) + \varphi_3(x) \\ &\qquad = \varphi_i(x + L_j e_j + L_3 e_3) - \varphi_3(x + L_j e_j) - \varphi_j(x) + n_{3j} \\ &\qquad = \varphi_3(x + L_j e_j + L_i e_i) + \varphi_i(x + L_j e_j) - \varphi_j(x) + n_{3j} + n_{i3} \\ &\qquad = \varphi_3(x + L_i e_i + L_j e_j) + \varphi_j(x + L_i e_i) - \varphi_i(x) + n_{3j} + n_{i3} + n_{i3}\,, \end{aligned} \tag{4.54}$$

on the other hand, namely,

$$n_{3i} + n_{j3} = 0\,, \tag{4.55}$$

and therefore $n_{13} = n_{23}$.

Different transition functions φ_μ do not necessarily reflect different physical situations, the difference might be a gauge transformation. To extract the gauge invariant content of the twisted boundary conditions, we will now derive the transformation properties of the twist tensor under a general gauge transformation, i.e., under a gauge transformation that is not necessarily C-periodic,

$$k_\mu(x)' = k_\mu(x) + \partial_\mu \varphi(x)\,. \tag{4.56}$$

While such transformations are inconsistent with purely C-periodic boundary conditions, they relate twisted boundary conditions with different transition functions but leave the

physical content, e.g. the field strength invariant. To see how the transition functions transform, we consider

$$\begin{aligned} k_\mu(x+L_ie_i)' &= k_\mu(x+L_ie_i) + \partial_\mu\varphi(x+L_ie_i) \\ &= -k_\mu(x) + \partial_\mu\varphi_i(x) + \partial_\mu\varphi(x+L_ie_i)\,, \\ k_\mu(x+L_ie_i)' &= -k_\mu(x)' + \partial_\mu\varphi_i(x)' \\ &= -k_\mu(x) - \partial_\mu\varphi(x) + \partial_\mu\varphi_i(x)'\,. \end{aligned} \tag{4.57}$$

From this we conclude that

$$\varphi_i(x)' = \varphi_i(x) + \varphi(x+L_ie_i) + \varphi(x) + n_i\,. \tag{4.58}$$

A similar transformation rule arises for the transition function in Euclidean time,

$$\begin{aligned} k_\mu(x+L_3e_3)' &= k_\mu(x+L_3e_3) + \partial_\mu\varphi(x+L_3e_3) \\ &= k_\mu(x) + \partial_\mu\varphi_3(x) + \partial_\mu\varphi(x+L_3e_3)\,, \\ k_\mu(x+L_3e_3)' &= k_\mu(x)' + \partial_\mu\varphi_3(x)' \\ &= k_\mu(x) + \partial_\mu\varphi(x) + \partial_\mu\varphi_3(x)'\,. \end{aligned} \tag{4.59}$$

Therefore the temporal transition function transforms as

$$\varphi_3(x)' = \varphi_3(x) + \varphi(x+L_3e_3) - \varphi(x) + n_3\,. \tag{4.60}$$

We now investigate how the spatial component of the twist tensor transforms

$$\begin{aligned} n'_{ij} &= \varphi_j(x+L_ie_i)' - \varphi_i(x+L_je_j)' - \varphi_i(x)' + \varphi_j(x)' \\ &= n_{ij} + \varphi(x+L_ie_i+L_je_j) + \varphi(x+L_ie_i) + n_j \\ &\qquad - \varphi(x+L_je_j+L_ie_i) - \varphi(x+L_je_j) - n_i \\ &\qquad - \varphi(x+L_ie_i) - \varphi(x) - n_i \\ &\qquad + \varphi(x+L_je_j) + \varphi(x) + n_j \\ &= n_{ij} + 2(n_j - n_i)\,, \end{aligned} \tag{4.61}$$

A similar calculation for the space-time components reads,

$$\begin{aligned} n'_{3i} &= \varphi_3(x+L_ie_i)' - \varphi_i(x+L_3e_3)' + \varphi_i(x)' + \varphi_3(x)' \\ &= n_{3i} + \varphi(x+L_ie_i+L_3e_3) - \varphi(x+L_ie_i) + n_3 \\ &\qquad - \varphi(x+L_3e_3+L_ie_i) - \varphi(x+L_3e_3) - n_i \\ &\qquad + \varphi(x+L_ie_i) + \varphi(x) + n_i \\ &\qquad + \varphi(x+L_3e_3) - \varphi(x) + n_3 \\ &= n_{3i} + 2n_3\,. \end{aligned} \tag{4.62}$$

With that we now investigate the gauge invariant content of the twist tensor. Previously

we have seen that $n_{3i} = n_{3j}$. This constraint is gauge invariant. The antisymmetric twist tensor therefore has two independent components, n_{12} and $n_{13} = n_{23}$. Under gauge transformations, they change by an even integer. Up to gauge transformations, we can thus distinguish the four physical situations characterized by

$$n_{12} \in \{0, 1\} \,, \qquad\qquad n_{13} \in \{0, 1\} \,. \tag{4.63}$$

We conclude this section with the following comment: The above calculation has been performed for the integer-valued pure gauge theory, and the twist tensor is therefore trivially integer-valued. Notably, for scalar QED the twist tensor is still quantized due to the additional cocycle condition for the matter field.

4.6. Duality and Boundary Conditions

The duality transformation in Section 4.2, allows us to identify the vortex with a dual charged particle, is set up in an infinite lattice. In this section we perform the duality transformation on a finite lattice to illuminate the relation between the boundary conditions of the original theory to the boundary conditions of the dual theory. Also here, we will sometimes make use of the explicit component notation. We start by briefly recalling the steps in the duality transformation, this time starting from the integer-valued dual gauge theory, but formulated on the original lattice,

$$Z = \left(\prod_{c_2} \sum_{k_{c_2} \in \mathbb{Z}} \right) \prod_{c_1} \widetilde{W}(\delta k_{c_1}) \,. \tag{4.64}$$

In the first step, the dual weights $\widetilde{W}$ are expressed by their Fourier representation as

$$Z = \left(\prod_{c_2} \sum_{k_{c_2} \in \mathbb{Z}} \prod_{c_1} \int_{-\pi}^{\pi} d\chi_{c_1} \right) \prod_{c_1} W(\chi_{c_1}) \exp(-i(\chi, \delta k)) \,. \tag{4.65}$$

Next a partial integration is performed. Here the boundary conditions need to be taken into account. In Appendix B we show that

$$(\chi, \delta k) = (d\chi, k) + (d\chi, \varphi)_b + P_1 n_{23} + P_2 n_{31} - P_3 n_{12} \,. \tag{4.66}$$

The P_i correspond to the Polyakov loops of the link variables χ, and n_{ij} is the twist tensor of the boundary conditions for the dual gauge theory. Furthermore, $(d\chi, \varphi)_b$ denotes a scalar product over the plaquettes at the boundaries where the 3-form, ϕ, is projected onto the plaquettes at the boundaries. The field χ is subject to C-periodic boundary conditions in space and periodic boundary conditions in time, without a twist. Now the

sum over k is performed, resulting in a constraint on the link variables,

$$Z = \left(\prod_{c_1} \int_{-\pi}^{\pi} d\chi_{c_1} \right) \prod_{c_2} \delta(d\chi_{c_2}) \prod_{c_1} W(\chi_{c_1}) \exp(-i(P_1 n_{23} + P_2 n_{31} - P_3 n_{12})) \,. \quad (4.67)$$

In the final step, the constrained integration over the link variables χ is replaced by an unconstrained integration over spin variables. In the infinite volume, this is justified by the Poincare lemma. In Appendix C, we show by an explicit construction that this is still justified in the finite volume, and that the P_i correspond to the twist in the boundary conditions of the spin theory, b_i,

$$\begin{aligned} \varphi(x + L_i e_i) &= -\varphi(x + L_i e_i) + b_i \,, \\ \varphi(x + L_3 e_3) &= \varphi(x + L_3 e_3) + b_3 \,, \end{aligned} \quad (4.68)$$

such that

$$\begin{aligned} Z = \frac{1}{2\pi} \left(\prod_{c_0} \int_{-\pi}^{\pi} d\phi_{c_0} \int_{-\pi}^{\pi} db_1 \sum_{b_2 \in \{b_1, b_1+\pi\}} \sum_{b_3 \in \{0,\pi\}} \right) \\ \times \prod_{c_1} W(d\phi_{c_1}) \exp(-i(b_1 - b_2) n_{31} - i b_3 n_{12}) \,. \end{aligned} \quad (4.69)$$

It is now apparent that the gauge invariant part of the boundary conditions of the dual gauge theory, the twist tensor, is related to the boundary conditions of the original spin model by a Fourier transform. Therefore, even if no twist is imposed on the dual gauge theory boundary conditions, it naturally appears in the boundary conditions of the original spin theory and the sectors that classically admit vortex solutions, i.e., $b_1 - b_2 = \pi$ are taken into account. We will therefore restrict the numerical calculation of the vortex mass and charge, presented in Chapter 5, to the $n_{ij} = 0$ sector of the gauge theory.

5. The Vortex in the Continuum Limit

5.1. The Continuum Limit at the Wilson-Fisher Fixed Point

In this chapter, we present the calculation of the finite volume vortex mass in the continuum limit at the Wilson-Fisher fixed point of the $(2+1)$-dimensional $O(2)$ model.

In the previous two chapters, we have discussed in detail how the correlation functions of the C-even and C-odd part of the vortex, $c_+(t)$ and $c_-(t)$, can be realized as path integrals of an ordinary but non-local operator in the integer gauge theory dual to the $(2+1)$-dimensional $O(2)$ model on the lattice, which can be evaluated with Monte Carlo techniques as described in Appendix D,

$$\begin{aligned} c_+(t) &= \frac{1}{Z}\prod_{{}^*c_2}\sum_{{}^*k_{{}^*c_2}\in\mathbb{Z}} \exp\left(-\frac{g^2}{2}\left\|d{}^*k\right\|^2\right)\phi_+(0)\phi_+(t)\,, \\ c_-(t) &= \frac{1}{Z}\prod_{{}^*c_2}\sum_{{}^*k_{{}^*c_2}\in\mathbb{Z}} \exp\left(-\frac{g^2}{2}\left\|d{}^*k\right\|^2\right)\phi_-(0)\phi_-(t)\,. \end{aligned} \tag{5.1}$$

For completeness, we also restate the definition of the operators,

$$\begin{aligned} \phi_+(t) &= \sum_{x_1,x_2} \mathrm{Re}\exp(-2\pi i(B_{x_1,x_2,t},{}^*k)) \\ \phi_-(t) &= \sum_{x_1,x_2} \mathrm{Im}\exp\left(i\frac{\pi}{L}(x_1+x_2)\right)\exp(-2\pi i(B_{x_1,x_2,t},{}^*k))\,. \end{aligned} \tag{5.2}$$

From these correlation functions, the vortex mass, m, and the energy of the lowest energy C-odd state, E, can be extracted. In order to relate such an observable of a lattice regularized quantum field theory to a universal physical quantity, a continuum limit has to be taken. The lattice has to be made finer and finer, and at the same time, the coupling has to be adjusted, such that a fundamental scale of the theory remains constant. Furthermore, the continuum limit result should be independent of the regularization, i.e., of the exact form of the action and the lattice structure.

This can be achieved as follows: If the lattice regularized quantum field theory has a continuous phase transition at some critical bare coupling with a divergent length-scale, ξ, the latter can be used as a fundamental scale for the continuum limit. From some starting bare coupling and lattice that extents over $N\times N\times N_t$ lattice sites, the bare coupling is tuned closer and closer to the phase transition, and the size of the lattice is

increased simultaneously, such that N/ξ remains constant. Because the length-scale ξ is divergent, the lattice can be made arbitrarily fine, limited only by computational power, if e.g. Monte Carlo simulations are performed. In addition, universality assures that the continuum limit of a physical quantity is indeed independent of the microscopic details of the regularization, i.e., of the specific choice of the action and the lattice geometry. In other words, all lattice regularizations in a given universality class give rise to the same quantum field theory in the continuum limit.

The critical properties of the lattice regularized $O(2)$ or XY model have been studied in great detail (see e.g., [81–85], or [9] for a comprehensive review of older work). It has a second order phase transition. We perform the continuum limit in the broken phase, where the vortices correspond to massive particles. The fundamental energy scale of this theory is the helicity modulus or spin stiffness. Its divergence approaching the phase transition from the broken phase is governed by the universal critical exponent ν. Taking into account the leading order corrections to scaling, it obeys [9]

$$\rho_s(t) = A_{\rho_s} t^{\nu} \left(1 + a_{\rho_s} t^{\omega} + b_{\rho_s} t + \ldots\right) , \tag{5.3}$$

where also the correction to scaling exponent ω is universal, and t is the reduced coupling, e.g.,

$$t = |g_c^2 - g^2| \tag{5.4}$$

for the Villain action. Other physical quantities, O, with the dimension of an energy, such as the vortex mass, obey the same scaling law with their respective amplitudes A_O and a_O. While the amplitudes depend on the microscopic details, amplitude ratios, A_{O_1}/A_{O_2}, are universal. The continuum limit of an observable subject to eq. (5.3) at the Wilson-Fisher fixed point, in units of the fundamental scale, that is the helicity modulus, is then simply A_O/A_{ρ_s}. In order to illustrate the universal nature of the vortex mass, we employ both the Villain action and the standard action.

After discussing the helicity modulus and its measurement in some more detail in Section 5.2, we give a detailed account on the setup of the continuum limit in Section 5.3.

5.2. The Helicity modulus

At small bare couplings in the symmetric phase, the spin-spin correlation function of the XY model decays exponentially as

$$\langle s(x)s(y)\rangle \propto \exp\left(-\frac{|x-y|}{\xi}\right) , \tag{5.5}$$

with the correlation length ξ. In the broken phase, that we are interested in, the correlation length diverges and a natural scale is provided by the helicity modulus [86] or spin stiffness, ρ_s. It measures the free energy response to a twist, α, in the boundary conditions, along a single dimension. The spin stiffness corresponds to the Goldstone boson

decay constant, the prefactor of the leading term in the effective action that describes the low-energy physics dominated by the Goldstone bosons [87]. It is a property of the infinite volume lattice theory at a given value of the coupling.

In a Monte Carlo simulation, ρ_s can be obtained from the finite-size behavior of the magnetic susceptibility and other observables [87, 88], or measured directly as

$$\rho_s = -\frac{L_1}{L_2 L_3} \frac{\partial^2 \log Z(\alpha)}{\partial^2 \alpha}\bigg|_{\alpha=0}. \tag{5.6}$$

By spreading out the twist throughout the lattice this formula can be evaluated to

$$\rho_s = \frac{1}{V}\left(\left\langle \sum_{c_1} s''(d\theta_{c_1})\right\rangle - \left\langle \left(\sum_{c_1} s'(d\theta_{c_1})\right)^2 \right\rangle\right). \tag{5.7}$$

Inserting the local form of the Villain action, we find

$$\rho_s = 4\frac{1}{g^2} + \frac{16\pi^2\left(1/g^2\right)^2}{V}\left(\left\langle \sum_{c_1\in\Lambda_1}\left(\frac{g_1(d\theta_{c_1})^2}{g_0(d\theta_{c_1})^2} - \frac{g_2(d\theta_{c_1})}{g_0(d\theta_{c_1})}\right)\right\rangle - \left\langle\left(\sum_{c_1}\left(\frac{d\theta_{c_1}}{2\pi} - \frac{g_1(d\theta_{c_1})}{g_0(d\theta_{c_1})}\right)\right)^2\right\rangle\right). \tag{5.8}$$

The sum is over all links, $c_1 \in \Lambda_1$, which point in the direction e_1, and

$$g_m(\mu) = \sum_{n\in\mathbb{Z}} n^m \exp\left(-\frac{1}{g^2}(\mu - 2\pi n)^2\right). \tag{5.9}$$

The analogous expression for the standard action is [89],

$$\rho_s = \frac{\beta}{L_1 L_2 L_3}\left\langle \sum_{c_1\in\Lambda_1} \cos\left(d\varphi_{c_1}\right)\right\rangle - \frac{\beta^2}{L_1 L_2 L_3}\left\langle\left(\sum_{c_1\in\Lambda_1}\sin\left(d\varphi_{c_1}\right)\right)^2\right\rangle. \tag{5.10}$$

The finite-size effects of this observable are proportional to L^{-3}.

To calculate the helicity modulus, ρ_s, as a function of the coupling, we perform simulations with the Wolff cluster algorithm [90] for the $(2+1)$-dimensional $O(2)$ model with the Villain action and measure ρ_s according to eq. (5.8). The minor modifications to the algorithm described in [90] due to the use of the Villain action are discussed in Appendix D. We use cubic lattices with periodic boundary conditions and extents $L = 12a, 24a, 48a, 64a$, and several couplings between $1/g^2 = 0.334$ and $1/g^2 = 0.46$, the critical coupling being $1/g^2 = 0.333068(7)$ [30]. At each coupling, we extrapolate ρ_s to the infinite volume limit by fitting a function of the form $\rho_s(L) = \rho_s + cL^{-3}$. For the two couplings closest to the critical point, the measurement for $L = 12a$ does not obey the scaling law and is omitted in the fits. For all values of $1/g^2$, the extrapolated results are

consistent with the direct measurement of the helicity modulus at $L = 64a$ and $L = 48a$. An example of the extrapolation to the infinite volume limit is shown in Figure 5.1.

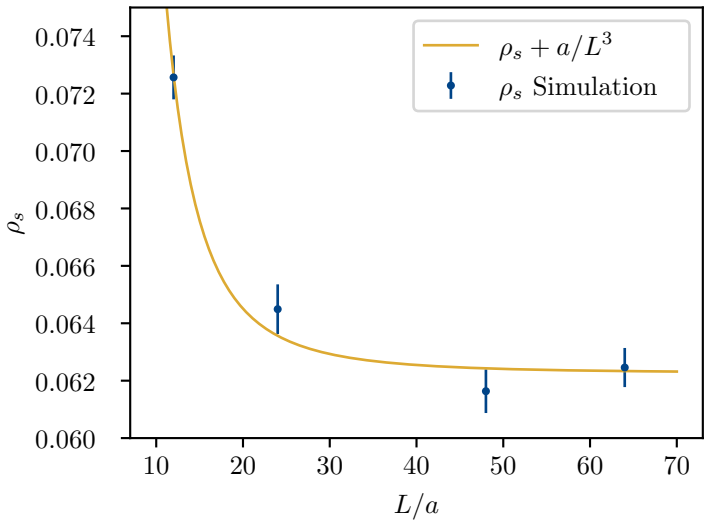

Figure 5.1.: The helicity modulus as a function of the lattice size, L, for $1/g^2 = 0.338$.

The coupling-dependence of the infinite-volume helicity modulus is very well described by eq. (5.3). A fit of this scaling form to the numerical data is shown in Figure 5.2. With the reduced coupling as $t = g_c^2 - g^2$. For the critical exponents we have taken the values from the literature [84], i.e.

$$\nu = 0.67169(7)\,, \qquad \omega = 0.789(4)\,. \tag{5.11}$$

The fit yields a χ^2 per degree of freedom of 0.6 and the best fit values for the amplitudes are

$$A_{\rho_s}^{(v)} = 0.531(3)\,, \qquad a_{\rho_s}^{(v)} = -0.25(2)\,, \qquad b_{\rho_s}^{(v)} = 0.11(2)\,. \tag{5.12}$$

Very accurate data for the helicity modulus are available in the literature for the standard action. Fitting the scaling form of eq. (5.3) to the data provided in [83] yields

$$A_{\rho_s}^{(s)} = 1.422(6)\,, \qquad b_{\rho_s}^{(s)} = -0.28(7)\,, \qquad e_{\rho_s}^{(s)} = -0.4(2)\,, \tag{5.13}$$

with a χ^2 per degree of freedom of 0.3. The fit is shown in Figure 5.3. With that, we have arrived at a formula for the helicity modulus as a function of the coupling for both the standard and the Villain action.

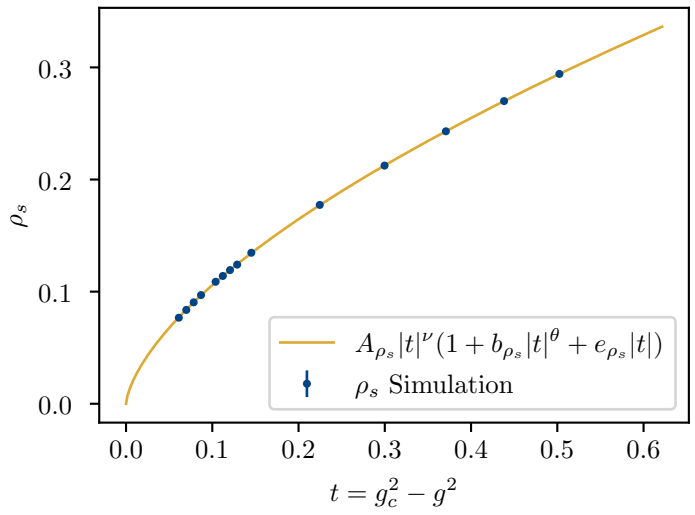

Figure 5.2.: The scaling of the helicity modulus as a function of the reduced coupling for the Villain action.

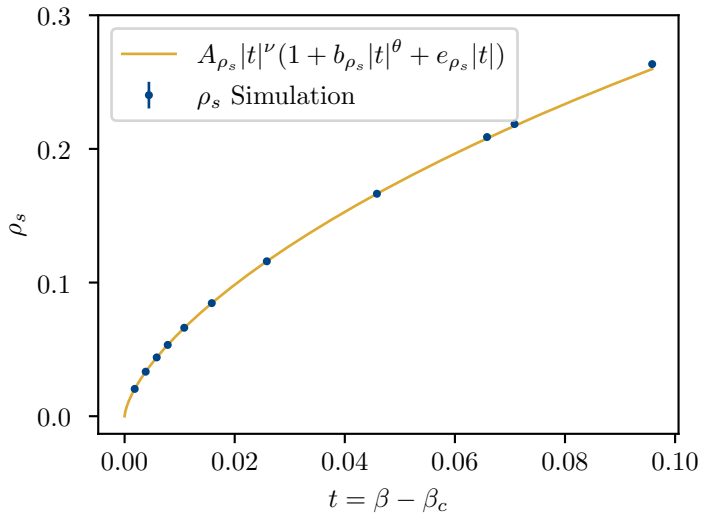

Figure 5.3.: The scaling of the helicity modulus as a function of the reduced coupling for the standard action. The data are taken from reference [83].

L_i	N_{ij}						
0.71(1)	4	6	8	10	12	14	16
1.43(2)	8	12	16	20	24	28	32
2.14(3)	12	18	24	30	36	42	48
2.85(4)	16	24	32	40	48	56	64
3.57(6)	20	30	40	50	60	70	80
4.28(7)	24	36	48	60	72	84	96
4.99(8)	28	42	56	70	84	98	112
5.71(9)	32	48	64	80	96	112	128
6.42(10)	36	54	72	90	108	126	144
$g_j^2/2$	1.38719	1.44099	1.46277	1.47400	1.48067	1.485	1.48800
β_j	0.50539	0.48103	0.47134	0.46634	0.46338	0.46145	0.46012

Table 5.1.: The values of the simulation parameters N, β, g^2, that have been used to calculate the vortex correlation function at different lattice spacings for the physical lattice extents L.

5.3. The Vortex Mass in the Continuum Limit

In order to calculate the finite volume vortex mass, we perform Monte Carlo simulations of the integer gauge theory dual to the $O(2)$ model with C-periodic boundary conditions in space and periodic boundary conditions in Euclidean time. The applied heat bath and Metropolis algorithms are outlined in Appendix D. The lattice extends over $N \times N \times N_t$ lattice sites. In all cases, we find that a Euclidean time extent of $N_t = 64$ is sufficient to reliably extract the vortex mass. We set up the continuum limit at different physical lattice extents, L_i. For each L_i, we perform simulations at several steps j towards the continuum limit, whereby the number of lattice sites, $N_{i,j}$ is increased and, at the same time, the coupling, g_j^2, is adjusted such that

$$L_i = N_{ij}\rho_s(g_j^2) \tag{5.14}$$

remains fixed. We choose $N_{ij} = i(2j+2)$, with $i \in \{1, \ldots, 9\}$ and $j \in \{1, \ldots, 7\}$, that is nine distinct physical volumes and seven steps towards to continuum limit for each of those. From a preliminary run, we know that simulations at $g^2 = 2.97$ and $N = 100$ are feasible. Taking this as a reference, the couplings were determined by numerically solving

$$N_{ij}\rho_s(g_j^2) = N_{i6}\rho_s(2.97)\,. \tag{5.15}$$

For the standard action, the values of β have then been calculated to yield the same physical extents. The resulting values for N_{ij}, g_j^2, β and L_i are summarized in Table 5.1. At each i, j, the vortex correlation functions $c_-(t)$ and $c_+(t)$ are evaluated as

follows. After 40'000 thermalization sweeps, 120'000 measurements are taken separated by 30 sweeps each, which are then averaged into 6000 bins. For all parameter values, the simulations were run in 60 identical replicas. For the standard action, only 40'000 measurements have been taken respectively and averaged into 2000 bins. Despite the binning, for couplings closer to the critical couplings a residual correlation in Monte Carlo time is present. The covariance matrix of the correlation functions is estimated according to the procedure described in [91]. A few examples of the C-even vortex correlation functions, alongside their correlation matrices are shown in Figure 5.4. The figure at the top shows three steps towards the continuum limit for the physical volume $L\rho_s = 1.43$ and the bottom figure for $L\rho_s = 5.00$. The points correspond to the results of the Monte Carlo simulations. The central region, where the correlation function is consistent with zero, is omitted in the plots. Furthermore, $c_+(t)$ follows the expected cosh behavior. Note that $c_+(t)$ is shown in lattice units, therefore we do not expect the curves to collapse to a continuum limit curve. Instead, the mass should approach zero for increasing j, this is seen as the decrease in the slope of $c_+(t)$ with increasing j. If the $c_+(t)$ were instead plotted against $t/N_{ij} \times L\rho_s$, the correlation functions would indeed approach a limiting curve. Beneath each $c_+(t)$, the corresponding correlation matrix,

$$\begin{aligned}\rho(c_+(t)c_+(t')) &= \frac{\mathrm{Cov}(c_+(t)c_+(t'))}{\sigma_{c_+(t)}\sigma_{c_+(t)}} \\ &= \frac{\langle c_+(t)c_+(t')\rangle - \langle c_+(t)\rangle \langle c_+(t')\rangle}{\sqrt{\left(\langle c_+^2(t)\rangle - \langle c_+(t)\rangle^2\right)\left(\langle c_+^2(t')\rangle - \langle c_+(t')\rangle^2\right)}}\end{aligned} \tag{5.16}$$

is shown. For large volumes and small couplings, the correlation matrices are diagonally dominated and correlations in Euclidean time are small. Correlations of the form $\rho_{c(t),c(T-t)}$ (visible as the cross shape in Figure 5.4) start to build up, when the critical point is approached. This can be attributed to the way $c_\pm(t)$ is measured. In each measurement, a hook time, t_h is chosen at random, and then, the value of $c_\pm((t_h - t) \mod N_t) = \phi(t_h)\phi^*(t)$ is updated for all t. In the next measurement, a different hook time t_h' is chosen. In the two steps,

$$\begin{aligned} c_\pm((t_h - t_h') \mod L_t) &= \phi(t_h)\phi(t_h') \\ c_\pm((t_h' - t_h) \mod L_t) &= \phi(t_h)\phi(t_h') \end{aligned} \tag{5.17}$$

are recorded, and the vortex operator evaluated at the same Euclidean times contributes to the vortex correlation function at Δt and at $L_t - \Delta t$. In this way, Monte Carlo time correlations manifest themselves as correlations in Euclidean time.

From the C-even vortex correlation function, $c_+(t)$, we retrieve the vortex mass $m(g^2, L)$ and from the C-odd vortex correlation function, $c_-(t)$, we obtain the minimal energy $E(g^2, L)$ by a single-cosh fit. The fitting routine is described in detail in Appendix E. The resulting energies follow the same scaling form as the helicity modulus. The vortex mass for the Villain action is depicted in Figure 5.5 as a function of the coupling, alongside

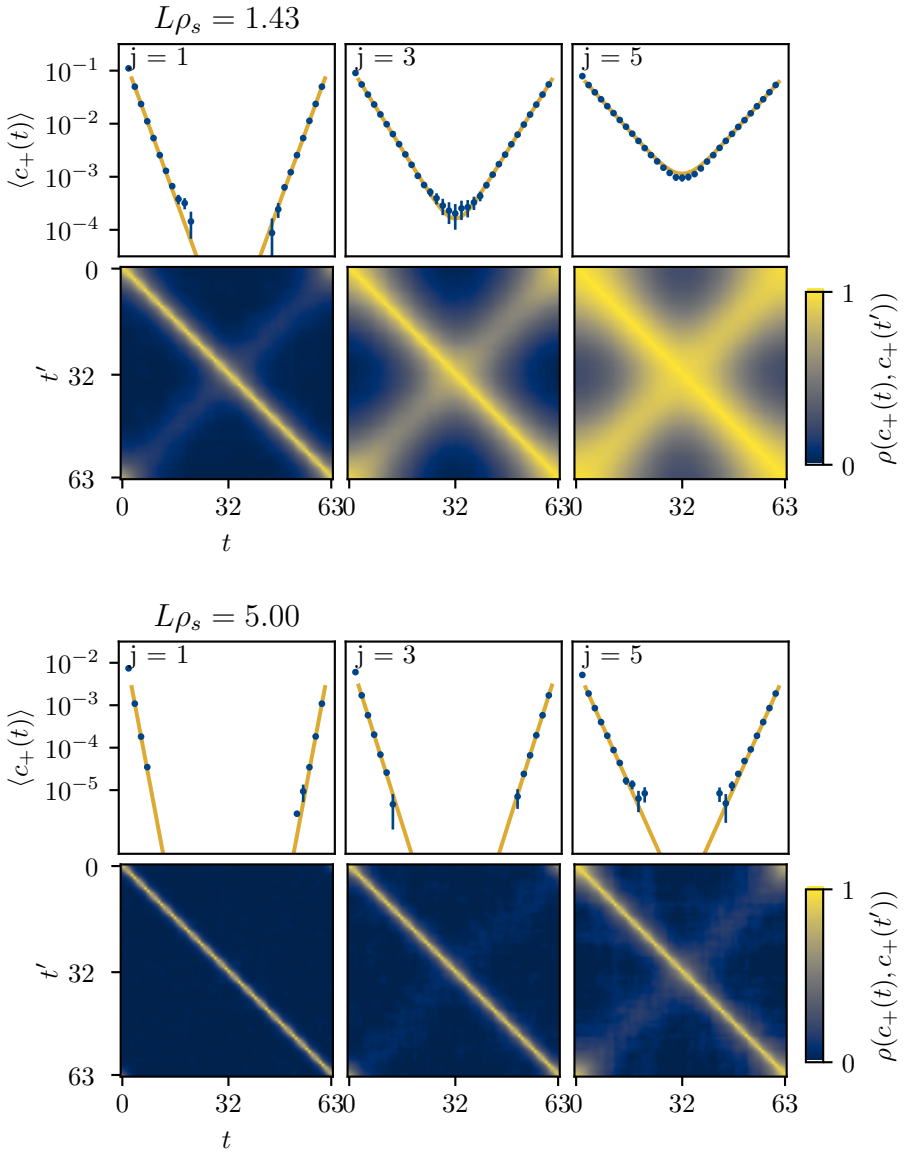

Figure 5.4.: Some examples of C-even vortex correlation functions, $c_+(t)$, from Monte Carlo simulations, alongside their covariance matrices. Two physical volumes are shown, $L\rho_s = 1.43$ (top) and $L\rho_s = 5.00$ (bottom) and three steps towards the continuum limit each.

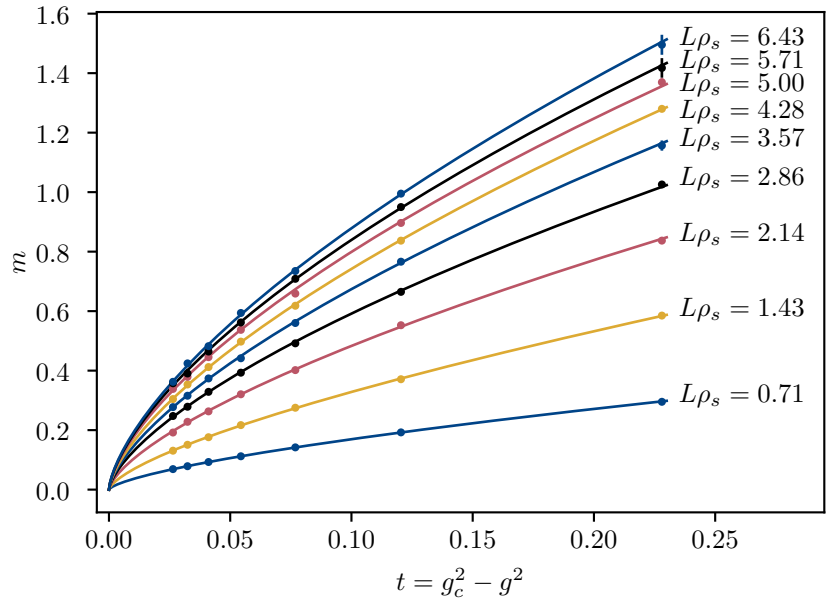

Figure 5.5.: The vortex mass for various physical volumes as a function of the reduced coupling. In lattice units, the mass approaches zero in the continuum limit.

with fits of the scaling form.

Therefore, $m(g^2, L)$ and $E(g^2, L)$ approach a finite continuum limit, when expressed in terms of the helicity modulus, confer Figure 5.6. In order to extract that continuum limit, we fit a function of the form

$$m(g^2, L) = A_{m_L}(g_c^2 - g^2)^\nu \left(1 + a_{m_L}(g_c^2 - g^2)^\omega\right) \tag{5.18}$$

to the masses and energies. The χ^2 per degree of freedom varies between 0.2 and 1.6, indicating that the masses obey the scaling law, and that their uncertainty is estimated in a reasonable way. The amplitude of the next order correction term, e_{m_L}, cannot be fitted reliably to our data, and is left out. The continuum limit of the vortex mass or energy in units of the vortex mass is then simply

$$m(L) = \frac{A_{m_L}}{A_{\rho_s}}\,. \tag{5.19}$$

The continuum limits of $m(L)$ and $E(L)$ are shown in Figure 5.7. As expected, we find that for larger L, the vortex mass diverges logarithmically with the physical extent L. For small values of L, the L dependence of m is not captured by this log behavior. In order to take into account the thereby induced systematic error due to the fit range selection, we employ the same method that we have used to fit the correlation functions.

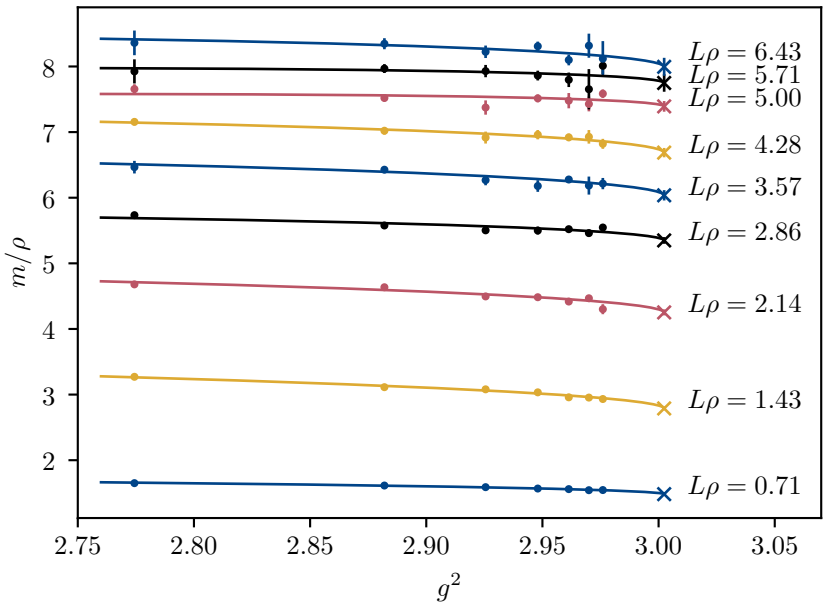

Figure 5.6.: The vortex mass expressed in units of the physical scale, ρ_s. It approaches a finite continuum limit, namely the universal amplitude ratio A_{m_L}/A_{ρ_s}.

Fitting a log of the form

$$m(L) = b \log\left(\frac{L}{L_0}\right) \tag{5.20}$$

yields a prefactor of

$$b = 3.55(9) \tag{5.21}$$

for the Villain action, and

$$b = 3.53(11) \tag{5.22}$$

for the Standard action. In Section 2.5 we have seen that for a classical point particle that interacts with itself in a C-periodic geometry via the Coulomb potential in two dimensions, the energy diverges logarithmically with the size of the box, and that the prefactor of this logarithmic divergence is nothing but the charge squared of the particle divided by 4π. We can thus identify the universal quantity $4\pi b$ with the charge of the vortex squared in units of the helicity modulus.

The energy of the C-odd state, E, asymptotically approaches m with the increasing physical volumes that we have considered. The vortex mass and E for the standard action show small but significant discrepancies to the results of the Villain action but only for volumes outside of the asymptotic regime. This indicates that there is a residual systematic error that is not accounted for. As the main focus of the present work lies on the extraction of the strength of the logarithmic divergence in the asymptotic regime,

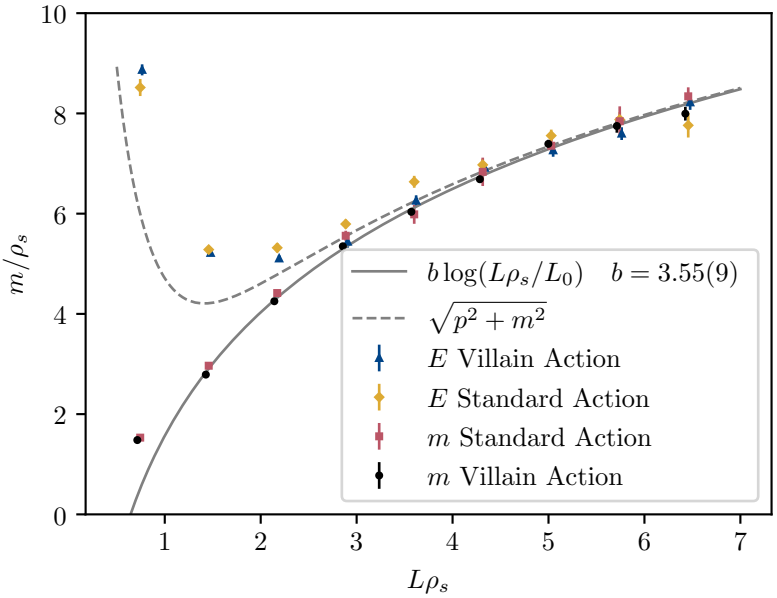

Figure 5.7.: The vortex mass, m and energy E in the continuum limit, as a function oft the physical volume, $L\rho_s$. As expected, the vortex mass diverges logarithmically, and the difference between E and m vanishes with increasing volume. Villain and standard action yield compatible results in the scaling regime. The markers were slightly shifted horizontally to increase visibility. The points for m from the Villain action are drawn at the true values of $L\rho_s$. The dashed gray line shows the energy of the energy of the state with the lowest possible non-zero momentum according to a relativistic dispersion relation with the mass taken from the logarithmic fit. The measured energies, E, do not follow this prediction.

where we find good agreement, we leave a detailed investigation of this discrepancy to be subject of future studies.

The extended infraparticle nature of the vortex spontaneously breaks Lorentz invariance [92, 93]. Therefore we do not expect a relativistic dispersion relation. In Figure 5.7 the energy of the state with the smallest possible non-zero momentum (i.e., $p = \pi/L$) according to such an energy momentum relation is shown. Indeed, the measurements do not follow this behavior.

Instead, motivated by a non-relativistic dispersion relation of the form $E = m + p^2/m_k$ that we assume for the state with the smallest allowed non-zero momentum, we define a kinetic mass for the vortex as

$$m_k = \frac{(\pi/L)^2}{2(E-m)}\,. \tag{5.23}$$

$L\rho_s$	0.71(1)	1.43(2)	2.14(3)
Villain action			
m_k/ρ_s	2.62(4)	1.99(5)	2.5(2)
m/ρ_s	1.48(1)	2.78(3)	4.25(5)
Standard action			
m_k/ρ_s	2.77(6)	2.08(7)	2.3(3)
m/ρ_s	1.53(1)	2.96(4)	4.41(6)

Table 5.2.: The kinetic mass of the vortex assuming a non-relativistic dispersion relation compared to its rest mass.

The resulting values for the cases where $E - m$ significantly differs from zero are summarized in Table 5.3. They differ substantially from the respective rest masses, confirming the spontaneous breaking of Lorentz invariance numerically.

6. Summary and Conclusions

We have studied the vortex in the $(2+1)$-dimensional $O(2)$ model in the continuum limit at the Wilson-Fisher fixed point approached from the broken phase. We have regularized the $O(2)$ model on the lattice and constructed the vortex two-point function according to the rigorous and non-perturbative scheme by Fröhlich and Marchetti [39]. In this formulation, the vortex two-point function is given as a ratio of partition functions which is not well-suited for numerical calculations. To overcome this difficulty, we have made use of the exact duality transformation that relates the $(2+1)$-dimensional $O(2)$ model to a gauge theory with integer-valued link variables. In order for configurations with a single vortex to exist in the finite volume, we have employed C-periodic boundary conditions. The duality relation also holds in the finite volume if C-periodic boundary conditions are used. The vortices in the $O(2)$ model are dual to charged scalar particles and their two-point function is an ordinary albeit non-local observable that can be calculated numerically.

We have taken a continuum limit of the vortex mass for several physical volumes at the Wilson-Fisher fixed point approached from the broken phase. In accordance with theoretical expectations from the infraparticle nature of the vortex, we find that its mass diverges logarithmically with the volume. Classical considerations of a charged particle in a C-periodic geometry imply that the prefactor of the logarithmic divergence can be identified with the Coulomb charge of the vortex squared. We have found that $e^2/4\pi\rho_s = 3.55(9)$. This is a new universal amplitude ratio associated with the Wilson-Fisher fixed point. To underscore the universal character of this quantity, we have used two different lattice actions for the $O(2)$ model, the Villain action and the standard action, and found that the numerical results are consistent.

Because of the extended infraparticle nature of the vortex, we do not expect a relativistic dispersion relation. We have confirmed that the energy of the state with the smallest allowed non-zero momentum does not follow such an energy momentum relation. Instead, we have defined a kinetic mass for the vortex according to a non-relativistic dispersion relation for the lowest non-zero momentum states, and found that it differs substantially from the rest mass of the vortex. This confirms numerically the spontaneous breaking of Lorentz invariance that is expected for infraparticles [92, 93]. The present dataset only allowed to calculate the kinetic mass at the three smallest volumes. It would be most interesting to further investigate the dispersion relation of the vortex, e.g., by looking into the energies of states with larger momentum or by increasing the statistics to take into account larger volumes.

Our results are in contradiction with the findings of [35], where the vortex mass was found to be finite. There, fixed boundary conditions were employed in order to enforce the presence of a vortex. The vortex mass was then obtained from a fit of an order

parameter profile from a semi-classical approximation. Fixed boundary conditions break translation invariance and often give rise to strong finite-volume effects. Furthermore, we think that the approach pursued in [35] is too semi-classical and not sufficiently well-founded to do justice to the subtle nature of the vortex.

Topological excitations such as the vortex are delicate objects, even more so if they are infraparticles. Nevertheless, the seminal work in the framework of algebraic quantum field theory [32–34, 39], makes it possible to treat them rigorously and non-perturbatively with lattice field theory methods. It would be interesting to study the inner structure of the vortex, e.g. its charge radius, beyond the semi-classical approximation with this approach.

It would also be most interesting to apply this methodology to other cases, such as in the continuum limit of the $(2 + 1)$-dimensional $O(2)$ model approached from the symmetric phase, where the vortices condense, or directly at the Wilson-Fisher fixed point in the conformal field theory. Another compelling case is the quantum XY-model, where it is an open question, whether vortices exist and can be described consistently. A more ambitious candidate are infraparticles with a non-Abelian charge, such as single quarks in QCD.

A. Differential Forms on the Lattice

A convenient formalism for lattice field theory is the one of differential forms. We adopt the notation in [72]. A lattice, Λ, consists of k-cells, c_k. For a three dimensional cubic lattice, the c_0 correspond to lattice points, c_1 to the links between the points, c_2 to the plaquettes that are surrounded by links, and finally, the c_3 to the cubes.

The dual lattice ${}^*\Lambda$, is obtained form the original lattice, by shifting it by half a lattice spacing in all directions. It consists of dual cells, ${}^*c_k$. The dual to a cubic lattice is again a cubic lattice. Its points, ${}^*c_3$, correspond to the centers of the cubes, c_3, of the original lattice, the dual links, ${}^*c_2$, that connect the dual lattice sites pierce the plaquettes, c_2, of the original lattice, the dual plaquettes, ${}^*c_1$, are themselves pierced by the links of the original lattice, c_1, and the dual cubes, ${}^*c_0$, have a point of the original lattice at the center. The k-cells are visualized for a three-dimensional cubic lattice in Figure A.1.

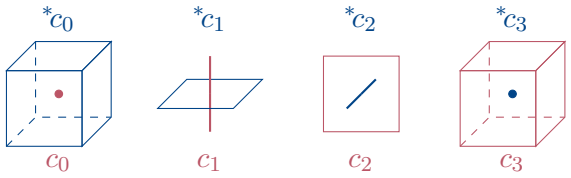

Figure A.1.: The different cells, that make up a three-dimensional cubic lattice, c_k.

The k-cells with $k > 0$ have a boundary, ∂c_k, which is the set of oriented $(k-1)$-cells that surround it. E.g., for a link, c_1, which extends from the site $c_0^{(1)}$ to the site $c_0^{(2)}$, the boundary consists of $c_0^{(2)}$ with positive orientation, and $c_0^{(1)}$ with negative orientation.

A k-form Φ associates a value, Φ_{c_k}, to each k-cell. The spin field of the $O(2)$ model, φ, for instance associates an angle to each site and therefore is a 0-form. The vector potential in a gauge theory on the other hand is a 1-form. An example for a 2-form is the field strength tensor.

The exterior derivative, d, maps a k-form, Φ, to a $k+1$ form, $d\Phi$, as

$$d\Phi_{c_{k+1}} = \sum_{c_k \in \partial c_{k+1}} \Phi_{c_k}, \tag{A.1}$$

where the sum is understood to be oriented. For instance, for a 0-form, φ, the value of its derivative on the link c_1 is

$$d\varphi_{c_1} = \varphi_{c_0^{(2)}} - \varphi_{c_0^{(1)}}, \tag{A.2}$$

where again, the link c_1 connects the site $c_0^{(1)}$ to the site $c_0^{(2)}$. The exterior derivative of a 1-form, on the other hand, is a 2-form that associates values to plaquettes. If a plaquette c_2 is surrounded counter-clockwise by the links $c_1^{(i)}$ with i ranging from one to four, the exterior derivative of the 1-form A on the plaquette c_2 is

$$dA_{c_2} = A_{c_1^{(1)}} + A_{c_1^{(2)}} - A_{c_1^{(3)}} - A_{c_1^{(4)}} \,. \tag{A.3}$$

The exterior derivative applied twice always gives zero, $d^2 = 0$. The field strength of a vector potential, A, in a gauge theory corresponds to $F = dA$. Furthermore, gauge transformations correspond to

$$A' = A + d\phi \,, \tag{A.4}$$

where ϕ is a 0-form. This trivially leaves $F = dA$ invariant because $d^2\phi = 0$.

The co-derivative, $\delta = {}^*d^*$, maps a k form to a $k-1$ form as

$$\delta\Phi_{c_{k-1}} = \sum_{{}^*c_k \in \partial {}^*c_{k-1}} \Phi_{c_k} \,. \tag{A.5}$$

For instance, the co-derivative of a 1-form, is a 0-form. It associates to a site the oriented sum of the values that are associated to all the links that point into or out of that site. The Laplacian in terms of differential forms corresponds to

$$\Delta = d\delta + \delta d \,, \tag{A.6}$$

and maps a k-form to a k-form.

A scalar product can be defined for two differential k-forms as

$$(\Phi, \Psi) = \sum_{c_k} \Phi_{c_k} \Psi_{c_k} \,. \tag{A.7}$$

It induces the norm

$$\|\Phi\|^2 = (\Phi, \Phi) \,, \tag{A.8}$$

and fulfills

$$(d\Phi, \Psi) = (\Phi, \delta\Psi) \,, \tag{A.9}$$

which corresponds to partial integration. Finally, each form can be Hodge decomposed into

$$\Phi = d\Delta^{-1}\delta\Phi + \delta\Delta^{-1}d\Phi \,. \tag{A.10}$$

We conclude this short account with some comments that apply in three dimensions. There, vector calculus can efficiently be described with differential forms (although not necessarily on the lattice.) A scalar field corresponds to a 0-form, a vector field to a 1-form, a pseudo-vector field to a 2-form and a pseudo-scalar field to a 3-form. The exterior derivative corresponds to the gradient, curl, and divergence respectively. The identities

$$\nabla \times (\nabla\phi) = 0 \,, \tag{A.11}$$

for a scalar field ϕ and

$$\nabla \cdot (\nabla \times V) = 0\,, \tag{A.12}$$

for a vector field V, are then simply manifestations of $d^2 = 0$.

B. Partial Integration with a Twist

In this appendix we show that

$$(\chi, \delta k) = (d\chi, k) + \sum_{i=1}^{3} (d\chi_{D_i}, \varphi_{D_i}) + P_1 n_{23} + P_2 n_{31} - P_3 n_{12} \,. \tag{B.1}$$

The expression $(\chi, \delta k)$ can be written explicitly as

$$\begin{aligned}(\chi, \delta k) = \sum_x \Big(& \chi_1(x)(k_{12}(x) - k_{31}(x) - k_{12}(x - e_2) + k_{31}(x - e_3)) \\ & + \chi_2(x)(k_{23}(x) - k_{12}(x) - k_{23}(x - e_3) + k_{12}(x - e_1)) \\ & + \chi_3(x)(k_{31}(x) - k_{23}(x) - k_{31}(x - e_1) + k_{23}(x - e_2)) \Big) \,.\end{aligned} \tag{B.2}$$

The terms can be regrouped into

$$\begin{aligned}(\chi, \delta k) = \sum_x \Big(& k_{12}(x)(\chi_1(x) - \chi_1(x + e_2) - \chi_2(x) + \chi_2(x + e_1)) \\ & + k_{23}(x)(\chi_2(x) - \chi_2(x + e_3) - \chi_3(x) + \chi_3(x + e_2)) \\ & + k_{31}(x)(\chi_3(x) - \chi_3(x + e_1) - \chi_1(x) + \chi_1(x + e_3)) \Big) \\ & + \sum_{x \in D_1} (\chi_2(x) k_{12}(x - e_1) - \chi_2(x + L e_1) k_{12}(x + (L - 1) e_1) \\ & \qquad - \chi_3(x) k_{31}(x - e_1) - \chi_3(x + L e_1) k_{r1}(x + (L - 1) e_1)) \\ & + \sum_{x \in D_2} (\chi_3(x) k_{23}(x - e_2) - \chi_3(x + L e_2) k_{23}(x + (L - 1) e_1) \\ & \qquad - \chi_1(x) k_{12}(x - e_2) - \chi_1(x + L e_2) k_{12}(x + (L - 1) e_2)) \\ & + \sum_{x \in D_3} (\chi_1(x) k_{31}(x - e_3) - \chi_1(x + L e_3) k_{31}(x + (L - 1) e_3) \\ & \qquad - \chi_2(x) k_{23}(x - e_3) - \chi_2(x + L e_3) k_{23}(x + (L - 1) e_3)) \,.\end{aligned} \tag{B.3}$$

The first sum is simply $(d\chi, k)$, and the remaining three sums, we will later on refer to them as B_i, account for possible corrections at the three boundaries $D_i = \{x | x_i = 0\}$. If A and χ obey C-periodic boundary conditions without a twist, they vanish and

$$(\chi, \delta k) = (d\chi, k) \,. \tag{B.4}$$

If the field k obeys twisted C-periodic boundary conditions, this is no longer true, the boundary conditions on k cannot be forged into boundary conditions of χ of the same form.

The transition functions, φ_j, are dual 0-forms and therefore 3-forms associated to the cubes. The boundary conditions on k are

$$\begin{aligned} A_{12}(x+e_iL) &= A_{12}(x) + \varphi_i(x) - \varphi_i(x-e_3) \\ A_{23}(x+e_iL) &= A_{23}(x) + \varphi_i(x) - \varphi_i(x-e_1) \\ A_{31}(x+e_iL) &= A_{31}(x) + \varphi_i(x) - \varphi_i(x-e_2)\,. \end{aligned} \tag{B.5}$$

The boundary terms are

$$\begin{aligned} B_1 &= \sum_{x\in D_1} \chi_2(x)(-\varphi_1(x)+\varphi_1(x-e_3)) - \chi_3(x)(-\varphi_1(x)+\varphi_1(x-e_2)) \\ B_2 &= \sum_{x\in D_2} \chi_3(x)(-\varphi_2(x)+\varphi_2(x-e_1)) - \chi_1(x)(-\varphi_2(x)+\varphi_2(x-e_3)) \\ B_3 &= \sum_{x\in D_3} \chi_1(x)(-\varphi_3(x)+\varphi_3(x-e_2)) - \chi_2(x)(-\varphi_3(x)+\varphi_3(x-e_1))\,. \end{aligned} \tag{B.6}$$

They can be interpreted as

$$B_i = (\chi_{D_i}, \delta\varphi_{D_i})\,, \tag{B.7}$$

where in this scalar product on the boundary, χ_{D_i} is the 1-form χ on the links of the boundary D_i and φ_{D_i} is the projection of the 3-form ϕ to the boundary D_i, where it now associates its values to plaquettes and therefore corresponds to a 2-form. We will now repeat the procedure we just applied in order to perform a partial integration in the boundary terms. This is again nontrivial because the transition function does not necessarily obey C-periodic boundary conditions. We rearrange the terms in B_1 to

$$\begin{aligned} B_1 &= \sum_{x\in D_1} \varphi_1(x)(\chi_3(x) - \chi_3(x+e_2) - \chi_2(x) + \chi_2(x+e_3)) \\ &\quad + \sum_{n=0}^{L-1} \varphi_1(ne_2-e_3)\chi_2(ne_2) - \varphi_1(ne_2+(L-1)e_3)\chi_2(ne_2+Le_3) \\ &\quad - \sum_{n=0}^{L-1} \varphi_1(ne_3-e_2)\chi_3(ne_2) - \varphi_1(ne_3+(L-1)e_2)\chi_2(ne_3+Le_2) \\ &= (d\chi_{D_1}, \phi_{D_1}) \\ &\quad + \sum_{n=0}^{L-1} \chi_2(ne_2)(\varphi_1(ne_2-e_3) - \varphi_1(ne_2+(L-1)e_3)) \\ &\quad - \sum_{n=0}^{L-1} \chi_3(ne_3)(\varphi_1(ne_3-e_2) + \varphi_1(ne_3+(L-1)e_2))\,. \end{aligned} \tag{B.8}$$

Note the difference in the sign in the last two lines. It is present because the boundary conditions in the Euclidean time direction, e_3, are periodic, and the boundary conditions in space are C-periodic. The terms for B_2 and B_3 are completely analogous. Let us now consider the sum of all three boundary terms

$$\begin{aligned} B_1 + B_2 + B_3 = \sum_{i=1}^{3} (d\chi_{D_l}, \varphi_{D_i}) + \\ + \sum_{n=0}^{L-1} \chi_3(ne_3) \Big((\varphi_2(ne_3 - e_1) + \varphi_2(ne_3 + (L-1)e_1)) \\ - (\varphi_1(ne_3 - e_2) + \varphi_1(ne_3 + (L-1)e_2)) \Big) \\ + \sum_{n=0}^{L-1} \chi_2(ne_2) \Big((\varphi_1(ne_2 - e_3) - \varphi_1(ne_2 + (L-1)e_3)) \\ - (\varphi_3(ne_2 - e_1) + \varphi_3(ne_2 + (L-1)e_1)) \Big) \\ + \sum_{n=0}^{L-1} \chi_1(ne_2) \Big((\varphi_3(ne_1 - e_2) + \varphi_3(ne_1 + (L-1)e_2)) \\ - (\varphi_2(ne_1 - e_3) - \varphi_2(ne_1 + (L-1)e_3)) \Big) . \end{aligned} \tag{B.9}$$

To make the appearance of the twist tensor in the boundary terms explicit, we make the substitutions

$$\tilde{\varphi}_1(x) = -\varphi_1(x - e_2 - e_3) , \quad \tilde{\varphi}_2(x) = -\varphi_2(x - e_1 - e_3) , \quad \tilde{\varphi}_3(x) = \varphi_3(x - e_1 - e_2) . \tag{B.10}$$

This substitution is equivalent to a general gauge transformation, and does therefore not affect the twist tensor. The sum over the boundary terms then reads,

$$\begin{aligned} B_1 + B_2 + B_3 = \sum_{i=1}^{3} (d\chi_{D_l}, \varphi_{D_i}) + \\ + \sum_{n=0}^{L-1} \chi_3(ne_3) \Big((-\tilde{\varphi}_2(ne_3 + e_3 + Le_1) - \tilde{\varphi}_2(ne_3 + e_3)) \\ - (-\tilde{\varphi}_1(ne_3 + e_3(L)e_2) - \tilde{\varphi}_1(ne_3 + e_3)) \Big) \\ + \sum_{n=0}^{L-1} \chi_2(ne_2) \Big((\tilde{\varphi}_1(ne_2 + e_2 + Le_3) - \tilde{\varphi}_1(ne_2 + e_2)) \\ - (\tilde{\varphi}_3(ne_2 + e_2 + Le_1) + \tilde{\varphi}_3(ne_2 + e_2)) \Big) \end{aligned}$$

$$+\sum_{n=0}^{L-1}\chi_1(ne_2)\Big((\tilde{\varphi}_3(ne_1+e_1Le_2)+\tilde{\varphi}_3(ne_1+e_1)) \\ -(\tilde{\varphi}_2(ne_1+e_1+Le_3)-\tilde{\varphi}_2(ne_1+e_1))\Big)\,. \tag{B.11}$$

Inserting the twist tensor, from eqs. (4.49) and (4.51), one arrives at the concise form

$$B_1+B_2+B_3=\sum_{i=1}^{3}(d\chi_{D_l},\phi_{D_i})+P_1n_{32}+P_2n_{13}-P_3n_{21}\,, \tag{B.12}$$

and indeed eq. (B.1) follows.

C. Closed and Exact Forms with Boundary Conditions

In the last step of the duality transformation, the integration over the 1-form χ with the constraint $d\chi = 0$, is replaced by an integration over the 0-form φ, with $\chi = d\varphi$. In the infinite volume the Poincaré Lemma assures that all closed forms are exact, i.e., for each χ with $d\chi = 0$ there exists a φ such that $d\varphi = \chi$.

In the finite volume this is no longer true. E.g., with periodic boundary conditions in the 3-direction, a constant 1-form with

$$\chi_1(x) = 0\,, \qquad \chi_2(x) = 0\,, \qquad \chi_3(x) = c\,, \tag{C.1}$$

obviously satisfies $d\chi = 0$ but cannot be written as $d\varphi$. This can be seen by looking at the Polyakov loop,

$$P_i = \sum_{n=0}^{N_i-1} \chi_i(ne_i). \tag{C.2}$$

If there is a 0-form φ such that $\chi = d\varphi$, P_i has to be zero, which clearly is not the case for a constant χ with $\chi_i(x) \neq 0$. For an example involving C-periodic boundary conditions consider

$$\chi_1(x) = \pi\,, \qquad \chi_2(x) = 0\,, \qquad \chi_3(x) = 0\,. \tag{C.3}$$

This 1-form satisfies $d\chi = 0 \mod 2\pi$. Furthermore,

$$P_1 - P_2 = \sum_{n=0}^{N_1-1} \chi_1(ne_1) - \sum_{n=0}^{N_2-1} \chi_2(ne_2) = N_1\pi\,. \tag{C.4}$$

If there exists a φ with $\chi = d\varphi$, from telescoping the sums one finds $P_1 = P_2$ and therefore $P_1 - P_2 = 0$. Thus, for N_1 odd, this 1-form is closed but not exact.

The 1-form χ of both examples can still be obtained as a derivative of a 0-form φ, if the proper twist is added to the boundary conditions of φ. In this appendix, we will give an explicit construction of such a 0-form, φ, plus boundary twists b_i, for any 1-form χ with $d\chi = 0$, such that $d\varphi = \chi$. We find it instructive to first consider periodic and then C-periodic boundary conditions in all directions, before discussing the actual case of interest, C-periodic boundary conditions in space and periodic boundary conditions in time. Note that the boundary conditions of χ in the constraint $d\chi = 0$ are strictly periodic or C-periodic. The twist on the boundary conditions of φ does not affect the boundary conditions of $d\varphi$.

This construction will not be unique. The additional redundancy corresponds to a global $O(2)$ symmetry in the spin system, which is not present in the link variables, χ. In the final step of the duality transform, the different boundary conditions will have to be summed over, and the redundancy be divided out.

Periodic Boundary Conditions

In the case of periodic boundary conditions, each χ can be written as $d\varphi$ for

$$\varphi(x,y,z) = \varphi(0,0,0) + \sum_{n=0}^{x-1} \chi_1(n,y,z) + \sum_{n=0}^{y-1} \chi_2(x,n,z) + \sum_{n=0}^{z-1} \chi_3(x,y,n) \tag{C.5}$$

with the boundary conditions,

$$\varphi(x + Le_i) = \varphi(x) + b_i\,, \tag{C.6}$$

where, $b_i = P_i$. The P_i are the Polyakov loops of the link variables χ and are given as

$$P_i = \sum_{n=1}^{L_i} \chi_i(x + ne_i)\,. \tag{C.7}$$

They are independent of x due to the constraint $d\chi = 0$. Then

$$\chi_i(x) = \varphi(x + e_i) - \varphi(x) \tag{C.8}$$

holds. The equation is trivially fulfilled in the bulk. On a link that extends over the boundary, it is easy to see that eq. (C.8) holds by considering, e.g.,

$$\begin{aligned}\varphi(L,y,z) - \varphi(L-1,y,z) &= \varphi(0,y,z) + b_1 - \varphi(L-1,y,z) \\ &= P_1 - \sum_{n=0}^{L-2} \chi_1(n,y,z) \\ &= \chi_1(L-1,y,z)\,.\end{aligned} \tag{C.9}$$

This construction fixes the boundary conditions and the field φ up to a global constant, $\varphi(0,0,0)$. In fact all 0-forms, φ with $d\varphi = \chi$, have to be of the form of eq. (C.5), since once $\varphi(0,0,0)$ is fixed, φ is uniquely determined by χ throughout the lattice. The redundancy corresponds to the global $O(2)$ symmetry of the spin model.

C-Periodic Boundary Conditions

For C-periodic boundary conditions, the situation is somewhat different. For a given field χ and boundary twists, b_i on φ, the value of $\varphi(x,y,z)$ is fixed by constraints from

any of the three lines that span the lattice through the point (x, y, z) as

$$\begin{aligned}
\varphi_{(1)}(x,y,z) &= \frac{1}{2}(b_1 + \sum_{n=0}^{x-1} \chi_1(n,y,z) - \sum_{n=x}^{L_1-1} \chi_1(n,y,z)) \\
\varphi_{(2)}(x,y,z) &= \frac{1}{2}(b_2 + \sum_{n=0}^{y-1} \chi_2(x,n,z) - \sum_{n=y}^{L_2-1} \chi_2(x,n,z)) \\
\varphi_{(3)}(x,y,z) &= \frac{1}{2}(b_3 + \sum_{n=0}^{z-1} \chi_3(n,y,n) - \sum_{n=z}^{L_3-1} \chi_3(x,y,n))\,. \qquad \text{(C.10)}
\end{aligned}$$

Because of the constraint $d\chi = 0$, the three values agree for suitable choices of b_i. Consider for instance,

$$\begin{aligned}
\varphi_{(1)}(x,y,z) - \varphi_{(2)}(x,y,z) &= \frac{1}{2}\Big(b_1 - b_2 + \sum_{n=0}^{x-1} \chi_1(n,y,z) - \sum_{n=x}^{L_1-1} \chi_1(n,y,z) \\
&\qquad - \sum_{n=0}^{y-1} \chi_2(x,n,z) + \sum_{n=y}^{L_2-1} \chi_2(x,n,z)\Big) \\
&= \frac{1}{2}\Big(b_1 - b_2 + \sum_{n=y}^{L_2-1} \chi_2(0,n,z) + \sum_{n=0}^{x-1} \chi_1(n,L_2,z) \\
&\qquad - \sum_{n=x}^{L_1-1} \chi_1(n,0,z) - \sum_{n=0}^{y-1} \chi_2(L_1,n,z)\Big) \\
&= \frac{1}{2}\Big(b_1 - b_2 + \sum_{n=y}^{L_2-1} \chi_2(0,n,z) - \sum_{n=0}^{x-1} \chi_1(n,0,z) \\
&\qquad - \sum_{n=x}^{L_1-1} \chi_1(n,0,z) + \sum_{n=0}^{y-1} \chi_2(0,n,z)\Big) \\
&= \frac{1}{2}\,(b_1 - b_2 + P_2 - P_1) \qquad \text{(C.11)}
\end{aligned}$$

If we choose b_i such that

$$b_i - b_j = P_i - P_j\,, \qquad \text{(C.12)}$$

for all i, j, then indeed, $\varphi_{(i)}(x,y,z) = \varphi_{(j)}(x,y,z)$. In the first step of the calculation above, we have made use of the fact that due to the constraint, $d\chi = 0$, the oriented sum of the links around any closed path inside the lattice vanishes. In particular, for the rectangular path from $(0,y,z)$ via (x,y,z) to (x,L_2,z) and back to $(0,y,z)$, we find

$$\sum_{n=0}^{x-1} \chi_1(n,y,z) + \sum_{n=y}^{L_2-1} \chi_2(x,n,z) - \sum_{n=0}^{x-1} \chi_1(n,L_2,z) - \sum_{n=y}^{L_2-1} \chi_2(0,n,z) = 0\,. \qquad \text{(C.13)}$$

An analogous relation holds for the path from $(x, 0, z)$ via (x, y, z) to (L_1, y, z) and back to $(x, 0, z)$. In the second step in eq. (C.11), we made use of the C-periodic boundary conditions.

The constraint, $d\chi = 0$, further restricts the values of P_i. Consider the sum over all plaquettes of a lattice boundary,

$$0 = \sum_{n_i=0}^{L_i} \sum_{n_j=0}^{L_j} d\chi_{ij}(n_i e_i + n_j e_j) = 2P_i - 2P_j \,. \tag{C.14}$$

This implies, that

$$b_i - b_j = 0 \mod \pi \,. \tag{C.15}$$

While in the case of periodic boundary conditions, $\varphi(0, 0, 0)$ was unconstrained by χ, for C-periodic boundary conditions one of the boundary twists b_i is free. As in the case of periodic boundary condition there is a global symmetry: $d\varphi$ is invariant under the change $\varphi' = \varphi + \delta$ and $b_i' = b_i + 2\delta$. The case of $\delta = \pi$, which leaves the boundary conditions invariant, corresponds to the $\mathbb{Z}_2$ symmetry that the global $O(2)$ symmetry is reduced to by the twisted C-periodic boundary conditions. From this global symmetry, as in the case of periodic boundary conditions, a redundancy of a factor of 2π arises.

Mixed Boundary Conditions

Let us now turn to the actual case of interest, namely C-periodic boundary conditions in space and periodic boundary conditions in time. Also here, we can give an explicit φ for a given $\chi = d\varphi$ as

$$\begin{aligned}
\varphi_{(1)}(x, y, z) &= \frac{1}{2}(b_1 + \sum_{n=0}^{x-1} \chi_1(n, y, z) - \sum_{n=x}^{L_1-1} \chi_1(n, y, z)) \\
\varphi_{(2)}(x, y, z) &= \frac{1}{2}(b_2 + \sum_{n=0}^{y-1} \chi_1(x, n, z) - \sum_{n=y}^{L_2-1} \chi_1(x, n, z)) \\
\varphi_{(3)}(x, y, z) &= \varphi_{(1,2)}(x, y, 0) + \sum_{n=0}^{z-1} \chi_1(n, y, n) \,.
\end{aligned} \tag{C.16}$$

Again, the constraint $d\chi = 0$ assures that the three definitions agree if the twists b_i are chosen such that

$$b_2 - b_1 = P_1 - P_2 \tag{C.17}$$

and

$$b_3 = P_3 \,. \tag{C.18}$$

The Polyakov loops P_i are restricted by the sum over all plaquettes of the lattice boundaries as

$$P_1 - P_2 = 0 \mod \pi \,, \tag{C.19}$$

and

$$0 = \sum_{n_3=0}^{L_3-1} \sum_{n_i=0}^{L_i-1} d\chi_{3i}(n_i e_i + n_3 e_3) = 2P_3 + P_i - P_i \,, \tag{C.20}$$

resulting in

$$b_1 - b_2 = 0 \mod \pi \,, \qquad\qquad b_3 = 0 \mod \pi \,. \tag{C.21}$$

The redundancy is the same as in the case of purely C-periodic boundary conditions. We obtain the final expression

$$Z = \frac{1}{2\pi} \left(\prod_{c_0} \int_{-\pi}^{\pi} d\varphi_{c_0} \int_{-\pi}^{\pi} db_1 \sum_{b_2 \in b_1, b_1+\pi} \sum_{b_3 \in 0,\pi} \right) \times \prod_{c_1} W(d\varphi_{c_1}) \exp(-i((b_1 - b_2)n_{23} - b_3 n_{12})) \,. \tag{C.22}$$

D. Monte Carlo Techniques

In lattice quantum field theory and statistical mechanics, one is interested in observables of the form

$$\langle O \rangle = \int \mathcal{D}\Phi W(\Phi) O(\Phi)\,, \tag{D.1}$$

where the integral is over all possible field configurations, i.e., an integral over the field values for each lattice site (or link in the case of a gauge theory). Except in some special cases, such an integral cannot be evaluated analytically, and one is forced to employ numerical techniques. Because the integral over $\mathcal{D}\Phi$ is extremely high-dimensional, also its numerical evaluation is a nontrivial endeavour.

Conventional numerical integration methods suffer from the curse of dimensionality [94], i.e., the required computational effort to achieve a certain precision grows exponentially with the number of dimensions of the integration domain. For an integral as in eq. (D.1), this corresponds to the number of points (or links, in the case of a gauge theory) of the lattice. In many interesting cases, the curse can be overcome with Monte Carlo techniques, where the high dimensional integration domain is sampled in a clever way: If the weight function $W(\Phi)$ is non-negative, it can be interpreted as a probability distribution and the integral in eq. (D.1) is then performed by evaluating O at configurations, Φ, drawn from that distribution.

This can be achieved by designing a Markov process, defined by an updating scheme that creates a new configuration Φ' from a current configuration, Φ, in a way that fulfills detailed balance,

$$\frac{P(\Phi \to \Phi')}{P(\Phi' \to \Phi)} = \frac{W(\Phi')}{W(\Phi)}\,, \tag{D.2}$$

and ergodicity. The term $P(\Phi \to \Phi')$ in the detailed balance condition refers to the probability that the configuration Φ' is obtained from the configuration Φ. The resulting configurations Φ then follow the distribution given by W, and $\langle O \rangle$ can be obtained as the mean of O evaluated at a set of configurations, generated in this way.

Metropolis Algorithm

Perhaps *the* paradigmatic Monte Carlo algorithm is the Metropolis algorithm [95, 96]. A new configuration Φ' that is obtained from Φ via a local change is proposed and then accepted according to the probability,

$$p = \min\left(1, \frac{W(\Phi')}{W(\Phi)}\right)\,, \tag{D.3}$$

to ensure detailed balance. The Metropolis algorithm can be applied to the integer gauge theory. There the field configuration corresponds to an integer ${}^*k$, associated to every link on the lattice.

A change is proposed as

$$ {}^*k'_{{}^*c_2} = {}^*k_{{}^*c_2} + \delta \,, \tag{D.4} $$

where ${}^*c_2$ is a random link and $\delta = \pm 1$ with a randomly chosen sign. The acceptance probability is then

$$ p = \min\left(1, \exp(-\Delta S)\right) \,, \tag{D.5} $$

where $\Delta S = S' - S$ is the change in the action induced by the proposed modification of the gauge field. The gauge field at a given link contributes to the field strength, $d{}^*k$, and thus to the action, at four different plaquettes, ${}^*c_1^{(n)}$, with the sign σ_n, such that

$$ \sigma_n d{}^*k_{{}^*c_1^{(n)}} = r_n^{\square} + {}^*k_{{}^*c_2} \,. \tag{D.6} $$

The four staple terms, $r_i^{\square}$ are independent of ${}^*k_{{}^*c_2}$. For the action dual to the Villain action, the overall change is,

$$ \begin{aligned} \Delta S &= \frac{g^2}{2} \left(\sum_{n=1}^{4} \left(k_{{}^*c_2} + \delta + r_n^{\square} \right)^2 - \sum_{n=1}^{4} \left(k_{{}^*c_2} + r_n^{\square} \right)^2 \right) \\ &= \frac{g^2}{2} \left(4\delta^2 + 8\delta k_{{}^*c_2} + 2\delta \sum_{n=1}^{4} r_n^{\square} \right) \,. \end{aligned} \tag{D.7} $$

For the action dual to the standard action, we find

$$ \exp(-\Delta S) = \prod_{n=1}^{4} \frac{I_{dk_{{}^*c_1^{(n)}} + \sigma_n \delta}(\beta)}{I_{dk_{{}^*c_1^{(i)}}}(\beta)} \,. \tag{D.8} $$

A sweep corresponds to $N_{\text{links}} = 3 \times N^2 \times N_t$ consecutive updates of the form described above, where N and N_t correspond to the spatial and Euclidean time extent of the lattice, respectively.

Heatbath Algorithm

In the heat bath algorithm, a new configuration is again obtained by a local update of a single degree of freedom. Detailed balance is fulfilled by setting

$$ P(\Phi \to \Phi') = c(\Phi) W(\Phi'), \tag{D.9} $$

where the constant, c, may depend on the configuration, but not on the degree of freedom that is updated, such that $c(\Phi) = c(\Phi')$.

We employ this method for the action dual to the Villain action. There the distribu-

tion, $W(\Phi)$, is Gaussian and thus straightforward to sample. It is realized as follows. A link, ${}^*c_2$, is chosen at random and the associated gauge field, ${}^*k_{{}^*c_2}$, is sampled from the distribution

$$p({}^*k'_{{}^*c_2}) = \exp\left(-\frac{g^2}{2}\left({}^*k'_{{}^*c_2} + \sum_{n=1}^{4} r_n^{\sqcap}\right)\right) . \tag{D.10}$$

Again, $3 \times N^2 \times N_t$ consecutive updates are referred to as a sweep.

Overrelaxation

A way to reduce simulation time auto-correlations in Monte Carlo calculations is to introduce deterministic overrelaxation sweeps between stochastic updates. In a micro-canonical overrelaxation step, the configuration is changed locally in a way that leaves the action invariant. For the gauge theory dual to the Villain action, this can be achieved by choosing

$${}^*k'_{{}^*c_2} = -{}^*k_{{}^*c_2} - \frac{1}{2}\sum_{n=1} r_n^{\sqcap}, \tag{D.11}$$

if the sum over the staple terms is even. If it is odd, no update is performed. In an overrelaxation sweep, the above transformation is applied to all links of the lattice as follows. In a loop over all lattice sites that passes systematically from timeslices to timeslice, at each site all three links that exit the site are updated. In the numerical calculations of the vortex mass for the Villain action, every fifth sweep is replaced by an overrelaxation sweep. A comparison of different updating schemes, Metropolis only, heatbath only, and heatbath with overrelaxation is shown in Figure D.1 for a test observable. The autocorrelation function decreases significantly faster if overrelaxation steps are inserted.

For the action dual to the standard action, the weight as a function of a local change, δ, in the Metropolis setup is not a symmetric function of δ, and therefore a simple overrelaxation step as described above is not possible.

Implementation of the Vortex Operator

We have seen that the vortex creation operator is

$$\Phi(x) = \exp(-2\pi i({}^*B_x, {}^*k)) = \exp(-2\pi i \Delta_2^{-1}\delta_2 {}^*k) . \tag{D.12}$$

In this section, we discuss how the vortex operator can be implemented in a Monte Carlo simulation. In order to be completely explicit, we will again use component notation and denote the integer gauge field as $k_i(x) = {}^*k({}^*c_2)$, where i denotes the direction the dual link, ${}^*c_2$, points to from the site x on the dual lattice.

In this explicit notation, the spatial divergence, of the dual gauge field $k_i(x)$ is given as

$$\delta_2 k(x) = k_1(x) - k_1(x - e_1) + k_2(x) - k_2(x - e_2) , \tag{D.13}$$

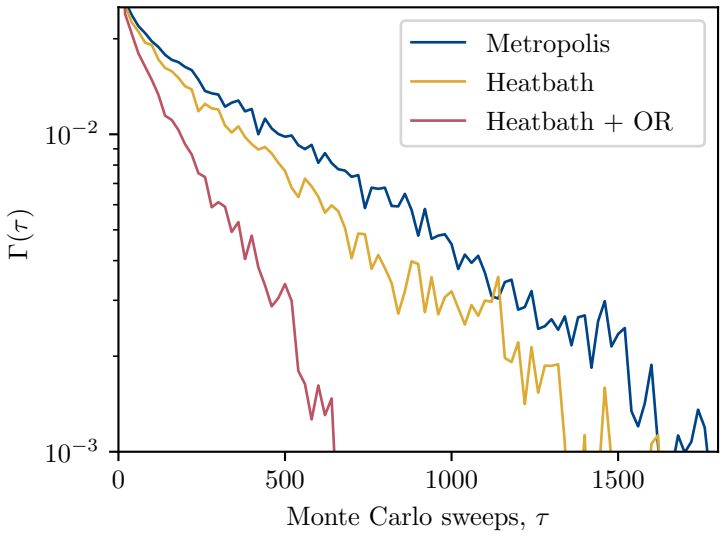

Figure D.1.: A comparison of different updating schemes. The autocorrelation function of a test observable, the vortex correlation function at euclidean time distance $t = a$, on an $8 \times 8 \times 16$ lattice. The action dual to the Villain action is used with coupling $g^2 = 2.94$. The Metropolis and heatbath schemes perform comparably. If every fifth sweep is replaced by an overrelaxation sweep ("Heatbath + OR"), the correlations decay much faster.

where C-periodic boundary conditions are employed. In lattice units, where $a = 1$, the inverse Laplacian for a generic field associated to the dual lattice sites, $\phi(x)$, can be constructed explicitly with the help of Fourier transforms as,

$$\Delta^{-1}\phi(x) = \frac{1}{N^2}\sum_{p}\frac{\exp(ipx)}{\hat{p}^2}\sum_{x'}\exp(-ipx')\phi(x')\,. \tag{D.14}$$

The summation extends over

$$p = \frac{2\pi}{N}\left(n_1 + \frac{1}{2}, n_2 + \frac{1}{2}\right)\,, \tag{D.15}$$

with $n_i \in \{0, \ldots, N-1\}$, and furthermore

$$\hat{p}^2 = 4 - 2\cos(p_1) - 2\cos(p_2)\,. \tag{D.16}$$

To convince ourselves that this is the inverse Laplacian, we consider

$$\begin{aligned}\Delta\Delta^{-1}\phi(x) &= 4\Delta^{-1}\phi(x) + \sum_{i=1}^{2}\left(\Delta^{-1}\phi(x-e_i) + \Delta^{-1}\phi(x+e_i)\right) \\ &= \frac{1}{N^2}\sum_p \left(4 - \sum_{i=1}^{2}\left(\exp(ip_i) + \exp(-ip_i)\right)\right)\frac{\exp(ipx)}{\hat{p}^2}\sum_{x'}\exp(-ipx')\phi(x') \\ &= \frac{1}{L^2}\sum_p \exp(ipx)\sum_{x'}\exp(-ipx')\phi(x') \\ &= \phi(x)\,. \end{aligned} \tag{D.17}$$

In the second line, we have used the fact that $\exp(ipx)$ is C-periodic due to the momentum shift of π/L. Had we worked with periodic boundary conditions, the above construction would formally work analogously, then without the momentum shift. In that case, $\hat{k}^2 = 0$ would be part of the summation and the above expression would thus be ill-defined. The operator can also be expressed in terms of the standard discrete Fourier transforms,

$$\begin{aligned} DFT(\phi)(n) &= \sum_{x_1=0}^{N-1}\sum_{x_2=0}^{N-1}\exp(-2\pi/Ni(x_1n_1 + x_2n_2))\phi(x) = \tilde{\phi}(n) \\ DFT^{-1}(\tilde{\phi})(x) &= \sum_{n_1=0}^{N-1}\sum_{n_2=0}^{N-1}\frac{1}{N^2}\exp(2\pi/Ni(x_1n_1 + x_2n_2))\tilde{\phi}(n) = \phi(x) \end{aligned} \tag{D.18}$$

In terms of these, the inverse Laplacian can be expressed as

$$\Delta^{-1}\phi(x) = \exp(i\pi/Lx)DFT^{-1}\left(\frac{DFT\left(\phi'\right)}{g}\right)(x) \tag{D.19}$$

with

$$\begin{aligned}\phi'(x) &= \exp\left(\frac{-i\pi x}{N}\right)\phi(x) \\ g(n) &= 4 + \cos(2\pi/L(n_1 + 1/2) + \cos(2\pi/L(n_2 + 1/2))\,. \end{aligned} \tag{D.20}$$

This version is used in the Monte Carlo calculation presented in this work. We employ the very efficient Fast Fourier Transform implementation from the FFTW library [97] to calculate the DFT.

Wolff Algorithm

For the $O(2)$ model, an extremely efficient cluster algorithm is available, namely the Wolff algorithm [90], an adaptation of the Swendsen-Wang algorithm [98] for Potts models to $O(n)$ models. In contrast to the local heatbath and Metropolis algorithms, where the

configuration is updated by changing a single degree of freedom at a time, in the Wolff cluster algorithm, the spin degrees of freedoms are grouped into clusters that are then updated jointly.

For the calculation of the helicity modulus in the spin formulation of the $O(2)$ model, we employ the Wolff algorithm in its single cluster version. For the $O(2)$ model, it works as follows.

1. Choose a random angle $w \in \{-\pi, \pi\}$, and a random starting site c_0. Add c_0 to the queue, and to the cluster, $\mathcal{C}$.

2. Remove a site, c_0, from the queue, and activate a bond on each link, c_1, attached to c_0 with probability, $p(c_1, w, \varphi)$. If the bond is activated and the site it connects to, c_0', is not in the cluster, append c_0' to the cluster and to the queue.

3. As long as the queue is not empty, go to step 2.

4. Flip the cluster at the angle w, i.e.,

$$\varphi'_{c_0} = 2w - \varphi_{c_0} \quad \forall c_0 \in \mathcal{C}\,. \tag{D.21}$$

The probabilities to add a bond at a given link are given by

$$p(c_1, w, \varphi) = 1 - \min\left(1, \frac{\exp(-s(d\varphi_{c_1}))}{\exp(-s(d\varphi'_{c_1}))}\right)\,, \tag{D.22}$$

where $s(d\varphi_{c_1})$, is the contribution of the link c_1 to the action and in $d\varphi'_{c1}$, one of the degrees of freedom, φ, attached to the link c_1 is flipped at w. For the standard action, this probability simplifies to

$$p(c_1, w, \varphi) = 1 - \min\Big(1, \exp(-2\beta\cos(\varphi_{c_0} - w)\cos(\varphi_{c_0'} - w)\Big)\,, \tag{D.23}$$

where the link c_1 connects the site c_0 to c_0'. For the Villain action, one cannot make such a simplification and we simply use

$$p(c_1, w, \varphi) = 1 - \min\left(1, \frac{\sum_{n\in\mathbb{Z}} \exp\left(-1/g^2(d\varphi_{c_1} + 2\pi n)^2\right)}{\sum_{n\in\mathbb{Z}} \exp\left(-1/g^2(d\varphi'_{c_1} + 2\pi n)^2\right)}\right)\,. \tag{D.24}$$

In the numerical simulations, the sums over n are truncated at $n = \pm 5$. At the couplings that are relevant for our purposes, the thereby introduced discrepancy to the true acceptance probability is smaller than machine precision.

E. Fitting Masses

The Monte Carlo simulations yield estimates for the vortex correlation function, $\langle c_{\pm}(t)\rangle$ and its covariance matrix, $\sigma_{tt'} = \mathrm{Cov}(c_{\pm}(t)c_{\pm}(t))$. A Euclidean time correlation function has the following form,

$$g(t) = \sum_n a_n \left(\exp(-E_n t) + \exp(-E_n(T-t))\right) . \tag{E.1}$$

At large Euclidean time separation, $g(t)$ is dominated by the contribution from the lowest energy state, E_0. Therefore, in order to retrieve m and E, we neglect contributions from excited state and fit

$$g(t) = a \left(\exp(-mt) + \exp(-m(T-t))\right) \tag{E.2}$$

to the Monte Carlo data by minimizing

$$\chi^2 = \sum_{t=t_0}^{T-t_0} \sum_{t'=t_0}^{T-t_0} \left(g(t) - \langle c(t)\rangle\right) (\sigma^{-1})_{tt'} \left(g(t') - \left\langle c(t')\right\rangle\right) . \tag{E.3}$$

The optimization is performed with the help of the SciPy library [67]. The approximation of the two-point function with eq. (E.2) is only justified for sufficiently large Euclidean time separations. That is, t_0 has to be chosen sufficiently large in the fit. This is a delicate matter and may be the source of a systematic error. Here we employ a Bayesian model averaging method [99], where the fit is performed for different values of t_0 between 0 and $t_0^{\max}$ and the retrieved masses are averaged according to

$$\langle m\rangle = \sum_{t_0=0}^{t_0^{\max}} \langle m\rangle_{t_0} \, pr(t_0|D) \tag{E.4}$$

In the above equation, $\langle m\rangle_{t_0}$ corresponds to the best fit result for m in a fit with a fixed value of t_0, according to eq. (E.3). In the cases where the vortex mass is large, for t larger than some t_t, the vortex correlation function is consistent with zero. In order to exclude the very unstable cases, where only values consistent with zero enter the fit, we use $t_0^{\max} = \max(3, t_t - 4)$. The term $pr(t_0|D)$ corresponds to the model weight, i.e., the probability assigned to the model, which in our case corresponds to a specific value of t_0, given the data. It can be approximated as [99]

$$-2\log(pr(t_0|D)) \approx -2\log(pr(t_0)) + \chi^2 + 2k + 4t_0 . \tag{E.5}$$

Here, k is the number of parameters in the model, i.e. $k = 2$ in our case and $pr(t_0)$ is the prior attributed to t_0. We use a flat prior distribution, i.e., $pr(t_0) = 1/(t_0^{\max} + 1)$. An uncertainty can be associated to m according to

$$\begin{aligned}\sigma_m^2 &= \langle m^2 \rangle - \langle m \rangle^2 \\ &= \sum_{t_0}^{t_0^{\max}} \sigma_{m,t_0}^2 pr(t_0|D) + \sum_{t_0}^{t_0^{\max}} \langle m^2 \rangle_{t+0} \, pr(t_0|D) - \left(\sum_{t_0=0}^{t_0^{\max}} \langle m^2 \rangle_{t_0} \, pr(t_0|D) \right)^2 . \end{aligned} \tag{E.6}$$

The first term corresponds to the model average of the statistical errors for the various fit ranges and the remaining terms account for systematic errors due to the choice of t_0. The procedure is illustrated in Figures E.1 and E.2, for two examples, from the dataset used in Chapter 5. In the case shown in Figure E.1, the mass is much smaller than for the case shown in Figure E.2, and $t_0^{\max}$ is therefore much larger. Both cases are handled well by the model averaging procedure.

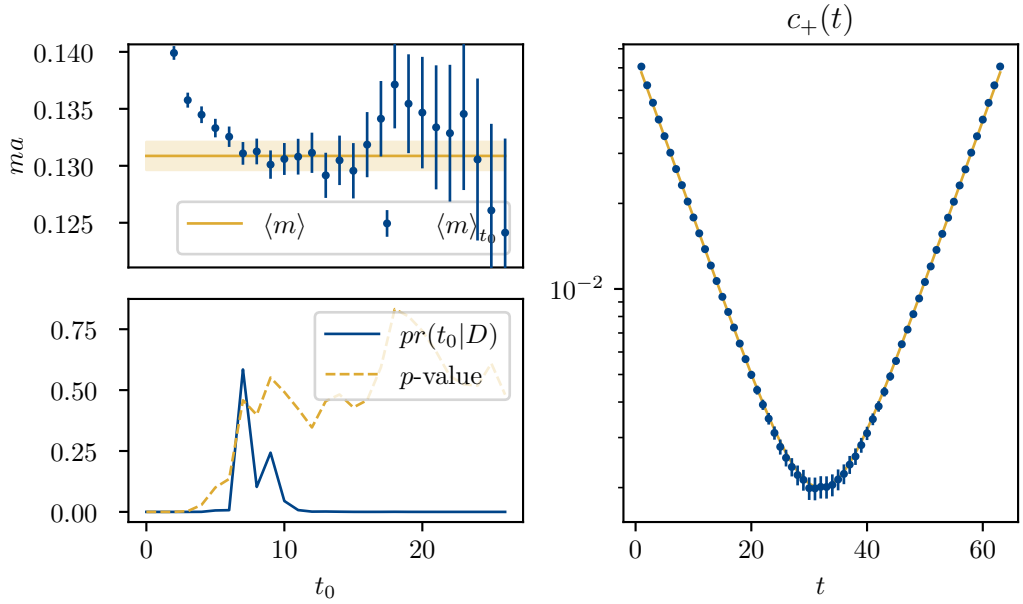

Figure E.1.: Illustration of the model averaging procedure to extract the vortex mass from $c_+(t)$ at $L = 1.43$ and $g^2 = 2.976$. The plot on the right shows the correlation function from Monte Carlo simulations and the best fit, using the model averaged parameters. On the left, the masses from fits with fixed $t_0 \in \{0, t_0^{\text{mass}}\}$ (top), and the model probability as well as the p-values of the fits are displayed. The latter refers to the probability, to draw a value bigger than the χ^2 of the fit from a χ^2-distribution, and is shown for comparison.

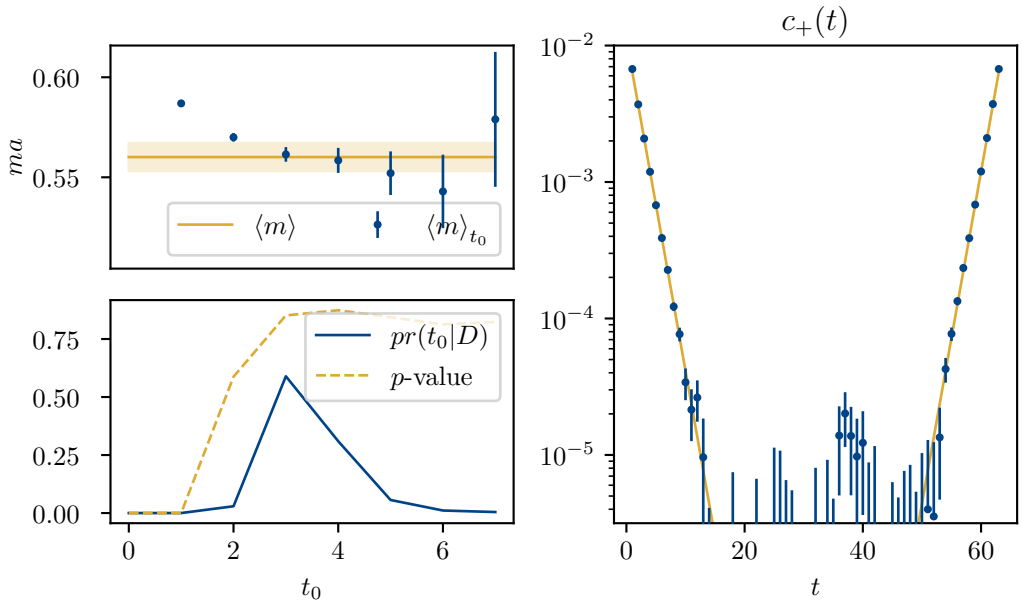

Figure E.2.: Illustration of the model averaging procedure to extract the vortex mass from $c_+(t)$, for $L = 3.57$ and $g^2 = 2.924$. The same plots as in Figure E.1

Part II.

Effective Low-Energy Theory for Spin Chains in a Strong Magnetic Field

7. The $SU(2)$ Spin Chain Close to Saturation

7.1. The XXZ Spin Chain

We consider a chain of N $SU(2)$ quantum spins in the fundamental representation, $\{2\}$. The length of the chain is $L = aN$, however, we will mostly work in the limit $N \to \infty$, otherwise periodic boundary conditions are assumed. Here a denotes the lattice spacing. The spins form the Hilbert space $\mathbb{C}^{2N}$, on which the local spin operators act. A local basis of the Hilbert space is given by

$$|s_0 s_a \dots s_{Na}\rangle = \bigotimes_x |s_x\rangle \tag{7.1}$$

with $s_x \in \{\uparrow, \downarrow\}$. The spin operators obey the following commutation relations

$$[S_x^a, S_y^b] = i\delta_{xy}\epsilon_{abc}S_x^c \,. \tag{7.2}$$

We choose the 3-direction as quantization axis. Then the spin operators are given in terms of the Pauli matrices

$$S_x^a = \frac{1}{2}\sigma_a \,. \tag{7.3}$$

From the spin operators, the rising and lowering operators are constructed as

$$S_x^{\pm} = S_x^1 \pm iS_x^2 \,. \tag{7.4}$$

We consider the XXZ-Hamiltonian with an external magnetic field, μ, in the 3-direction.

$$H = J\sum_x \left(\frac{1}{2}(S_x^+ S_{x+a}^- + S_x^- S_{x+a}^+) + \Delta S_x^3 S_{x+a}^3\right) - \mu\sum_x S_x^3 \,. \tag{7.5}$$

Furthermore, we restrict the discussion to the case of $|\Delta| > 1$.

This model has a $U(1)$ symmetry generated by $S^3 = \sum_x S_x^3$, and a full $SU(2)$ symmetry for $\Delta = 1$ and $\mu = 0$ (the isotropic Heisenberg Hamiltonian). This can be seen from the

following expression,

$$\begin{aligned}
[H, S^a] &= J \sum_y \left[\sum_x S^1_x S^1_{x+a} + S^2_x S^2_{x+a} + \Delta S^3_x S^3_{x+a}, S^a_y \right] \\
&= J \sum_x \Big([S^1_x, S^a_x](S^1_{x-a} + S^1_{x+a}) + [S^2_x, S^a_x](S^2_{x-a} + S^2_{x+a}) \\
&\qquad + \Delta [S^3_x, S^a_x](S^3_{x-a} + S^3_{x+a}) \Big) \\
&= iJ \sum_x \Big(\epsilon_{1ac} S^c_x (S^1_{x-a} + S^1_{x+a}) + \epsilon_{2ac} S^c_x (S^2_{x-a} + S^2_{x+a}) \\
&\qquad + \Delta \epsilon_{3ac} S^c_x (S^3_{x-a} + S^3_{x+a}) \Big) \,. \qquad (7.6)
\end{aligned}$$

For $a = 3$, the commutator vanishes for arbitrary Δ, and for $\Delta = 1$ it vanishes for all a. The term μS^3 in the Hamiltonian only commutes with S^3 and therefore breaks the global $SU(2)$ symmetry, even for $\Delta = 1$. The remaining $U(1)$ symmetry allows us to investigate the Hamiltonian in sectors of fixed magnetization, S^3. In addition there is translation symmetry by one lattice spacing, i.e., the Hamiltonian commutes with the translation operator T_a. This symmetry allows us to characterize the eigenstates of the Hamiltonian in terms of their momenta, the eigenvalues of the translation operator. For $J < 0$, this is a model for ferromagnetism and for $J > 0$ for antiferromagnetism.

In addition, for N even, there is a unitary transformation

$$U = \prod_{x=a}^{Na/2} 2 S^3_{2x} \,, \qquad (7.7)$$

that maps $J \to -J$ and $\Delta \to -\Delta$, as

$$\begin{aligned}
UHU^\dagger &= U \left(J \sum_x \left(\frac{1}{2} (S^+_x S^-_{x+a} + S^-_x S^+_{x+a}) + \Delta S^3_x S^3_{x+a} \right) - \mu \sum_x S^3_x \right) U^\dagger \\
&= -J \sum_x \left(\frac{1}{2} (S^+_x S^-_{x+a} + S^-_x S^+_{x+a}) - \Delta S^3_x S^3_{x+a} \right) - \mu \sum_x S^3_x \,. \qquad (7.8)
\end{aligned}$$

Therefore, two Hamiltonians with $J_1 = -J_2$ and $\Delta_1 = -\Delta_2$ have the same spectrum. E.g., a ferromagnet ($J < 0$) with $\Delta = -1$ is unitarily equivalent to an isotropic antiferromagnet ($J > 0, \Delta = 1$). The respective eigenstates are related as $|\psi_1\rangle = U |\psi_2\rangle$.

In the presence of a strong magnetic field, $\mu \gg |J\Delta|$, the ground state of the Hamiltonian is the state with all spins aligned along the magnetic field,

$$|S\rangle = |\uparrow\uparrow \ldots \uparrow\rangle \,, \qquad (7.9)$$

the unique state with the largest possible S^3-magnetization,

$$S^3 |S\rangle = N\frac{1}{2} |S\rangle \ . \tag{7.10}$$

Its energy is

$$H |S\rangle = E_s |S\rangle = \left(\frac{JN\Delta}{4} - \frac{\mu N}{2}\right) |S\rangle \ . \tag{7.11}$$

In the following we will diagonalize the Hamiltonian in the magnetization sectors $\Delta S^3 = -1$ and $\Delta S^3 = -2$, corresponding to one and two flipped spins, in the background of the saturated state respectively. These flipped spins will be referred to as defects. Even though the spin one-half XXZ chain is exactly diagonalizable with the Bethe ansatz [100, 101], we will pursue a more elementary (and more explicit) approach and directly solve the stationary Schrödinger equation in the symmetry sectors that contain the states we are interested in. This method is also applicable to the $SU(3)$ spin chain.

7.2. Defects Close to Saturation

We start with the $\Delta S^3 = -1$ sector, i.e., one flipped spin in the saturated background. A complete basis of this sector consists of the states with all spins except one up and one spin down. We will refer to such states as $|x\rangle$, where x refers to the location of the down spin. Up to normalization such a state corresponds to

$$|x\rangle = S^-_x |S\rangle \ . \tag{7.12}$$

The Hamiltonian acts on $|x\rangle$ as

$$H |x\rangle = \left(J\Delta\frac{(N-4)}{4} - \mu\frac{(N-2)}{2}\right) |x\rangle + \frac{J}{2} |x+a\rangle + \frac{J}{2} |x-a\rangle \ . \tag{7.13}$$

We can construct eigenstates of the translation operator for each momentum in the Brillouin zone, $p \in \{0, \pm 2\pi/L, \ldots, \pm\pi/a\}$,

$$|p\rangle = \sum \exp(ipx) |x\rangle \ . \tag{7.14}$$

It is easy to see, that those are eigenstates of the XXZ-Hamiltonian,

$$H |p\rangle = (J\Delta(N-4)/4 - \mu(N-2)/2 + J\cos(ap)) |p\rangle \ , \tag{7.15}$$

and therefore have the well defined energy

$$E_p = E_S - J\Delta + \mu + J\cos(ap) \, . \tag{7.16}$$

For a ferromagnetic coupling, $J < 0$, the low-energy physics of that sector is concentrated around $p = 0$, and for an antiferromagnetic coupling, $J > 0$, around $p = \pi/a$. This is

consistent with the unitary equivalence of two models with $J_1 = -J_2$ and $\Delta_1 = -\Delta_2$, since under the transformation U, that maps $\Delta \to -\Delta$ and $J \to -J$, the states $|p\rangle$ transform as

$$\begin{aligned} U|p\rangle &= \sum_x \exp(ipx) U|x\rangle = \sum_x \exp(ipx)(-1)^{x/a}|x\rangle \\ &= \sum_x \exp(i(p+\pi/a)x)|x\rangle = |p+\pi/a\rangle \ . \end{aligned} \tag{7.17}$$

Let us now turn to the $\Delta S^3 = -2$ sector, i.e., two flipped spins in a saturated background. We diagonalize the Hamiltonian in this sector by imposing stability conditions on the solutions to the recursion relation corresponding to the stationary Schrödinger equation.

Up to normalization, a basis of this sector consists of the $N(N-1)/2$ states

$$|x,y\rangle := S_x^- S_y^- |S\rangle \ , \tag{7.18}$$

with $y \geq x + a$. From those, a translation invariant basis can be constructed as

$$|p,r\rangle := \sum_x \exp(ipx)|x, x+r\rangle \ . \tag{7.19}$$

In this set, there are again $N(N-1)/2$ states: we have N momenta in the Brillouin zone, for each of which r can vary from 1 to $N-1$, however in that way each state is counted twice, giving the factor of $1/2$. Under the unitary transformation U, the states $|p,r\rangle$ transform as

$$U|p,r\rangle = \sum_x \exp(ipx)(-1)^{x/a}(-1)^{(x+r)/a}|x,x+r\rangle = \exp(i\pi r/a)|p,r\rangle \ . \tag{7.20}$$

In the $\Delta S^3 = -1$ sector, translation invariance is sufficient to diagonalize the Hamiltonian which is not the case here. With

$$\begin{aligned} H|x,x+r\rangle = &\left(\frac{J\Delta}{4}(N-8) - \frac{\mu}{2}(N-4)\right)|x,x+r\rangle \\ &+ \frac{J}{2}\left(|x+a,x+r\rangle + |x-a,x+r\rangle + |x,x+r+a\rangle + |x,x+r-a\rangle\right) \end{aligned} \tag{7.21}$$

for $r > a$, and

$$\begin{aligned} H|x,x+a\rangle = &\left(\frac{J\Delta}{4}(N-4) - \frac{\mu}{2}(N-4)\right)|x,x+a\rangle \\ &+ \frac{J}{2}\left(|x-a,x+a\rangle + |x,x+2a\rangle\right) \ , \end{aligned} \tag{7.22}$$

we find that the states, $|p, r\rangle$, transform as

$$\begin{aligned} H\,|p,r\rangle &= \left(\frac{J\Delta}{4}(N-8) - \frac{\mu}{2}(N-4)\right)|p,r\rangle + J\left(w\,|p,r+a\rangle + \overline{w}\,|p,r-a\rangle\right) \\ H\,|p,a\rangle &= \left(\frac{J\Delta}{4}(N-4) - \frac{\mu}{2}(N-4)\right)|p,r\rangle + J\left(w\,|p,2a\rangle\right)\,. \end{aligned} \tag{7.23}$$

We have introduced the notation $w = (1 + \exp(ipa))/2$. To find eigenstates of the Hamiltonian, we make the general ansatz

$$|\psi, p\rangle = \sum_r \psi(r)\,|p,r\rangle\ , \tag{7.24}$$

and act on it with the Hamiltonian,

$$\begin{aligned} H\,|\psi,p\rangle = &\left[J\overline{w}\psi(2a) + \left(\frac{J\Delta}{4}(N-4) - \frac{\mu}{2}(N-4)\right)\psi(a)\right]|p,a\rangle \\ &+ \sum_r \left[J\left(w\psi(r-a) + \overline{w}\psi(r+a)\right) + \left(\frac{J\Delta}{4}(N-8) - \frac{\mu}{2}(N-4)\right)\psi(r)\right]|p,r\rangle\,. \end{aligned} \tag{7.25}$$

The stationary Schrödinger equation, i.e., the condition that $|\psi, p\rangle$ is an eigenstate of H,

$$H\,|\psi,p\rangle = E\,|\psi,p\rangle\ , \tag{7.26}$$

gives a second order recursion relation for the wave function $\psi(r)$,

$$\begin{aligned} \epsilon\psi(r) &= w\psi(r-a) + \overline{w}\psi(r+a) && r > a \\ (\epsilon - \Delta)\psi(a) &= \overline{w}\psi(2a) && r = a\,, \end{aligned} \tag{7.27}$$

where we have introduced the dimensionless energy parameter

$$\epsilon = \frac{1}{J}\left(E - \frac{J\Delta}{4}(N-8) + \frac{\mu}{2}(N-4)\right) = \frac{1}{J}\left(E - E_S + 2J\Delta - 2\mu\right)\,. \tag{7.28}$$

This recursion relation can be brought into matrix form

$$\begin{pmatrix}\psi(r+a)\\ \psi(r)\end{pmatrix} = M\begin{pmatrix}\psi(r)\\ \psi(r-a)\end{pmatrix}, \tag{7.29}$$

where the matrix, M, is

$$M = \begin{pmatrix}\epsilon/\overline{w} & -w/\overline{w}\\ 1 & 0\end{pmatrix}\,. \tag{7.30}$$

In the limit $N \to \infty$, the recursion is solved by

$$\begin{pmatrix} \psi(r) \\ \psi(r-a) \end{pmatrix} = M^{r/a-2} \begin{pmatrix} \psi(2a) \\ \psi(a) \end{pmatrix} . \tag{7.31}$$

Writing $(\psi(2a), \psi(a))^T$ in terms of eigenvectors of M, assuming that $\lambda_+ \neq \lambda_-$, gives

$$\psi(r) = A\lambda_+^{r/a} + B\lambda_-^{r/a} . \tag{7.32}$$

This solution is implicit, as the matrix M depends on ϵ, which is still unknown. From stability considerations, we now derive conditions on ϵ to obtain explicit solutions. We consider an infinite system, and impose that the states are normalizable, either to 1, which will lead us to localized states or to a delta function, which gives scattering states.

7.3. Localized Two-Defect States

A necessary condition on the state $|\psi, p\rangle$ to be normalizable to 1 in the limit $N \to \infty$, is $\psi(r) \to 0$ for $r \to \infty$. The solution to the recursion relation, eq. (7.31), can be of that form if M has at least one eigenvalue of absolute value less than one. The matrix M has eigenvalues and eigenvectors,

$$\begin{aligned} \lambda_+ &= \frac{\epsilon + \sqrt{\epsilon^2 - 4w\overline{w}}}{2\overline{w}} & \lambda_- &= \frac{\epsilon - \sqrt{\epsilon^2 - 4w\overline{w}}}{2\overline{w}} \\ v_+ &= \begin{pmatrix} \lambda_+ \\ 1 \end{pmatrix} & v_- &= \begin{pmatrix} \lambda_- \\ 1 \end{pmatrix} . \end{aligned} \tag{7.33}$$

The absolute value of $\lambda_\pm$ is plotted in Figure 7.1. Since $|\lambda_+| < 1$ implies $|\lambda_-| > 1$ and vice versa, at most one eigenvalue is of absolute value less than one at any given ϵ. A localized state is therefore possible only if the initial condition vector, $(\psi(2a), \psi(a))^T$, is proportional to the eigenvector with eigenvalue of absolute value smaller than one. This condition corresponds to the following equation,

$$\lambda_\pm = \frac{\epsilon - \Delta}{\bar{w}} , \tag{7.34}$$

which has a solution that is valid in both cases, + and −, namely

$$\epsilon = \frac{w\bar{w} + \Delta^2}{\Delta} = \frac{\cos(ap) + 2\Delta^2 + 1}{2\Delta} . \tag{7.35}$$

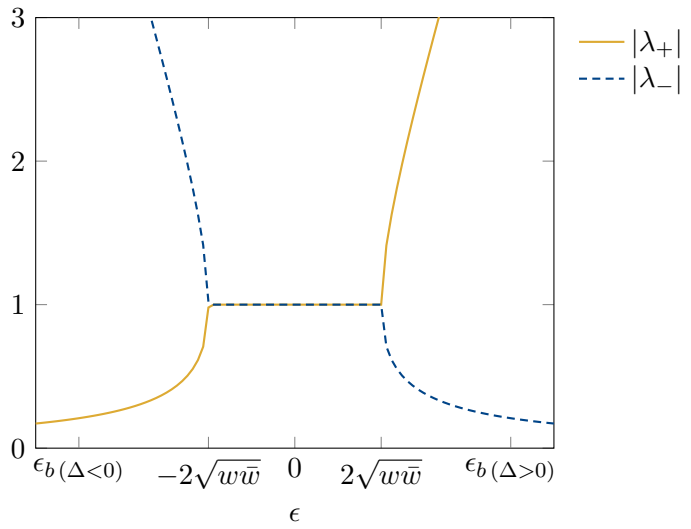

Figure 7.1.: The absolute values of $\lambda_\pm$ (the eigenvalues of the recursion relation matrix M). Note that $|\lambda_+| < 1$ implies $|\lambda_-| > 1$.

It depends on the sign of Δ, which of the eigenvalues is of magnitude less than one. If we plug the resulting ϵ back into the expressions for $\lambda_\pm$, we find

$$\begin{aligned}\lambda_\pm &= \frac{1}{2\Delta\overline{w}}\left(w\overline{w} + \Delta^2 \pm \Delta\sqrt{\frac{\left(\Delta^2 - w\overline{w}\right)^2}{\Delta^2}}\right) \\ &= \frac{1}{2\Delta\overline{w}}\left(w\overline{w} + \Delta^2 \pm \operatorname{sgn}(\Delta)(\Delta^2 - w\overline{w})\right)\,.\end{aligned} \tag{7.36}$$

In the second line we have imposed that $|\Delta| \geq 1$. Simplifying further, we find

$$\begin{aligned}\Delta > 0: &\qquad \lambda_+ = \frac{\Delta}{\overline{w}}\,, &&\qquad \lambda_- = \frac{w}{\Delta}\,, \\ \Delta < 0: &\qquad \lambda_- = \frac{\Delta}{\overline{w}}\,, &&\qquad \lambda_+ = \frac{w}{\Delta}\,.\end{aligned} \tag{7.37}$$

The eigenvalue of absolute value less than 1 is therefore always w/Δ, corresponding to λ_- for $\Delta > 0$ and to λ_+ for $\Delta < 0$.

The reduced energy, ϵ, from eq. (7.35) corresponds to a total energy for the localized state of

$$E_{\text{loc}} = E_S - J\Delta + 2\mu + J\left(\frac{\cos(ap)+1}{2\Delta}\right)\,. \tag{7.38}$$

Note that for $\Delta = 1$ and $\mu = 0$, we recover the well known result for the bound state energy $E = E_S - J\sin^2(ap/2)$ for the isotropic Heisenberg Model [100]. The wave

function $\psi(r)$ follows from eq. (7.31) as

$$\begin{aligned}\psi(r) &= \lambda_{\pm}^{r/a-1}\psi(a) = C\lambda_{\pm}^{r/a} = C\left(\frac{w}{\Delta}\right)^{r/a} \\ &= C\left(\frac{\cos(ap/2)}{\Delta}\right)^{r/a}\exp(ipr/2) \\ &= C\exp(\kappa_l r)\exp(ipr/2)\,. \end{aligned} \tag{7.39}$$

In expressing $w = \exp(iap/2)\cos(ap/2)$, it seems that we have introduced a sign ambiguity since the division of p by 2 gives rise to a phase ambiguity of π. This ambiguity is, however, canceled by the multiplication of the two terms. We can therefore safely assume that $-\pi/2a < p/2 < \pi/2a$. The constant κ_l in the exponent,

$$\kappa_l = \frac{1}{a}\log\left(\frac{\cos\left(ap/2\right)}{\Delta}\right)\,, \tag{7.40}$$

is indeed negative for $\Delta > 0$, and the wave function is thus exponentially suppressed for large r. For $\Delta < 0$, an additional factor of $(-1)^{r/a}$ has to be included in the phase factor, $\exp(ipr/2)$, in order to give a positive argument to the logarithm. Note that this staggering phase factor is also produced by the transformation of $|p, r\rangle$ under the unitary transformation U, that maps $J \to -J$ and $\Delta \to -\Delta$. This is also what we would expect, as the energy of a localized state with momentum p is unaffected by the transformation U. In contrast to the one-defect sector, where the transformation U corresponds to a momentum shift by π/a, for the localized two-defect states it introduces a staggering factor in the relative coordinate, that is not captured by a total momentum shift.

To retrieve the full wave function, $\psi(x, y)$, which we will later use in order to compare the results to an effective theory, we plug $\psi(r)$ and the definition of the translation invariant states, eq. (7.19), into our ansatz, eq. (7.24), and obtain

$$|\psi, p\rangle = \sum_{y>x}\psi(y-x)\exp(ipx)\,|x, y\rangle = C\sum_{y>x}\exp(ip(x+y)/2)\exp(\kappa_l(y-x))\,|x, y\rangle\,, \tag{7.41}$$

where the sum is over all x and all y with $y > x$. From here we can read off

$$\psi(x, y) = C\exp(ip(x+y)/2)\exp(\kappa_l(y-x))\,. \tag{7.42}$$

7.4. Scattering of Defects

Let us now turn to the scattering states. As scattering states, we refer to states for which the wave function $\psi(r)$ is not vanishing but bounded for large r. They resemble plane wave states. Their wave function and energy is again derived from the recursion relation.

In the region $-2\sqrt{w\overline{w}} < \epsilon < 2\sqrt{w\overline{w}}$, the eigenvalues of the recursion matrix M are pure complex phases and thus the solutions specified in eq. (7.31) are bounded for all

initial conditions. Expressing the right-hand side of eq. (7.31) in terms of eigenvectors of M yields

$$\psi(r) = \lambda_+^{r/a} A + \lambda_-^{r/a} B\,, \tag{7.43}$$

where so far A and B are unspecified constants. Since in this regime $\lambda_\pm$ are pure complex phases, we introduce

$$\lambda_+ = \exp(iaq), \tag{7.44}$$

which implies that

$$\lambda_- = \exp(-iaq)\frac{w}{\overline{w}} = \exp(-iaq)\exp(iap)\,. \tag{7.45}$$

From eq. (7.44), we obtain the dispersion relation

$$\begin{aligned} \lambda_+ &= \exp(iaq)\,, \\ \epsilon + \sqrt{\epsilon^2 - 4w\overline{w}} &= 2\overline{w}\exp(iaq)\,. \end{aligned} \tag{7.46}$$

Taking the real part on both sides yields

$$\epsilon = \cos(aq) + \cos(aq - ap)\,. \tag{7.47}$$

The wave function becomes

$$\psi(r) = A\exp(iqr) + B\exp(-iqr)\exp(ipr)\,, \tag{7.48}$$

where the ratio of A and B is further constrained by the boundary condition equations,

$$\begin{aligned} \psi(2a) &= \frac{\epsilon - \Delta}{\overline{w}}\psi(a) \\ \lambda_+^2 A + \lambda_-^2 B &= \frac{\epsilon - \Delta}{\overline{w}}(A\lambda_+ + B\lambda_-)\,, \end{aligned} \tag{7.49}$$

from which we obtain that

$$\frac{A}{B} = -\frac{1 + \exp(iap) - 2\Delta\exp(ia(p-q))}{1 + \exp(iap) - 2\Delta\exp(iaq)}\,. \tag{7.50}$$

The full wave function $\psi(x, y)$ is

$$\begin{aligned} \psi(x,y) &= \psi(y-x)\exp(ipx) \\ &= A\exp(iqy + i(p-q)x) + B\exp(iqx + i(p-q)y)\,, \end{aligned} \tag{7.51}$$

and the total energy of the scattering states is

$$E_{sc} = E_S - 2J\Delta + 2\mu + J\cos(aq) + J\cos(aq - ap)\,. \tag{7.52}$$

7.5. Discussion

The energy levels and the corresponding eigenstates of the three considered sectors are summarized in Table 7.1. We now continue with discussing a few specific cases in more detail. The energy levels of the selected cases are illustrated in Figure 7.2.

Table 7.1.: Energies of defect states.

Sector	State	Energy
$\Delta S^3 = 0$	$\|S\rangle$	$E_S = \frac{JN\Delta}{4} - \frac{\mu N}{2}$
$\Delta S^3 = -1$	$\|p\rangle$	$E_p = E_S - J\Delta + \mu + J\cos(ap)$
$\Delta S^3 = -2$	$\|\mathrm{loc}, p\rangle$	$E_l = E_S - J\Delta + 2\mu + J\frac{\cos(ap)+1}{2\Delta}$
	$\|sc, p, q\rangle$	$E_{sc} = E_S - 2J\Delta + 2\mu + J\cos(aq) + J\cos(aq - ap)$

First, we consider a ferromagnet with weak anisotropy, $\Delta = 1 + \delta$. For any $\mu > 0$, the saturated state is the lowest energy state and the energy gap to the sector $\Delta S^3 = -1$ is $|\mu| + \delta|J|$. The low-energy physics of each sector is centered around $p = 0$ and $q = 0$. The localized state is a bound state, in the sense that its energy, for $p = 0$, is lower than the energy of the lowest energy scattering state where $p = q = 0$. To see this, consider

$$E_{\mathrm{loc}} - E_{sc} = \frac{J\delta^2}{1+\delta}, \tag{7.53}$$

which is negative for $J < 0$.

In the antiferromagnetic case, the situation presents itself differently. Without an external magnetic field, $\mu = 0$, the spectrum corresponds to the one of a ferromagnetic Hamiltonian, but it is inverted. While the saturated state is the ground state in the ferromagnetic case, it is the highest excited state in the antiferromagnetic case, confer Figure 7.2. In a large external magnetic field, the saturated state becomes the ground state due to the contribution of μS^3 to the energy. There exists a value of $\mu = \mu_c$ for which the one and two-defect sectors have the same energy as the saturated states, namely for $p = \pi/a$ in the one-defect sector and for $p = 0$, $q = \pi/a$ in the two-defect sectors. This value is

$$\mu_c = -J(1 + \Delta) \tag{7.54}$$

for both states $|p = \pi/a\rangle$ and $|sc, 0, \pi/a\rangle$. The low energy physics is centered around $p = \pi/a$ in the $\Delta S^3 = -1$ sector and around $p = 0$ and $q = \pi/a$ in the $\Delta S^3 = -2$ sector.

Two models with $J_1 = -J_2$ and $\Delta_1 = -\Delta_2$ are unitarily equivalent and the respective Hamiltonians have the same eigenvalues but not necessarily the same eigenstates. Rather, the eigenstates are related by the unitary transformation U. While the saturated state

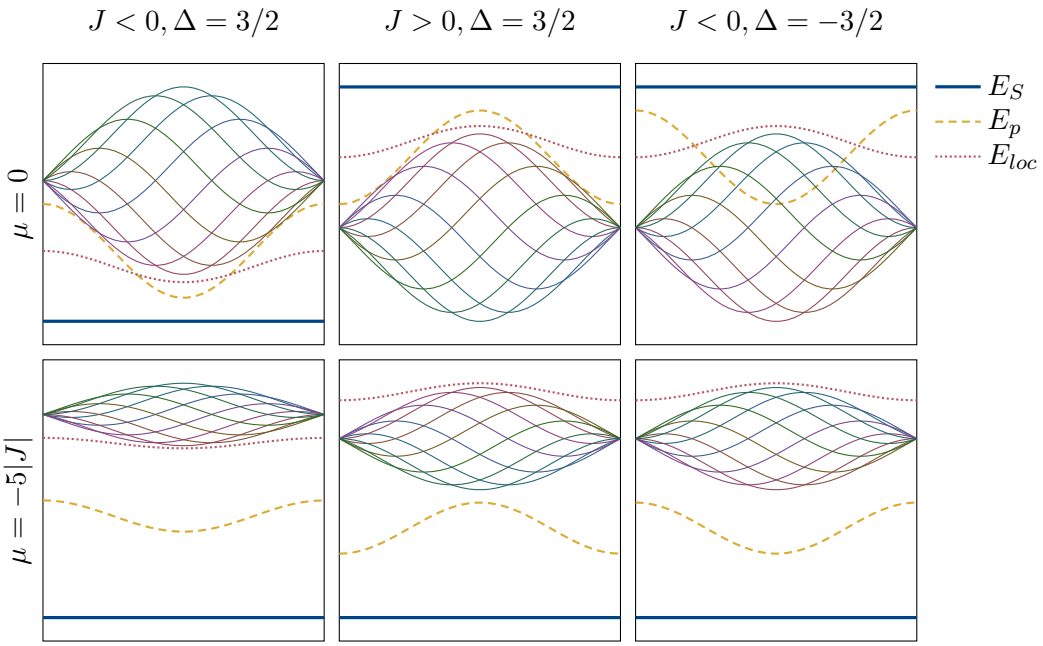

Figure 7.2.: Energy levels for various XXZ-models as a function of total momentum p ranging from $-\pi/a$ to π/a. The thick blue line corresponds to the energy of the saturated state, the dashed line to the one-defect sector. The dotted line represents the localized state energy and the thin lines correspond to the scattering state energies for various q (magenta for $q = 0$ and blue green for $q = \pi/a$).

is invariant under U, the one- and two-defect states transform as

$$\begin{aligned} U\,|p\rangle &= |p + \pi/a\rangle \ , \\ U\,|sc, p, q\rangle &= |sc, p, q + \pi/a\rangle \ , \\ U\,|\mathrm{loc}, p\rangle &= \sum_{r>0} \exp(ipr/2) \exp(\kappa_l r) \exp(i\pi r/a)\,|p, r\rangle \ . \end{aligned} \tag{7.55}$$

This implies that in the sector $\Delta S^3 = -1$, the momentum p is shifted by π/a, and in the sector $\Delta S^3 = -2$, the relative momentum q is shifted by π/a. Since localized states do not have relative momentum, the transformation U gives rise to an additional staggering factor.

In Figure 7.2, this can be appreciated as follows. The models in the second and third column are unitarily equivalent. The energy of the one-defect state is shifted by π/a, while the energy of the localized state is not shifted. For the energy of the scattering states, the internal momentum q is shifted by π/a, i.e., the energy of the scattering state with $q = 0$ is interchanged with the energy of the scattering state with $q = \pi/a$.

8. The $SU(3)$ Spin Chain Close to Saturation

8.1. The $SU(3)$ Spin Chain

We consider a bipartite chain of $SU(3)$ quantum spins, a one-dimensional version of the spin ladder that is employed as a regularization of the $\mathbb{C}P(2)$ model in [66]. The spins on the even sites, referred to as sublattice A, are in the fundamental representation $\{3\}$ and the spins on the odd sites, sublattice B, in the anti-fundamental representation $\{\bar{3}\}$ of $SU(3)$. Their interaction is governed by an antiferromagnetic Heisenberg type Hamiltonian,

$$H_0 = J\left(\sum_{x\in A} T^b_x \overline{T}^b_{x+a} + \sum_{y\in B} \overline{T}^b_y T^b_{y+a}\right) \tag{8.1}$$

where a denotes the lattice spacing, and sometimes an index of the $SU(3)$ algebra. Furthermore, we restrict the discussion to $J > 0$. T^b_x and $\overline{T}^b_y$ are the generators of the fundamental and anti-fundamental representations of $SU(3)$ respectively. The spin chain extends over $L = Na$, but as in Chapter 7, we will work in the limit where $N \to \infty$. The $SU(3)$ generators obey the commutation relations

$$[T^a_x, T^b_{x'}] = i\delta_{xx'} f_{abc} T^c_x\,, \qquad [\overline{T}^a_x, \overline{T}^b_{x'}] = i\delta_{xx'} f_{abc} \overline{T}^c_x\,, \tag{8.2}$$

where f_{abc} are the structure constants. In the basis where T^3_x and T^8_x are diagonal, the T^a correspond to the Gell-Mann matrices

$$T^a_x = \frac{1}{2}\lambda_a\,. \tag{8.3}$$

Analogous to the case of $SU(2)$, one can rewrite the Hamiltonian in terms of shift operators

$$T^\pm_x = T^1_x \pm iT^2_x\,, \qquad V^\pm_x = T^4_x \pm iT^5_x\,, \qquad U^\pm_x = T^6_x \pm iT^7_x\,, \tag{8.4}$$

as

$$\begin{aligned} H_0 = \frac{J}{2}\sum_{x\in A}\Big(&T^+_x\overline{T}^-_{x+a} + T^-_x\overline{T}^+_{x+a} + V^+_x\overline{V}^-_{x+a} + V^-_x\overline{V}^+_{x+a} + U^+_x\overline{U}^-_{x+a} + U^-_x\overline{U}^+_{x+a} \\ &+ 2T^3_x\overline{T}^3_{x+a} + 2T^8_x\overline{T}^8_{x+a}\Big) \\ + \frac{J}{2}\sum_{y\in B}\Big(&\overline{T}^+_y T^-_{y+a} + \overline{T}^-_y T^+_{y+a} + \overline{V}^+_y V^-_{y+a} + \overline{V}^-_y V^+_{y+a} + \overline{U}^+_y U^-_{y+a} + \overline{U}^-_y U^+_{y+a} \\ &+ 2\overline{T}^3_x T^3_{x+a} + 2\overline{T}^8_x T^8_{x+a}\Big)\,. \end{aligned} \tag{8.5}$$

This system has a global $SU(3)$ symmetry, generated by

$$T^a = \sum_{x\in A} T^a_x + \sum_{x\in B}\overline{T}^a_y\,. \tag{8.6}$$

Therefore, the eigenstates of H fall in different charge sectors of the two conserved charges T^3 and T^8. A basis of the Hilbert space is given by

$$|f_a \dots f_{Na}\rangle = \bigotimes_{x\in A} |f_x\rangle \otimes |\bar{f}_{x+a}\rangle\ , \tag{8.7}$$

with $f_x \in \{u,d,s\}$ and $\bar{f}_y \in \{\bar{u},\bar{d},\bar{s}\}$, such that $|f_x\rangle$ and $|\bar{f}_x\rangle$ are simultaneous eigenstates of T^3_x as well as T^8_x and $\overline{T}^3_x$ as well as $\overline{T}^8_x$ respectively. The action of the shift operators on theses states is visualized in Figure 8.1.

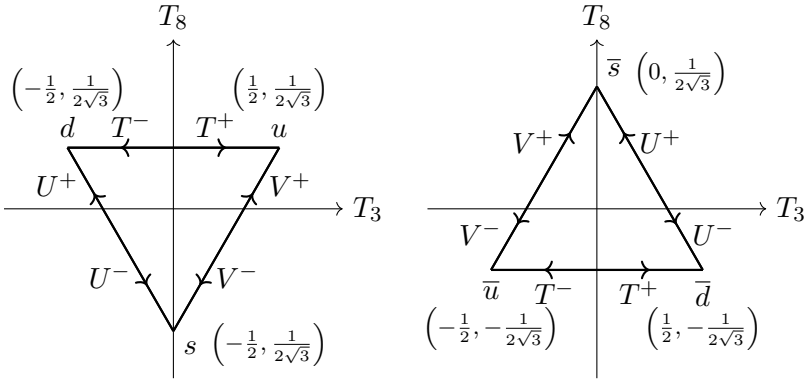

Figure 8.1.: The action of the shift operators on the states $|u\rangle$, $|d\rangle$, and $|s\rangle$, that form the fundamental representation, $\{3\}$ (on the left), as well as $|\bar{u}\rangle$, $|d\rangle$, $|s\rangle$, that form the anti-fundamental representation (on the right). The states are drawn at coordinates corresponding to their eigenvalues with respect to T^3 and T^8.

We will also add a chemical potential coupled to T^3

$$H = H_0 - \mu_3 T^3 \,. \tag{8.8}$$

This term reduces the global $SU(3)$ symmetry to $U(1)_3 \times U(1)_8$. Because of the alternating fundamental and anti-fundamental representations, this Hamiltonian is only invariant under translations by two lattice spacings. It is, however, invariant under T^8-charge conjugation (which maps $\bar{d} \leftrightarrow u, \bar{u} \leftrightarrow d, \bar{s} \leftrightarrow s$) combined with translation by one lattice spacing. It is this operator that we will denote by $\widetilde{T}$, whose eigenvalues will be referred to as momenta in the following. They take on values in the full Brillouin Zone $p \in [-\pi/a, \pi/a]$. In contrast to $SU(2)$, the (anti-)fundamental representation of $SU(3)$ is complex and there is no unitary transformation that relates this system to a ferromagnetic one.

As in $SU(2)$, for sufficiently large chemical potential $\mu_3 \gg J$, the system saturates to the unique state with the largest possible T^3 charge, namely

$$|S\rangle = \bigotimes_{x \in A} |u_x\rangle \otimes |\bar{d}_{x+a}\rangle \,. \tag{8.9}$$

This state is an eigenstate, and for μ_3 sufficiently large, it is the ground state of H with

$$H\,|S\rangle = \left(\frac{JN}{6} - \mu_3 \frac{N}{2}\right) |S\rangle \,. \tag{8.10}$$

In the following we will examine the behavior of different defects in this saturated state and the scattering thereof.

8.2. Defects Close to Saturation

We start by introducing the following defect operators in terms of the $SU(3)$ ladder operators,

$$\begin{aligned} \hat{s}_x &:= \begin{cases} V_x^- & x \in A \\ U_x^+ & x \in B \end{cases} , \\ \hat{\phi}_x &:= T_x^- - \hat{s}_x \hat{s}_{x+a} - \hat{s}_x \hat{s}_{x-a} \,, \\ \hat{\chi}_x &:= T_x^- + \hat{s}_x \hat{s}_{x+a} + T_{x+a}^- \,. \end{aligned} \tag{8.11}$$

The defect states, up to normalization, are generated by acting with these operators on the saturated state as

$$|s_x\rangle := \hat{s}_x\,|S\rangle \,, \qquad |\phi_x\rangle := \hat{\phi}_x\,|S\rangle \,, \qquad |\chi_x\rangle := \hat{\chi}_x\,|S\rangle \,. \tag{8.12}$$

In this way, $\hat{s}_x$ replaces a u with an s and a $\bar{d}$ with an $\bar{s}$. T_x^- replaces a u with a d and a $\bar{d}$ with a u. The operators $\hat{\phi}_x$ and $\hat{\chi}_x$ thus generate composite extended defects,

e.g. for $x \in A$,

$$\begin{aligned}
|\phi_x\rangle &= |d_x\rangle \otimes \bigotimes_{y\in A\setminus\{x\}} |u_y\rangle \bigotimes_{y\in B} |\bar{d}_y\rangle \\
&\quad - |s_x\rangle \otimes |\bar{s}_{x+a}\rangle \otimes \bigotimes_{y\in A\setminus\{x\}} |u_y\rangle \bigotimes_{y\in B\setminus\{x+a\}} |\bar{d}_y\rangle \\
&\quad - |s_x\rangle \otimes |\bar{s}_{x-a}\rangle \otimes \bigotimes_{y\in A\setminus\{x\}} |u_y\rangle \bigotimes_{y\in B\setminus\{x-a\}} |\bar{d}_y\rangle \\
|\chi_x\rangle &= |d_x\rangle \otimes \bigotimes_{y\in A\setminus\{x\}} |u_y\rangle \bigotimes_{y\in B} |\bar{d}_y\rangle \\
&\quad + |s_x\rangle \otimes |\bar{s}_{x+a}\rangle \otimes \bigotimes_{y\in A\setminus\{x\}} |u_y\rangle \bigotimes_{y\in B\setminus\{x+a\}} |\bar{d}_y\rangle \\
&\quad + |d_{x+a}\rangle \otimes |\bar{s}_{x-a}\rangle \otimes \bigotimes_{y\in A\setminus\{x+a\}} |u_y\rangle \bigotimes_{y\in B} |\bar{d}_y\rangle \ .
\end{aligned} \tag{8.13}$$

The states $|s_x\rangle$, form a basis of the Hilbert space in the sector $\Delta T^3 = -\frac{1}{2}$. The sector $\Delta T^3 = -1$, is spanned by $|\phi_x\rangle$, $|\chi_x\rangle$, and $\hat{s}_x\hat{s}_y\,|S\rangle$, where $y > x + a$. As we will see, the use of this seemingly strange basis significantly facilitates the solution of the Schrödinger equation since they form subspaces closed under the action of the Hamiltonian.

While $|s_x\rangle$ and $|\phi_x\rangle$ are eigenstates of H, $|\chi_x\rangle$ transforms as

$$H\,|\chi_x\rangle = \left(E_S - \frac{J3}{2} + \mu_3\right)|\chi_x\rangle - \frac{J}{2}\,|\chi_{x+a}\rangle - \frac{J}{2}\,|\chi_{x-a}\rangle \ , \tag{8.14}$$

akin to a one-defect state of an $SU(2)$-XXZ model with $\Delta = -3/2$.

Under translation, the defect states transform as

$$\widetilde{T}\hat{s}_x\,|S\rangle = \hat{s}_{x+a}\,|S\rangle \ , \qquad \widetilde{T}\hat{\phi}_x\,|S\rangle = \hat{\phi}_{x+a}\,|S\rangle \ , \qquad \widetilde{T}\hat{\chi}_x\,|S\rangle = \hat{\chi}_{x+a}\,|S\rangle \ , \tag{8.15}$$

we can therefore introduce

$$\hat{s}_p = \sum_x \exp(ipx)\hat{s}_x \, , \qquad \hat{\phi}_p = \sum_x \exp(ipx)\hat{\phi}_x \, , \qquad \hat{\chi}_p = \sum_x \exp(ipx)\hat{\chi}_x \, . \tag{8.16}$$

The translation invariant defect states generated by these operators are all eigenstates of the Hamiltonian

$$\begin{aligned}
H\hat{s}_p\,|S\rangle &= \left(E_S + \frac{1}{2}\mu_3\right)\hat{s}_p\,|S\rangle \\
H\hat{\phi}_p\,|S\rangle &= (E_S + \mu_3)\,\hat{\phi}_p\,|S\rangle \\
H\hat{\chi}_p\,|S\rangle &= \left(E_S + \mu_3 - \frac{3J}{2} - J\cos(ap)\right)\hat{\phi}_p\,|S\rangle \ .
\end{aligned} \tag{8.17}$$

As expected from the fact that $|s_x\rangle$ and $|\phi_x\rangle$ are already eigenstates, the eigenvalue of the s- and ϕ-type translation invariant defects do not depend on the momentum, these states are immobile. Note that (as in the antiferromagnetic XXZ models) there is a critical chemical potential, where the energy of $\chi_0 |S\rangle$ is lower than the energy of the saturated state, and the latter is no longer the ground state, namely,

$$\mu_c = \frac{5}{2} J \,. \tag{8.18}$$

At this chemical potential, saturation occurs. In the following, we will look into two-defect states, that involve a dynamical χ-type defect.

8.3. χ-ϕ Scattering

The two particle state is defined as

$$|\chi, \phi, x, y\rangle = \hat{\chi}_x \hat{\phi}_y |S\rangle \tag{8.19}$$

with $y \geq x + 2a$ or $y \leq x - 3a$. We define translation invariant states as

$$|\chi, \phi, r, p\rangle = \sum_y \exp(ipy) |\chi, \phi, y + r, y\rangle \,. \tag{8.20}$$

For $r \geq 3a$ or $r \leq -4a$, the Hamiltonian acts on those as

$$H |\chi, \phi, r, p\rangle = \left(E_S + 2\mu_3 - \frac{3}{2} J \right) |\chi, \phi, r, p\rangle - \frac{J}{2} |\chi, \phi, r + a, p\rangle - \frac{J}{2} |\chi, \phi, r - a, p\rangle \,. \tag{8.21}$$

The states $|\chi, \phi, a\rangle$ and $|\chi, \phi, -2a\rangle$ are defined by imposing that $|\chi, \phi, 3a\rangle$ and $|\chi, \phi, -4a\rangle$ transform under the Hamiltonian as the states $|\chi, \phi, r\rangle$ for $r > 3a$ or $r < -4a$. This is achieved by imposing eq. (8.21) also for $r = 2a$ and $r = -3a$. The resulting states are,

$$\begin{aligned} |\chi, \phi, a, p\rangle &= -\frac{2}{J} \left(H |\chi, \phi, 2a, p\rangle - \left(E_S + 2\mu_3 - \frac{3}{2} J \right) |\chi, \phi, 2a, p\rangle + \frac{J}{2} |\chi, \phi, 3a, p\rangle \right) \\ |\chi, \phi, -2a, p\rangle &= -\frac{2}{J} \left(H |\chi, \phi, -3a, p\rangle - \left(E_S + 2\mu_3 - \frac{3}{2} J \right) |\chi, \phi, -3a, p\rangle \right. \\ &\qquad \left. + \frac{J}{2} |\chi, \phi, -4a, p\rangle \right) . \end{aligned} \tag{8.22}$$

Under the Hamiltonian, they transform as

$$\begin{aligned} H\left|\chi,\phi,a,p\right\rangle &= \left(E_S + 2\mu_3 - \frac{3}{2}J\right)\left|\chi,\phi,a,p\right\rangle \\ &\quad - \frac{J}{2}\left|\chi,\phi,2a,p\right\rangle - \frac{J}{2}\exp(-2iap)\left|\chi,\phi,-2a\right\rangle \\ H\left|\chi,\phi,-2a,p\right\rangle &= \left(E_S + 2\mu_3 - \frac{3}{2}J\right)\left|\chi,\phi,-2a,p\right\rangle \\ &\quad - \frac{J}{2}\left|\phi,\chi,-3a,p\right\rangle - \frac{J}{2}\exp(2iap)\left|\chi,\phi,a,p\right\rangle \ . \end{aligned} \tag{8.23}$$

Remarkably, this set of states, $\{\left|\chi,\phi,r,p\right\rangle, r \geq a \text{ or } r \leq -2a\}$, is closed under the action of the Hamiltonian, and to obtain energy eigenstates we can proceed exactly as in the case of $SU(2)$ by making an ansatz of the form

$$\left|\psi_{\chi\phi},p\right\rangle = \sum_{r\leq -2a}\psi_{\chi\phi}(r)\left|\chi,\phi,r,p\right\rangle + \sum_{r\geq a}\psi_{\chi\phi}(r)\left|\chi,\phi,r,p\right\rangle \ . \tag{8.24}$$

The equation $H\left|\psi_{\chi\phi},p\right\rangle = E\left|\psi_{\chi\phi},p\right\rangle$, translates into two recursion relations for $\psi_{\chi\phi}(r)$, namely,

$$\begin{aligned} r \geq 2a: &\qquad \begin{pmatrix}\psi_{\chi\phi}(r+a)\\ \psi_{\chi\phi}(r)\end{pmatrix} = \begin{pmatrix}\epsilon_{\chi\phi} & -1\\ 1 & 0\end{pmatrix}\begin{pmatrix}\psi_{\chi\phi}(r)\\ \psi_{\chi\phi}(r-a)\end{pmatrix}, \\ r \leq -3a: &\qquad \begin{pmatrix}\psi_{\chi\phi}(r-a)\\ \psi_{\chi\phi}(r)\end{pmatrix} = \begin{pmatrix}\epsilon_{\chi\phi} & -1\\ 1 & 0\end{pmatrix}\begin{pmatrix}\psi_{\chi\phi}(r)\\ \psi_{\chi\phi}(r+a)\end{pmatrix}, \end{aligned} \tag{8.25}$$

with

$$\epsilon_{\chi\phi} = \frac{2}{J}\left(E_S - E - \frac{3}{2}J + 2\mu_3\right), \tag{8.26}$$

and the coupled boundary conditions

$$\begin{aligned} \epsilon_{\chi\phi}\psi_{\chi\phi}(a) &= \psi_{\chi\phi}(2a) + \exp(+2iap)\psi_{\chi\phi}(-2a)\,, \\ \epsilon_{\chi\phi}\psi_{\chi\phi}(-2a) &= \psi_{\chi\phi}(-3a) + \exp(-2iap)\psi_{\chi\phi}(a)\,. \end{aligned} \tag{8.27}$$

The recursion relation matrix has the spectral structure familiar from the discussion of the $SU(2)$-XXZ Hamiltonian, with the additional simplification of $w = 1$. Thus, for a given $\epsilon_{\chi\phi}$, at most one eigenvalue is smaller than 1 in absolute value and in the region, $\epsilon_{\chi\phi} \in [-2,2]$, $|\lambda_\pm| = 1$ holds. The eigenvalues and eigenvectors are

$$\begin{aligned} \lambda_+ &= \frac{1}{2}\left(\epsilon_{\chi\phi} + \sqrt{\epsilon_{\chi\phi}^2 - 4}\right), & \lambda_- &= \frac{1}{2}\left(\epsilon_{\chi\phi} - \sqrt{\epsilon_{\chi\phi}^2 - 4}\right), \\ v_+ &= \begin{pmatrix}\lambda_+\\ 1\end{pmatrix}, & v_- &= \begin{pmatrix}\lambda_-\\ 1\end{pmatrix}. \end{aligned} \tag{8.28}$$

The general solution of the coupled recursion relations, eq. (8.25), is

$$\begin{aligned} r > 0: \qquad & \psi_{\chi\phi}(r) = A\lambda_+^{r/a} + B\lambda_-^{r/a}\,, \\ r < 0: \qquad & \psi_{\chi\phi}(r) = C\lambda_+^{-r/a} + D\lambda_-^{-r/a}\,, \end{aligned} \tag{8.29}$$

where, making use of $\epsilon_{\chi\phi} = \lambda_+ + \lambda_-$, A, B, C, and D are related by the boundary conditions, eqs. (8.27), as

$$\begin{aligned} A &= -\frac{\exp(2iap)\left(C\lambda_-\lambda_+^3 - C\lambda_+^2 + D\lambda_-^2\left(\lambda_+^2 - 1\right)\right)}{(\lambda_- - \lambda_+)\,\lambda_+} = D\exp(2iap)\lambda_+^{-2} \\ B &= \frac{\exp(2iap)\left(\lambda_-^2\left(C\lambda_+^2 - C\right) - C\lambda_+^2 + D\lambda_+\lambda_-^3\right)}{\lambda_-\,(\lambda_- - \lambda_+)} = C\exp(2iap)\lambda_+^2\,. \end{aligned} \tag{8.30}$$

We have made use of the relation $\lambda_- = \lambda_+^{-1}$. For a localized state to exist, one of the eigenvalues, $\lambda_\pm$, has to be smaller than 1 in absolute value, which in turn implies that the other is larger than 1 in absolute value. This implies either $A = C = 0$ or $B = D = 0$, which is incompatible with eqs. (8.30). Therefore no localized state exists.

The scattering states correspond to the region $\epsilon_{\chi\phi} \in [-2, 2]$, where λ_+ and λ_- are pure complex phases and conjugate to each other. Defining

$$\exp(\pm iaq) := \lambda_\pm\,, \tag{8.31}$$

the wave function, eq. (8.29), becomes

$$\psi_{\chi\phi}(r) = \begin{cases} A\exp(iqr) + B\exp(-iqr), & r \geq a \\ C\exp(-iqr) + D\exp(iqr), & r \leq -2a \end{cases}\,, \tag{8.32}$$

with

$$\begin{aligned} A &= D\exp(2ia(p-q))\,, \\ B &= C\exp(2ia(p+q))\,. \end{aligned} \tag{8.33}$$

The dispersion relation is obtained from

$$\epsilon_{\chi\phi} = \lambda_+ + \lambda_- = 2\cos(aq)\,. \tag{8.34}$$

Expressed as total energy eigenvalue of H, it reads

$$E = E_S - \frac{3}{2}J + 2\mu_3 - J\cos(aq)\,. \tag{8.35}$$

8.4. χ-s Scattering

The scattering of a χ- and an s-type defect is almost completely equivalent to the scattering of a χ- and a ϕ-type defect. The two-particle states are defined as

$$\begin{aligned} |\chi, s, x, y\rangle &= \hat{\chi}_x \hat{s}_y |S\rangle \,, \\ |\chi, s, r, p\rangle &= \sum_y \exp(ipy) |\chi, s, y+r, y\rangle \,, \end{aligned} \tag{8.36}$$

where $x \geq y + a$ or $x \leq y - 2a$. For $r \geq 2a$ or $r \leq -3a$, the translation invariant states transform under the Hamiltonian as

$$H |\chi, s, r, p\rangle = \left(E_S + \frac{3}{2}\mu_3 - \frac{3}{2}J\right) |\chi, s, r, p\rangle - \frac{J}{2} |\chi, s, r+a, p\rangle - \frac{J}{2} |\chi, s, r-a, p\rangle \,. \tag{8.37}$$

For $r = a$ and $r = -2a$ we find

$$\begin{aligned} H |\chi, s, a, p\rangle &= \left(E_S + \frac{3}{2}\mu_3 - \frac{3}{2}J\right) |\chi, s, a, p\rangle - \frac{J}{2} |\chi, s, 2a, p\rangle \\ &\quad - \frac{J}{2} \exp(-2iap) |\chi, s, -2a\rangle \\ H |\chi, s, -2a, p\rangle &= \left(E_S + \frac{3}{2}\mu_3 - \frac{3}{2}J\right) |\chi, s, -2a, p\rangle - \frac{J}{2} |\phi, s, -3a, p\rangle \\ &\quad - \frac{J}{2} \exp(+2iap) |\chi, s, a, p\rangle \,. \end{aligned} \tag{8.38}$$

Up to a constant energy shift of $1/2\mu_3$, due to the different charges of the s- and ϕ-type defect, this is exactly what we have found for χ-ϕ scattering. We can therefore immediately write down the energy and wave function of the scattering state as

$$\begin{aligned} \psi_{\chi s}(r) &= \begin{cases} A \exp(iqr) + B \exp(-iqr), & r \geq a \\ C \exp(-iqr) + D \exp(iqr), & r \leq -2a \end{cases} \\ E &= E_S - \frac{3}{2}J + \frac{3}{2}\mu_3 - J\cos(aq) \,, \end{aligned} \tag{8.39}$$

where again,

$$\begin{aligned} A &= D \exp(2ia(p-q)) \,, \\ B &= C \exp(2ia(p+q)) \,. \end{aligned} \tag{8.40}$$

Therefore, as in χ-ϕ scattering, no localized state exists.

8.5. χ-χ Scattering

We now turn to the most interesting case of two dynamical defects of χ-type. The two-defect states are

$$|\chi,\chi,x,y\rangle = \hat{\chi}_x\hat{\chi}_y\,|S\rangle \tag{8.41}$$

with $y \geq x+2a$, since the two defects are now indistinguishable. Introducing the relative coordinate r, we define translation invariant states as

$$|\chi,\chi,r,p\rangle = \sum_x \exp(ipx)\,|\chi,\chi,x,x+r\rangle\ . \tag{8.42}$$

For $r \geq 2a$, they transform under the Hamiltonian as

$$H\,|\chi,\chi,r,p\rangle = (E_S+2\mu_3-3J)\,|\chi,\chi,r,p\rangle - Jw\,|\chi,\chi,r+a,p\rangle - J\bar{w}\,|\chi,\chi,r-a,p\rangle\ , \tag{8.43}$$

where again $w = \frac{1}{2}\left(1+\exp(iap)\right)$. As for χ-ϕ scattering, the state $|\chi,\chi,a,p\rangle$ is defined by imposing the action of the Hamiltonian for $r > 2a$, eq. (8.43), for $r = 2a$ as,

$$|\chi,\chi,a,p\rangle = -\frac{1}{J\bar{w}}\left(H\,|\chi,\chi,2a,p\rangle - (E_S+2\mu_3-3J)\,|\chi,\chi,2a,p\rangle + Jw\,|\chi,\chi,3a,p\rangle\right)\ . \tag{8.44}$$

The set of states $\{|\chi,\chi,r,p\rangle\,, r \geq a\}$ is again closed under the action of the Hamiltonian since

$$H\,|\chi,\chi,a,p\rangle = \left(E_S+2\mu_3-\frac{3}{2}J\right)|\chi,\chi,a,p\rangle - Jw\,|\chi,\chi,2a,p\rangle\ . \tag{8.45}$$

To find eigenstates of the Hamiltonian, we proceed as before and make the ansatz

$$|\psi_{\chi,\chi},p\rangle = \sum_{r\geq a}\psi_{\chi\chi}(r)\,|\chi,\chi,r,p\rangle\ . \tag{8.46}$$

Plugging it into the stationary Schrödinger equation then gives the recursion relation for the wave function $\psi_{\chi\chi}$,

$$\begin{pmatrix}\psi_{\chi\chi}(r+a)\\ \psi_{\chi\chi}(r)\end{pmatrix} = \begin{pmatrix}\epsilon_{\chi\chi}/\bar{w} & -w/\bar{w}\\ 1 & 0\end{pmatrix}\begin{pmatrix}\psi_{\chi\chi}(r)\\ \psi_{\chi\chi}(r-a)\end{pmatrix}\ , \tag{8.47}$$

with

$$\epsilon_{\chi\chi} = \frac{1}{-J}\left(E-E_S-2\mu_3+3J\right)\ . \tag{8.48}$$

Eq. (8.47) is valid for all $r \geq 2a$. The interaction point, eq. (8.45), gives a constraint on the boundary conditions of the recursion relation, namely

$$\begin{pmatrix}\psi_{\chi\chi}(2a)\\ \psi_{\chi\chi}(a)\end{pmatrix} = \begin{pmatrix}\left(\epsilon_{\chi\chi}+\frac{3}{2}\right)/\bar{w}\\ 1\end{pmatrix}\psi_{\chi\chi}(a)\,. \tag{8.49}$$

This recursion relation and its boundary condition correspond to the ones encountered for the two-defect sector of the $SU(2) - XXZ$ model for $J_{XXZ} = -J$ and $\Delta = -3/2$, a model unitarily equivalent to an anisotropic antiferromagnet. This case is discussed thoroughly in Section 7.1, and we will therefore simply state the results here. The localized state wave function is obtained from eq. (7.39)

$$\psi_{\chi\chi}(r) = C(-2\frac{w}{3})^{r/a} = C\exp(\kappa_l^{\chi\chi} r)(-1)^{r/a}\exp\left(\frac{ipr}{2}\right), \tag{8.50}$$

where

$$\kappa_l^{\chi\chi} = \frac{1}{a}\log\left(\frac{2\cos(ap/2)}{3}\right). \tag{8.51}$$

The corresponding $\epsilon_{\chi\chi}$ is obtained from eq. (7.35) as

$$\epsilon_{\chi\chi} = -\frac{1}{3}\cos(ap) - \frac{11}{6}. \tag{8.52}$$

With that, we find for the full energy,

$$E = E_S + \frac{1}{3}J\cos(ap) - \frac{7J}{6} + 2\mu. \tag{8.53}$$

For scattering states we obtain the wave function,

$$\psi_{\chi\chi}(r) = A\exp(iqr) + B\exp(-iqr)\exp(ipr). \tag{8.54}$$

with

$$\frac{A}{B} = -\frac{1+\exp(iap)+3\exp(ia(p-q))}{1+\exp(iap)+3\exp(iaq)}. \tag{8.55}$$

The dispersion relation follows from $\epsilon_{\chi\chi} = \cos(aq) + \cos(aq - ap)$ and reads

$$E = E_S - 3J + 2\mu - J\cos(a(p-q)) - J\cos(aq). \tag{8.56}$$

The energies for the various defect states we have considered are summarized in Figure 8.2.

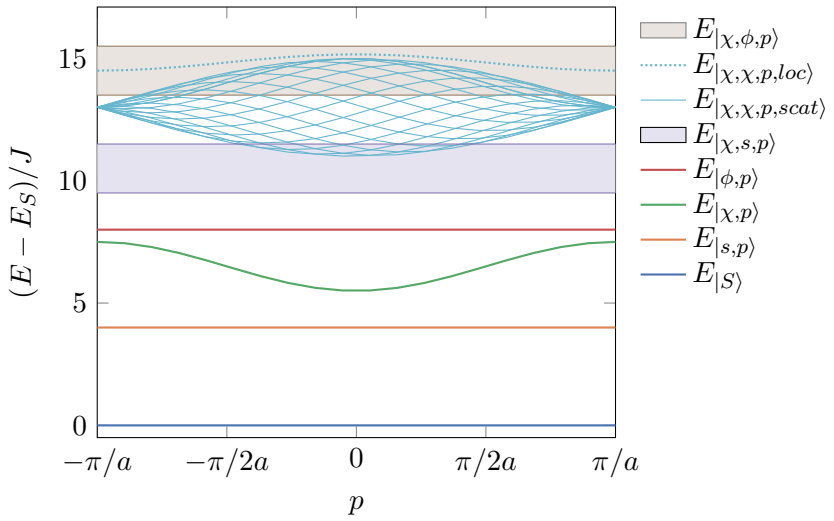

Figure 8.2.: The energy levels of the $SU(3)$ spin chain. The energy of the scattering states, $|\chi, s, p\rangle$ and $|\chi, \phi, p\rangle$, only depend on the internal momentum q, and are represented by extended bands. The energies of the states $|\chi, p\rangle, |\chi, \chi, p, \text{scat}\rangle, |\chi, \chi, p, \text{loc}\rangle$ correspond to the ones of an XXZ Hamiltonian with $J_{XXZ} = -J$ and $\Delta = -\frac{3}{2}$.

9. Effective Low-Energy Quantum Mechanics

9.1. An Effective Hamiltonian

The various defects in the saturated states of the $SU(2)$ and $SU(3)$ spin chains discussed in the previous chapters can effectively be described as quantum mechanical point particles. In the following, we will look into this effective quantum mechanics, for the various charge sectors. By the term "effective quantum mechanics", we refer to a quantum mechanical System in continuous space, defined by a Hamiltonian H_e alongside a matching prescription that specifies the way in which the wave function of the point particles in the effective theory is to be compared to the wave functions of the defects in the exact solution.

The effective theory only captures the low-energy physics of a given sector, characterized by a low-energy expansion parameter, e.g. the momentum of the one-defect state for the $SU(2)$ XXZ-spin chain with $J < 0$. We impose, that the wave functions and energies of continuum and lattice theory match up to second order in this expansion parameter. In the two-defect sectors, the effective theory will be obtained by matching the scattering state wave function and energies. The predictions for the localized state are regarded as a consistency check. In all cases, we will set $E_S = 0$. We start, by discussing the quantum mechanics of non-relativistic point particles with contact interactions, our candidate for the effective description.

The Hamiltonian of a free non-relativistic point particle is

$$H_e^{(1)} = M_0 + \frac{\hat{p}^2}{2m} = M_0 - \frac{\partial_x^2}{2m}\,, \tag{9.1}$$

with rest energy M_0 and kinetic mass m. It has the eigenstate wave functions

$$\psi_e(x) = \exp(ip_e x) \tag{9.2}$$

with energy eigenvalues

$$E_e^{(1)}(p) = M_0 + \frac{p_e^2}{2m}\,. \tag{9.3}$$

The contact interaction of two such particles is described by the Hamiltonian

$$H_e^{(2)} = 2M_0 + \frac{\hat{p}_1^2}{2m} + \frac{\hat{p}_2^2}{2m} + \text{“contact interaction”}\,, \tag{9.4}$$

where the term "contact interaction" means that the domain of the wave functions is $\mathcal{D}(\psi) = \{(x,y) \in \mathbb{R}^2, x \neq y\}$ with a boundary condition at $x = y$ that characterizes the interaction. Introducing center of mass and relative coordinates, the Hamiltonian takes the form

$$H_e^{(2)} = 2M_0 + \frac{\hat{P}^2}{4m} + \frac{\hat{q}^2}{m} + \text{"contact interaction"}\,, \tag{9.5}$$

with

$$\begin{aligned} r &= x_1 - x_2\,, & R &= \frac{x_1 + x_2}{2}\,, \\ \hat{q} &= \frac{1}{2}(\hat{p}_1 - \hat{p}_2)\,, & \hat{P} &= \hat{p_1} + \hat{p_2}\,. \end{aligned} \tag{9.6}$$

According to the theory of self-adjoint extensions, the most general boundary condition at $r = 0$, that leaves H self-adjoint and at the same time permits eigenstates that respect parity is

$$\lim_{\epsilon \to 0^+} \begin{pmatrix} \psi_e(r,R) \\ \partial_r \psi_e(r,R) \end{pmatrix}_{r=+\epsilon} = \begin{pmatrix} a & b \\ c & a \end{pmatrix} \lim_{\epsilon \to 0^+} \begin{pmatrix} \psi_e(r,R) \\ \partial_r \psi_e(r,R) \end{pmatrix}_{r=-\epsilon}\,, \tag{9.7}$$

with a, b, c real and $a^2 - bc = 1$. This Hamiltonian has the symmetric scattering eigenstate wave function

$$\psi_e(R,r) = \exp(ip_eR) \begin{cases} A_e \exp(iq_er) + B_e \exp(-iq_er)\,, & r > 0 \\ A_e \exp(-iq_er) + B_e \exp(iq_er)\,, & r < 0 \end{cases}\,, \tag{9.8}$$

where the boundary condition, eq. (9.7), fixes the ratio

$$\frac{A_e}{B_e} = \frac{q_e + i\kappa_e}{q_e - i\kappa_e}\,, \tag{9.9}$$

with

$$\kappa_e = \frac{-c}{a+1}\,. \tag{9.10}$$

The scattering state energy is

$$E_s(p_e, q_e) = 2M_0 + \frac{p_e^2}{4m} + \frac{q_e^2}{m}\,. \tag{9.11}$$

For $\kappa_e > 0$, the contact interaction allows a bound state with the wave function

$$\psi(R,r) = C \exp(ip_eR) \begin{cases} \exp(-\kappa_e r)\,, & r > 0 \\ \exp(+\kappa_e r)\,, & r < 0 \end{cases} \tag{9.12}$$

and energy

$$E_b(p_e) = 2M_0 + \frac{p_e^2}{4m} - \frac{\kappa_e^2}{m}\,. \tag{9.13}$$

This Hamiltonian is invariant under Galilean boosts. The relative coordinate wave func-

tion, especially the ratio of A_e/B_e, does not depend on the total momentum. On the microscopic side, on the other hand, boost invariance is broken by the lattice, and the relative coordinate wave functions do depend on the total momentum. Therefore, in the two defect charge sector, each total momentum sector is described by its own effective theory, only valid at the respective total momentum.

The low-energy physics of the effective theory is centered around $p_e = 0$ for $H^{(1)}$ and around $q_e = 0$ for each p_e for $H^{(2)}$. Therefore, p_e and q_e serve as expansion parameters and are mapped to a suitable counterpart of the exact solution.

9.2. Effective Description of Defects in an $SU(2)$ Ferromagnet

In the case of a ferromagnetic $SU(2)$ spin chain, where $J < 0$, the low-energy physics of the exact solution of the $\Delta S^3 = -1$ sector is centered around $p = 0$. Employing the obvious matching prescription

$$\psi(x) \stackrel{!}{=} \psi_e(x)\,, \tag{9.14}$$

and identifying $p_e = p$, lattice and continuum wave functions agree to all orders in p_e. Expanding the lattice energy to second order in p_e yields (recall that we set $E_S = 0$),

$$E = J(1-\Delta) - \mu - J\frac{a^2 p_e^2}{2} + O(a^3 p_e^3)\,. \tag{9.15}$$

Comparing this expression to the effective energy, eq. (9.3), gives

$$\begin{aligned} M_0 &= J(1-\Delta) - \mu\,, \\ m &= \frac{-1}{Ja^2}\,. \end{aligned} \tag{9.16}$$

For the effective description of the two-defect sector, $\Delta S^3 = -2$, the matching prescription becomes more subtle. In order to obtain consistent results, the contact point has to be explicitly removed. We start by bringing the lattice wave function to a form comparable to the one of the effective theory, namely,

$$\psi(x,y) = \exp\left(i\frac{p}{2}(x+y)\right)\left(A\exp\left(i\left(q-\frac{p}{2}\right)r\right) + B\exp\left(-i\left(q-\frac{p}{2}\right)r\right)\right)\,, \tag{9.17}$$

where the sign ambiguity introduced by the division of p by 2 cancels. We therefore impose that $-\pi/2a \leq p/2 \leq \pi/2a$. Matching the momenta as

$$q_e = q - \frac{p}{2}\,, \tag{9.18}$$

we recover the form of the continuum wave function, eq. (9.8), with $p_e = p$. Note that the low-energy physics of each p-sector of the lattice theory is centered around $q_e = 0$.

The energy is

$$E = -2\Delta J - 2\mu + 2J\cos\left(\frac{ap_e}{2}\right)\cos(aq_e)\,. \tag{9.19}$$

In terms of the momentum q_e, the ratio A/B reads

$$\frac{A}{B} = -\frac{\cos\left(\frac{ap_e}{2}\right) - \Delta\exp(-iaq_e)}{\cos\left(\frac{ap_e}{2}\right) - \Delta\exp(+iaq_e)}\,. \tag{9.20}$$

Explicitly excluding the contact point, the lattice and effective wave functions are matched regarding the prescription

$$\psi_e(x + a/2, y - a/2) \stackrel{!}{=} \psi(x, y)\,, \qquad y > x + a\,, \tag{9.21}$$

where we assume $y > x + a$ and symmetric continuation of the effective wave function. At this stage, this matching prescription seems somewhat arbitrary. We will comment on that in Section 9.5. The amplitude ratio is compared according to

$$\frac{A}{B}\exp(2iq_e a) = \frac{A_e}{B_e}\,. \tag{9.22}$$

Expanding both sides to second order in q_e gives

$$-1 + \frac{2iaq_e\cos\left(\frac{ap_e}{2}\right)}{\Delta - \cos\left(\frac{ap_e}{2}\right)} + \frac{2a^2q_e^2\left(\cos\left(\frac{ap_e}{2}\right)\right)^2}{\left(\Delta - \cos\left(\frac{ap_e}{2}\right)\right)^2} = -1 + \frac{2iq_e}{\kappa_e} + \frac{2q_e^2}{\kappa_e^2}\,, \tag{9.23}$$

from where we can identify

$$\kappa_e = \frac{\Delta\left(\cos\left(\frac{ap_e}{2}\right)\right)^{-1} - 1}{a}\,. \tag{9.24}$$

The kinetic mass and rest energy are obtained from the comparison of the energy dispersion relations, expanded to second order in p_e and q_e.

$$\begin{aligned} E &= -2\Delta J - 2\mu + 2J\cos\left(\frac{ap_e}{2}\right)\cos(aq_e) \\ &\approx -2\Delta J + 2J - 2\mu - \frac{1}{4}a^2Jp_e^2 - a^2Jq_e^2\,, \\ E_e &= 2M_0 + \frac{p_e^2}{4m} + \frac{q_e^2}{m}\,. \end{aligned} \tag{9.25}$$

From this we find, in agreement with the one-defect sector,

$$m = \frac{-1}{Ja^2}\,, \qquad\qquad M_0 = J(1-\Delta) - \mu\,. \tag{9.26}$$

In the case of a weakly anisotropic ferromagnet, $\Delta = 1 + \delta$ the effective theory predicts

a bound state with energy

$$\begin{aligned} E_{b,e} &= 2M_0 + \frac{p_e^2}{4m} - \frac{\kappa_e^2}{m} \\ &\approx J(\delta^2 - 2\delta) - 2\mu - \frac{1}{4}a^2 J p_e^2 + \frac{1}{4}a^2\delta J p_e^2 + \frac{J}{4}a^2\delta^2 J p_e^2 \end{aligned} \tag{9.27}$$

whereas from the microscopic lattice calculation, we have

$$\begin{aligned} E_b &= \frac{J(\cos(ap_e)+1)}{2\Delta} - \Delta J - 2\mu \\ &\approx J(\delta^2 - 2\delta) - 2\mu - \frac{1}{4}a^2 J p_e^2 + \frac{1}{4}a^2\delta J p_e^2 - \frac{J}{4}a^2\delta^2 J p_e^2 \,. \end{aligned} \tag{9.28}$$

The lattice and effective energy agree up to and including order $O(p_e^2)$ and $O(\delta^2)$. In addition, we can also compare the decay length of the localized state wave function,

$$\begin{aligned} \kappa &= \frac{1}{a}\log\left(\frac{\cos\left(\frac{ap_e}{2}\right)}{\Delta}\right) \approx -\frac{\delta}{a} - \frac{ap_e^2}{8} + \frac{\delta^2}{2a} \\ -\kappa_e &= \frac{1}{a}\left(\frac{\Delta}{\cos\left(\frac{ap_e}{2}\right)} - 1\right) \approx -\frac{\delta}{a} - \frac{ap_e^2}{8} - \frac{1}{8}a\delta p_e^2 \end{aligned} \tag{9.29}$$

and find that they agree up to second order in p_e and to first order in δ. For a model unitarily equivalent to an antiferromagnet, i.e., $\Delta < -1$, we find that $\kappa_e < 0$, and the effective theory does not have a bound state.

9.3. Effective Description for Defects in an $SU(2)$ Antiferromagnet

For $J > 0$, the low-energy physics of the exact solution in the one-defect sector, $\Delta S^3 = -1$, is centered around $p = \pi/a$. The rapid oscillation of such a state cannot be incorporated into a continuum theory and is explicitly excluded in the matching prescription for the wave functions as

$$\psi(x)\exp(i\pi x/a) \stackrel{!}{=} \psi_e(x)\,. \tag{9.30}$$

The expansion parameter of the continuum theory p_e is identified with the lattice momentum shifted by π/a,

$$p_e = p - \pi/a\,. \tag{9.31}$$

The wave functions again agree to all orders in p_e. Expanding the exact energy to second order in p_e gives

$$E = -J(\Delta+1) - \mu + J\frac{a^2 p_e^2}{2} + O(a^3 p_e^3)\,, \tag{9.32}$$

from where we can read off the rest energy and kinetic mass,

$$M_0 = J(-1-\Delta) - \mu\,, \qquad\qquad m = \frac{1}{Ja^2}\,. \tag{9.33}$$

These results are consistent with the ones obtained for $J < 0$, regarding the unitary equivalence ($J \to -J$ and $\Delta \to -\Delta$).

The low-energy physics of the $\Delta S^3 = -2$ sector scattering state is centered around $q - p/2 = \pi/a$. The relative momenta are therefore identified as $q_e = q - p/2 - \pi/a$ and the total momenta as $p_e = p$. Explicitly excluding the rapid oscillation as well as the contact point, we employ the following matching prescription for the wave function,

$$\psi_e(x + a/2, y - a/2) \stackrel{!}{=} \psi(x,y) \exp\left(i\pi \frac{y-x}{a}\right)\,, \qquad y > x + a\,. \tag{9.34}$$

In terms of q_e, the ratio A/B is

$$\frac{A}{B} = -\frac{\cos\left(\frac{ap_e}{2}\right) + \Delta \exp(-iaq_e)}{\cos\left(\frac{ap_e}{2}\right) + \Delta \exp(+iaq_e)}\,, \tag{9.35}$$

equivalent to the $J < 0$ case, but with flipped sign of Δ, as it should be, regarding the unitary equivalence of the two models. The wave function in terms of q_e is

$$\psi(x,y) = \exp(ip/2(x+y)) \exp\left(i\pi \frac{r}{a}\right) \left(A \exp(iq_e r) + B \exp(-iq_e r)\right)\,. \tag{9.36}$$

Matching the wave functions according to eq. (9.34) results in the condition

$$\frac{A}{B} \exp(2iq_e a) = \frac{A_e}{B_e}\,, \tag{9.37}$$

which is equivalent to the condition we had in the discussion of the ferromagnetic case, eq. (9.22). Thus the discussion there applies, but with Δ replaced by $-\Delta$.

9.4. Effective Quantum Mechanics for the $SU(3)$ Spin Chain

Completely analogous to the XXZ-chain, the single-defect eigenstates of the $SU(3)$ spin chain Hamiltonian are effectively described by a quantum mechanical free particle Hamiltonian. The low-energy physics of the χ-type defect is centered around $p = 0$. The non-dynamical defects can be described by particles with an infinite kinetic mass. Comparing the energy eigenvalues of the one particle states, eq. (8.15), to second order in p with eq. (9.3) and again disregarding the trivial constant E_S, we obtain the following effective

masses for the single defects,

$$\begin{aligned} M_s^{(0)} &= \frac{1}{2}\mu_3\,, & m_s &= \infty\,, \\ M_\phi^{(0)} &= \mu_3\,, & m_\phi &= \infty\,, \\ M_\chi^{(0)} &= \mu_3 - \frac{5J}{2}\,, & m_\chi &= \frac{1}{Ja^2}\,. \end{aligned} \tag{9.38}$$

In the exact solution of the $SU(3)$ spin chain, we have encountered sectors describing scattering of distinguishable defects, namely χ- and ϕ-type defects as well as χ- and s-type defects. For both cases we have found the same results except for an energy shift due to the T^3 charge difference of the ϕ- and the s-type defect. We can therefore restrict the following discussion to χ-ϕ scattering.

As an effective theory, we again employ the contact interaction Hamiltonian, but this time without symmetrizing the resulting wave functions. The effective Hamiltonian in terms of the total rest mass, M_0^t, and the total and reduced kinetic masses m_t, and m_r is

$$H_e^{(2)} = M_0^t + \frac{p^2}{2m_t} + \frac{q^2}{2m_r}\,, \tag{9.39}$$

this time with the more general boundary condition

$$\lim_{\epsilon\to 0^+} \begin{pmatrix} \psi_e(r,R) \\ \partial_r\psi_e(r,R) \end{pmatrix}_{r=+\epsilon} = \exp(i\theta) \begin{pmatrix} a & b \\ c & d \end{pmatrix} \lim_{\epsilon\to 0^+} \begin{pmatrix} \psi_e(r,R) \\ \partial_r\psi_e(r,R) \end{pmatrix}_{r=-\epsilon}\,. \tag{9.40}$$

An ansatz of the following form is an eigenstate of this Hamiltonian,

$$\psi(R,r) = \exp(ip_eR) \begin{cases} \exp(iq_er) + R\exp(-iq_er) & r<0 \\ T\exp(iq_er) & r>0 \end{cases}\,. \tag{9.41}$$

The boundary conditions at the contact point, eq. (9.40), yields the reflection and transmission amplitudes

$$R_e = -\frac{-iaq_e + bq_e^2 + c + idq_e}{-iaq_e - bq_e^2 + c - idq_e}\,, \qquad T_e = \frac{2\exp(i\theta)q_e}{aq_e - ibq_e^2 + ic + dq_e}\,. \tag{9.42}$$

If we impose the interaction to be parity invariant ($a = d$, $\theta = 0$), the reflection and transmission coefficients simplify to

$$R_e = -\frac{bq_e^2 + c}{-2iaq_e - bq_e^2 + c} \qquad ,T_e = \frac{2q_e}{2aq_e - ibq_e^2 + ic}\,. \tag{9.43}$$

In order to match the effective quantum mechanics to the exact results, we start by

recalling the wave function from the exact solution

$$\psi_{\chi\phi}(x,y) = \exp(ipy) \begin{cases} A\exp(iq(x-y)) + B\exp(-iq(x-y))\,, & x > y \\ C\exp(-iq(x-y)) + D\exp(iq(x-y))\,, & x < y-a \end{cases} . \tag{9.44}$$

Since the ϕ defect is infinitely heavy, the center of mass coordinates are

$$R = y\,, \qquad\qquad r = x - y\,, \tag{9.45}$$

and the exact lattice wave function is of the same form as the one in the continuum, eq. (9.41), if we identify $p_e = p$ and $q_e = q$. The reflection and transmission coefficients are obtained from eq. (8.33) by setting $D = 1$, $C = R$, and $B = 0$ as

$$R = 0\,, \qquad\qquad T = \exp(2iap - 2iaq)\,. \tag{9.46}$$

The phase shift in the transmission coefficient is a consequence of the immobile defect being moved by two lattice spacings during the scattering event. This should not reflect itself in the continuum effective theory and we explicitly exclude it by using the following non-trivial matching condition

$$\begin{aligned} &\psi_e(R,r) = \psi(R,r)\,, && r < 0\,, \\ &\psi_e(R,r) = \psi(R-2a, r+2a)\,, && r > 0\,. \end{aligned} \tag{9.47}$$

For exact and effective reflection and transmission coefficients this implies,

$$R_e = R\,, \qquad\qquad T_e = T\exp(-2iap_e + 2iaq_e)\,, \tag{9.48}$$

and therefore

$$R_e = 0\,, T_e = 1\,. \tag{9.49}$$

Thus the effective theory is completely free.

Since the ϕ defect has infinite kinetic mass, the total and reduced kinetic masses are $m_t = m_\phi = \infty$ and $m_r = m_\chi$. With that the dispersion relation of the effective theory becomes

$$E_e = M_\phi^{(0)} + M_\chi^{(0)} + \frac{q_e^2}{2m_\chi}\,. \tag{9.50}$$

The exact dispersion relation to second order, on the other hand, again disregarding the constant energy shift of E_S, is

$$E = \left(2\mu_3 - \frac{5J}{2}\right) + \frac{1}{2}a^2 J q_e^2\,. \tag{9.51}$$

Equating eqs. (9.51) and (9.50), we can identify

$$m_\chi = \frac{1}{Ja^2}\,, \qquad\qquad M_\phi^{(0)} + M_\chi^{(0)} = \left(2\mu_3 - \frac{5J}{2}\right)\,, \tag{9.52}$$

which is consistent with the rest and kinetic masses obtained by matching the one-particle wave functions to a free one particle effective quantum mechanics, as listed in eq. (9.38).

Let us now turn to the final case, the scattering of two χ-type defects. Since the exact solution of this sector is equivalent to the one for an XXZ Hamiltonian with $J < 0$ and $\Delta = -3/2$, the same is true for its effective description. The χ-type defects are effectively described by particles that interact with a (repulsive) contact interaction characterized by the parameter

$$\kappa_e = -\frac{1}{a}\left(\frac{3}{2}\cos^{-1}\left(\frac{ap_e}{2}\right) + 1\right)\,. \tag{9.53}$$

The rest energy and kinetic mass are consistent with the one-particle effective quantum mechanics.

9.5. The Non-trivial Matching Prescription

In the previous sections, we have explicitly excluded the contact point in the matching of lattice and effective two-defect scattering wave functions. This is necessary in order to obtain a consistent description of the low-energy physics. Seemingly arbitrary, we have employed the matching condition

$$\psi_e(x + \alpha/2, y - \alpha/2) = \psi(x, y)\,, \tag{9.54}$$

with $\alpha = a$. In the following we will show, that this is the only choice for α, that gives consistent predictions for the existence of a bound state for the $SU(2)$ spin chain with arbitrary Δ.

We now examine what happens for $\alpha \neq a$. In that case, we retrieve for two $SU(2)$ defects with $J < 0$,

$$\kappa(\alpha) = \frac{\Delta - \cos\left(\frac{ap}{2}\right)}{a\Delta - \alpha\Delta + \alpha\cos\left(\frac{ap}{2}\right)}\,. \tag{9.55}$$

For total momentum zero, this expression simplifies to

$$\kappa(\alpha) = \frac{\Delta - 1}{-\Delta\alpha + a\Delta + \alpha} = \frac{1}{a}\left(\frac{-1}{\alpha/a - \gamma}\right)\,. \tag{9.56}$$

with $\gamma := \Delta/(\Delta - 1)$. For the considered case of $|\Delta| \geq 1$, we find that $\gamma > 0$.

From the microscopic solution we know that for $\Delta > 1$ the effective theory should support a bound state and for $\Delta < -1$ it should not. The existence of a bound state is determined by the sign of κ and therefore by the sign of $\gamma - \alpha/a$. Consistency with the

microscopic solution implies

$$\begin{aligned} \Delta > 1 \quad &\Rightarrow \quad \alpha/a < \gamma\,, \\ \Delta < -1 \quad &\Rightarrow \quad \alpha/a > \gamma\,. \end{aligned} \tag{9.57}$$

If we impose that the effective theory gives consistent results for arbitrary $|\Delta| \geq 1$, the limits $\Delta \to \pm\infty$ constrain α/a to 1 and therefore imply that

$$\alpha = a\,. \tag{9.58}$$

We conclude this section with the following comment. An alternative but equivalent procedure to the non-trivial matching prescription is to employ a contact interaction of finite extent with a trivial matching prescription as effective theory. The Hamiltonian is again a free Hamiltonian but with an interval of finite extent, $[-\alpha, \alpha]$, excluded instead of just a point. In that case, the boundary conditions are applied not to the contact point but to the edges of the excluded interval, i.e., to the points $r = \pm\alpha$. In that case, we find, e.g., for the ratio of

$$\frac{A}{B} = \exp(-2i\alpha q)\frac{q + i\kappa}{q - i\kappa}\,. \tag{9.59}$$

The additional phase factor $\exp(-2i\alpha q)$ then arises not from the matching but from the extended contact interaction.

10. Summary and Conclusions

The low-energy physics of spin 1/2 XXZ-Heisenberg chains and the $SU(3)$ spin chain in a strong magnetic field is well described by an effective quantum mechanics, where the spin defects are represented by non-relativistic point particles with a contact interaction.

For $J < 0$, the effective theory captures the physics around zero momentum. The masses of the one- and two-particle (or defect) sector are retrieved consistently. For a weak anisotropy $\Delta = 1 + \delta$, the effective theory predicts a weakly bound state in accordance with the exact results. The predicted effective bound state energy agrees up to and including $O(p_e^2)$ and $O(\delta^2)$, and the bound state wave function decay length, κ, agrees up to and including $O(p_e^2)$ and $O(\delta)$. For a model with $\Delta < -1$, the contact interaction does not permit a localized state. Although such a state is present in the exact solution, it is not part of the low-energy physics of the $\Delta S^3 = -2$ sector and therefore not expected to be part of the effective description. In the case of $J > 0$, the effective theory predictions are completely consistent with the results for $J < 0$, regarding the unitary transformation U.

The defects in the saturated state of the $SU(3)$ spin chain are classified into two types of static and one type of dynamical defects. Remarkably, the dynamical defect is completely analogous to a defect in the saturated state for an XXZ model with $\Delta = -3/2$ and $J < 0$, both in its exact and effective description. The dynamical defects do not form a bound state, they interact repulsively. In the matching of the effective theory to the exact solution a subtlety arises. The contact point has to be explicitly excluded in order to obtain a consistent description of the low-energy physics at arbitrary Δ.

This illustrates, on the one side, the power of effective theory methods but also, on the other side, that great care has to be taken in the application of such techniques. Even for the simple case considered here, unexpected subtleties may arise.

One motivation for the investigation of the defects in the saturated state of the $SU(3)$ symmetric spin chain is the possibility of an additional phase transition in the $\mathbb{C}P(2)$ model that can be regularized with an $SU(3)$ spin ladder. The repulsive interaction of the dynamical defects is a hint that no additional phase transition occurs. In order to make a definite statement, it would be interesting to generalize this result to the case of a spin ladder, a two dimensional system.

Bibliography

[1] D. C. Mattis, *The Theory of Magnetism I: Statics and Dynamics*, ed. by D. C. Mattis, Springer Series in Solid-State Sciences, Berlin, Heidelberg: Springer, 1981, pp. 1–38.

[2] C. Sander, *Intellect. Hist. Rev.* 30 (2020), 523.

[3] B. Abi et al., *Phys. Rev. Lett.* 126 (2021), 141801.

[4] W. Heisenberg, *Z. Physik* 49 (1928), 619.

[5] H. E. Stanley, *Rev. Mod. Phys.* 71 (1999), 358.

[6] L. P. Kadanoff, *Phys. Phys. Fiz.* 2 (1966), 263.

[7] K. G. Wilson, *Phys. Rev. B* 4 (1971), 3174.

[8] K. G. Wilson, *Phys. Rev. B* 4 (1971), 3184.

[9] A. Pelissetto and E. Vicari, *Phys. Rep.* 368 (2002), 549.

[10] L. Onsager, *Nuovo Cim.* 6 (1949), 279.

[11] R. Feynman, *Progress in Low Temperature Physics*, vol. 1, Elsevier, 1955, pp. 17–53.

[12] A. A. Abrikosov, *J. Phys. Chem. Solids* 2 (1957), 199.

[13] H. E. Hall, W. F. Vinen, and D. Shoenberg, *Proc. R. Soc. A* 238 (1956), 204.

[14] W. F. Vinen and D. Shoenberg, *Proc. R. Soc. A* 260 (1961), 218.

[15] V. N. Popov, *Sov. Phys. JETP* 37 (1972), 341.

[16] J.-M. Duan, *Phys. Rev. B* 49 (1994), 12381.

[17] G. Baym and E. Chandler, *J. Low Temp. Phys.* 50 (1983), 57.

[18] N. Kopnin, *JETP Lett.* 27 (1978).

[19] N. B. Kopnin and M. M. Salomaa, *Phys. Rev. B* 44 (1991), 9667.

[20] G. E. Volovik, *JETP Lett.* 67 (1998), 528.

[21] D. J. Thouless and J. R. Anglin, *Phys. Rev. Lett.* 99 (2007), 105301.

[22] E. P. Gross, *Nuovo Cim.* 20 (1961), 454.

[23] L. P. Pitaevskii, *Sov. Phys. JETP* 13 (1961), 451.

[24] T. Simula, *Phys. Rev. A* 97 (2018), 023609.

[25] T. Banks, R. Myerson, and J. Kogut, *Nucl. Phys. B* 129 (1977), 493.

[26] R. Savit, *Phys. Rev. B* 17 (1978), 1340.

[27] M. E. Peskin, *Ann. Phys. (N.Y.)* 113 (1978), 122.

[28] K. Kajantie et al., *Nucl. Phys. B* 559 (1999), 395.

[29] K. Kajantie et al., *Nucl. Phys. B* 546 (1999), 351.

[30] T. Neuhaus, A. Rajantie, and K. Rummukainen, *Phys. Rev. B* 67 (2003), 014525.

[31] K. Kajantie et al., *Nucl. Phys. B* 699 (2004), 632.

[32] J. Fröhlich, G. Morchio, and F. Strocchi, *Ann. Phys. (N.Y.)* 119 (1979), 241.

[33] D. Buchholz, *Phys. Lett. B* 174 (1986), 331.

[34] H.-J. Borchers and D. Buchholz, *Quantum Field Theory: A Selection of Papers in Memoriam Kurt Symanzik*, ed. by A. Jaffe, H. Lehmann, and G. Mack, Berlin, Heidelberg: Springer, 1985, pp. 169–185.

[35] G. Delfino, W. Selke, and A. Squarcini, *Phys. Rev. Lett.* 122 (2019), 050602.

[36] N. H. Christ and T. D. Lee, *Phys. Rev. D* 12 (1975), 1606.

[37] R. Rajaraman, *Solitons and Instantons*, North-Holland, 1982.

[38] L. P. Kadanoff and H. Ceva, *Phys. Rev. B* 3 (1971), 3918.

[39] J. Fröhlich and P. A. Marchetti, *Comm. Math. Phys.* 112 (1987), 343.

[40] J. Fröhlich and P. A. Marchetti, *Commun.Math. Phys.* 121 (1989), 177.

[41] J. Fröhlich and P. A. Marchetti, *Europhys. Lett.* 2 (1986), 933.

[42] P. A. Marchetti, *EPL* 4 (1987), 663.

[43] A. S. Kronfeld and U.-J. Wiese, *Nucl. Phys. B* 357 (1991), 521.

[44] A. S. Kronfeld and U.-J. Wiese, *Nuclear Physics B* 401 (1993), 190.

[45] D. Horn, *Phys. Lett. B* 100 (1981), 149.

[46] P. Orland and D. Rohrlich, *Nucl. Phys. B* 338 (1990), 647.

[47] S. Chandrasekharan and U.-J. Wiese, *Nucl. Phys. B* 492 (1997), 455.

[48] R. Brower, S. Chandrasekharan, and U.-J. Wiese, *Phys. Rev. D* 60 (1999), 094502.

[49] R. Brower et al., *Nucl. Phys. B* 693 (2004), 149.

[50] K. G. Wilson, *Phys. Rev. D* 10 (1974), 2445.

[51] A. Bazavov et al., *Rev. Mod. Phys.* 82 (2010), 1349.

[52] S. Dürr et al., *Science* 322 (2008), 1224.

[53] P. de Forcrand, *Proceedings of The XXVII International Symposium on Lattice Field Theory — PoS(LAT2009)*, vol. 91, SISSA Medialab, 2010, p. 010.

[54] R. P. Feynman, *Int. J. Theor. Phys.* 21 (1982), 467.

[55] J. I. Cirac and P. Zoller, *Nat. Phys.* 8 (4 2012), 264.

[56] S. Lloyd, *Science* 273 (1996), 1073.

[57] D. Jaksch et al., *Phys. Rev. Lett.* 81 (1998), 3108.

[58] I. Bloch, J. Dalibard, and S. Nascimbène, *Nat. Phys.* 8 (4 2012), 267.

[59] M. Lewenstein, A. Sanpera, and V. Ahufinger, *Ultracold Atoms in Optical Lattices: Simulating Quantum Many-Body Systems*, Oxford University Press, 2012.

[60] U.-J. Wiese, *Nucl. Phys. A* 931 (2014), 246.

[61] H. Eichenherr, *Nucl. Phys. B* 146 (1978), 215.

[62] A. D'Adda, M. Lüscher, and P. Di Vecchia, *Nucl. Phys. B* 146 (1978), 63.

[63] B. B. Beard et al., *Phys. Rev. Lett.* 94 (2005), 010603.

[64] B. B. Beard et al., *Comput. Phys. Commun.* 175 (2006), 629.

[65] C. Laflamme et al., *Ann. Phys. (N.Y.)* 370 (2016), 117.

[66] W. Evans et al., *Ann. Phys. (N.Y.)* 398 (2018), 94.

[67] P. Virtanen et al., *Nat. Methods* 17 (3 2020), 261.

[68] R. K. Guy, *Am. Math. Mon.* 95 (1988), 697.

[69] V. G. Vaks and A. I. Larkin, *Sov. Phys. JETP* 22 (1966), 678.

[70] R. G. Bowers and G. S. Joyce, *Phys. Rev. Lett.* 19 (1967), 630.

[71] J. Villain, *J. Phys. France* 36 (1975), 581.

[72] L. Polley and U.-J. Wiese, *Nucl. Phys. B* 356 (1991), 629.

[73] M. F. Atiyah, "Duality in Mathematics and Physics", Lecture Notes, Institut de Matematica de la Universitat de Barcelona, 2007.

[74] H. A. Kramers and G. H. Wannier, *Phys. Rev.* 60 (1941), 252.

[75] R. Savit, *Rev. Mod. Phys.* 52 (1980), 453.

[76] K. Drühl and H. Wagner, *Ann. Phys. (N.Y.)* 141 (1982), 225.

[77] C. R. Gattringer, S. Jaimungal, and G. W. Semenoff, *Phys. Lett. B* 425 (1998), 282.

[78] V. M. Buchstaber and M. I. Monastyrsky, *J. Phys. A: Math. Gen.* 36 (2003), 7679.

[79] P. A. M. Dirac, *Can. J. Phys.* 33 (1955), 650.

[80] G. 't Hooft, *Nucl. Phys. B* 153 (1979), 141.

[81] M. Campostrini et al., *Phys. Rev. B* 63 (2001), 214503.

[82] M. Hasenbusch, *J. Stat. Mech.* 2006 (2006), 08019.

[83] M. Hasenbusch, *J. Stat. Mech.* 2008 (2008), 12006.

[84] M. Hasenbusch, *Phys. Rev. B* 100 (2019), 224517.

[85] S. M. Chester et al., *J. High Energ. Phys.* 2020 (2020), 142.

[86] M. E. Fisher, M. N. Barber, and D. Jasnow, *Phys. Rev. A* 8 (1973), 1111.

[87] P. Hasenfratz and H. Leutwyler, *Nucl. Phys. B* 343 (1990), 241.

[88] S.-i. Tominaga and H. Yoneyama, *Phys. Rev. B* 51 (1995), 8243.

[89] Y.-H. Li and S. Teitel, *Phys. Rev. B* 40 (1989), 9122.

[90] U. Wolff, *Phys. Rev. Lett.* 62 (1989), 361.

[91] U. Wolff, *Comput. Phys. Commun.* 156 (2004), 143.

[92] J. .-.-L. Gervais and D. Zwanziger, *Physics Letters B* 94 (1980), 389.

[93] J. Fröhlich, G. Morchio, and F. Strocchi, *Physics Letters B* 89 (1979), 61.

[94] R. Bellman, *Dynamic Programming*, Princeton University Press, 1957.

[95] N. Metropolis et al., *J. Chem. Phys.* 21 (1953), 1087.

[96] W. K. Hastings, *Biometrika* 57 (1970), 97.

[97] M. Frigo, *Proceedings of the ACM SIGPLAN 1999 Conference on Programming Language Design and Implementation*, PLDI '99, New York, NY, USA: Association for Computing Machinery, 1999, pp. 169–180.

[98] R. H. Swendsen and J.-S. Wang, *Phys. Rev. Lett.* 58 (1987), 86.

[99] W. I. Jay and E. T. Neil, arXiv: `2008.01069`.

[100] H. Bethe, *Z. Phys.* 71 (1931), 205.

[101] C. N. Yang and C. P. Yang, *Phys. Rev.* 150 (1966), 321.